Selective Irradiation of the Vascular Endothelium

By

Bradley W. Schuller

B.A., Physics, 2003
College of the Holy Cross

SUBMITTED TO THE DEPARTMENT OF NUCLEAR SCIENCE AND ENGINEERING ON AUGUST 10, 2007 IN PARTIAL FULFILLMENT OF THE REQUIREMENTS FOR THE DEGREE OF

DOCTOR OF PHILOSOPHY IN NUCLEAR SCIENCE AND ENGINEERING
AT THE
MASSACHUSETTS INSTITUTE OF TECHNOLOGY

SEPTEMBER 2007

Signature of Author: _____
Department of Nuclear Science and Engineering
August 7, 2007

Certified by: _____
Jeffrey A. Coderre
Associate Professor of Nuclear Science and Engineering
Thesis Supervisor

Certified by: _____
Jacquelyn C. Yanch
Professor of Nuclear Science and Engineering
Thesis Reader

Accepted by: _____
Jeffrey A.Coderre
Associate Professor of Nuclear Science and Engineering
Chair, Committee for Graduate Students

Selective Irradiation of the Vascular Endothelium

by
Bradley W. Schuller

Submitted to the Department of Nuclear Science and Engineering on August 10, 2007 in partial fulfillment of the requirements for the degree of Doctor of Philosophy in Nuclear Science and Engineering

ABSTRACT

We developed a unique methodology to selectively irradiate the vascular endothelium *in vivo* to better understand the role of vascular damage in causing normal tissue radiation side-effects.The relationship between vascular endothelial cell apoptosis and intestinal crypt stem cell death was evaluated using uniform whole-body and selective vascular irradiation techniques. Mice received whole-body epithermal neutron beam irradiation. Additional dose was selectively targeted to endothelial cells from the short-ranged (5-9 μm) particles released from neutron capture reactions in ^{10}B confined to the blood by incorporation into 70-90 nm-diameter liposomes. Mice also received uniform photon doses above and below the threshold for death from the gastrointestinal (GI) syndrome. When plotted versus neutron beam dose, the crypt microcolony assay showed the same dose response for both the neutron beam-only and neutron beam plus boronated liposome groups. The added dose selectively delivered to the microvasculature did not cause any additional crypt loss. Jejunal cross-sections were prepared 4 hrs after irradiation and stained with TUNEL to observe and score apoptotic cells in the villus lamina propria. To uniquely identify the type of cell undergoing apoptosis in the lamina propria, intestinal specimens from various mice in the TUNEL studies were sectioned and stained with Meca-32 to identify endothelial cells and caspase-3 to identify apoptotic cells and visualized using dual-fluorescence microscopy. The TUNEL data showed a low level (~2 apoptotic cells per villus) of apoptosis in the lamina propria for both the uniform (photon or neutron) and selective vascular irradiation conditions that was independent of the administered dose. The dual-fluorescence studies indicated that most apoptotic bodies in the lamina propria were not endothelial cells but, rather, apoptotic leukocytes. These data demonstrate that there is no causal relationship between vascular endothelial cell apoptosis and crypt stem cell death in the mouse small intestine.

Thesis Supervisor: Jeffrey A. Coderre, Ph.D., Associate Professor of Nuclear Science and Engineering, Massachusetts Institute of Technology

ACKNOWLEDGEMENTS

Science is never a solitary pursuit. The thesis presented here would be a mere spectre had it not been for the incredible influence and guidance from the wonderful people with whom I have had the pleasure of working. Their impact on me extends beyond the brevity of these acknowledgements, and my only concern is that these futile words will only serve to belittle my true appreciation for them. For that I apologize.

First, I would like to thank my advisor, Prof. Jeff Coderre. He was the unwavering pillar of support and guidance during my studies with him. Always a source of inspiration, he revealed the true process of science by allowing me to explore while also providing profound insight into new problems. He taught me how to be a good scientist, and for that I will always be grateful.

I would like to extend my appreciation to Dr. Kent Riley, Dr. Peter Binns and Prof. Otto Harling for maintaining impeccable neutron irradiation facilities as well as providing their expertise and invaluable insight into radiation dosimetry, data analysis and experimental design. This project would not have been possible without them.

Special thanks are due to Prof. Jackie Yanch, Prof. David Schauer and Prof. Alan Jasanoff for serving on my thesis committee and providing valuable instruction and guidance during the course of the project.

Many thanks are due to Dr. Arlin Rogers, Dr. Prashant Nambiar and Kathy Cormier (Division of Comparative Medicine, MIT) for providing and maintaining an elegant histology service and for allowing me a glimpse of the fine art of pathology and histological scoring. Their beautiful tissue staining provided unprecedented clarity into the wonderful world of tissue architecture.

I am grateful to Prof. M. Fred Hawthorne and Richard Julius (University of Missouri) for providing the boron compound that ultimately formed the core of this thesis and for endorsing the major results of this project in front of the National Academy of Sciences.

My time at MIT would have been far less pleasant without the wonderful friendships offered to me over the past four years. Specifically, I would like to express my deepest appreciation to Rong Wang and Antonio Damato (my office mates) as well as Yoonsun Chung, Vered Anzenberg, Jingli Liu Kiger and Rebecca Raabe. Special thanks are due to Rachel Batista for her friendship and willingness to listen during the good times and the bad times.

I would like to specifically thank Prof. Janine Shertzer (College of the Holy Cross) for convincing a freshman english major that physics is the true language of the universe. She sparked in me an unquenchable curiosity and passion for science.

I will never be able to express how grateful I am for the unconditional love and support from my family. They have always been such a source of inspiration and happiness for me, and they will never know how much they have shaped who I am today. I am honored to be a part of them.

Finally, I would like to extend my deepest love and appreciation to my dear fiancée, Gabrielle Deifik. Words cannot express how grateful I am for her love and support, which I too often take for granted. She is always there for me through thick and thin, and she is always my biggest cheerleader. We have battled the Harpies together, and I am looking forward to spending my life with her.

TABLE OF CONTENTS

LIST OF FIGURES

Chapter 1

Chapter 2

Chapter 3

Chapter 4

Chapter 4 Appendix

Chapter 5

LIST OF TABLES

Chapter 1: Introduction

1.1 Motivation

The role of vascular damage in normal tissue radiation side effects (both acute and late) has been a matter of considerable debate for many years. The debate is largely centered on the role of vascular damage (apoptosis) in acute radiation effects, although there are some unanswered questions regarding the role of vascular damage in the onset of late radiation effects as well. These debates still exist largely due to the lack of experimental techniques to selectively increase the radiation dose to one target cell population *in vivo* (e.g. the vascular endothelium) while keeping all others relatively unscathed. Conventional irradiation techniques only allow for uniform irradiation where all cells in the tissue receive the same radiation dose.

Our goal in this project was to develop a methodology to selectively irradiate the vascular endothelium in order to address and hopefully resolve some of the unanswered questions and unresolved controversies that still exist in the radiation biology community. A selective vascular irradiation methodology exists in the central nervous system (CNS) where the blood-brain barrier can be exploited to gain vascular specificity (these techniques will be described later). However, we wanted to find a general technique that could be applied to any tissue or tumor where it would be interesting to explore the effects of vascular damage in that system. This thesis will describe a generalized methodology for

selective vascular irradiation and will present the proof-of-principle results that were obtained in a very interesting tissue system: the mouse small intestine.

1.2 Background

1.2.1 Radiation damage in normal tissues (acute and late)

The critical events that lead to the ultimate depletion of tissue structure and function are initiated at the time of irradiation. The eventual manifestation of radiation effects critically depends on tissue type and cell turnover kinetics as well as the magnitude of the radiation dose. Radiation damage in normal tissue is traditionally separated into 'early' (acute) and 'late' effects, where, for late effects, there may be a clinically 'silent' period before the damage manifests itself. Stem cell based, rapidly-renewing tissues such as the small intestine, bone marrow and oral mucosa are classic examples of acute responding tissues. It is generally accepted that damage to the regenerative stem cell populations is the initiating lesion leading to radiation effects in these tissues. Once the regenerative stem cell populations die due to radiation exposure, the loss of tissue structure and function is very quick to follow, usually within a few days or weeks after radiation exposure [1]. There is, however, a hypothesis that exists in the radiation biology community that claims that vascular damage, rather than direct stem cell damage, is the cause of acute radiation effects.

Late radiation effects typically occur in slowly proliferating tissues such as the lung, kidney, liver and CNS. Fibrosis, atrophy, vascular damage, neural damage and negative growth effects are the typical radiation-induced late effects, and they tend to develop months to years after radiation exposure [1]. Researchers now believe that vascular damage may be responsible for promoting the conditions required for late effects, namely chronic inflammation (more on this later).

1.2.2 The role of vascular damage in normal tissue toxicity (late effects)

1.2.2.1 Late radiation effects in the small intestine

Once surviving crypt stem cells have repopulated the intestinal epithelium to fully regain optimal tissue function after radiation exposure, it would seem that the tissue has thwarted severe and long-lasting effects. However, at sufficiently high radiation doses (but still below those that would result in death from the gastrointestinal (GI) syndrome) the small intestine is susceptible to late radiation-induced fibrosis that occurs months to even years after exposure [2]. It has been hypothesized that radiation damage to the vascular endothelium plays a critical role in the onset of late tissue fibrosis [3], although the exact mechanism remains unclear. Regardless, the onset of tissue fibrosis is the direct result of the complex interplay between interconnected cell signaling networks [2, 4]. It has been proposed that vascular damage is responsible for the onset of a chronic

inflammatory state, where inflammatory cytokine signaling persists beyond the point of normal wound healing to ultimately result in tissue scarring, or fibrosis.

Up-regulation of various inflammatory cytokines, including transforming growth factor-β (TGF-β) [5], tumor necrosis factor-α (TNF-α) and interleukin-1 (IL-1) has been reported in irradiated tissue [6]. Impairment of microvascular function has been implicated in the late radiation response of the small intestine in reports showing a dose-dependent decrease in microvascular thrombomodulin, which results in elevated levels of thrombin. Elevated thrombin levels will then activate the inflammation response, and the active feedback loop in TGF-β and TNF-α maintains the suppressed thrombomodulin levels, thus perpetuating inflammatory signaling [4, 7]. Thus, there is strong, yet indirect, evidence showing that microvascular radiation damage mediates the late radiation response in the small intestine.

1.2.2.2 Late radiation effects in the CNS

Researchers have previously employed a selective vascular irradiation methodology in the rat CNS where the blood-brain barrier was used to restrict the widely used boron neutron capture therapy (BNCT) compound, sulfhydryl boron hydride ($Na_2B_{12}H_{11}SH$, BSH), to the blood. Subsequent irradiation with thermal neutrons selectively elevated the dose delivered to the CNS microvasculature (more detail on this technique later). They were able to show that vascular damage was responsible for the onset of late (7 months) necrosis in the rat

spinal cord [8-12]. In these studies, O-2A glial progenitor cells survived selective vascular irradiation conditions, which indicated that vascular radiation damage played a critical role in the onset of late radiation effects but had no effect on the early radiation response in that system. Similar studies were carried out in the rat brain where the loss of neural precursor cells was correlated with stem cell dose and not the added dose selectively delivered to the vasculature [13].

There is clear evidence from the studies outlined above that vascular damage plays a role in the onset of late radiation effects in normal tissue (the exact damage mechanisms are still unknown). However, the primary controversy surrounding the role of vascular damage in normal tissue radiation toxicity is centered on acute radiation effects.

1.2.3 Controversies surrounding the proposed role of vascular damage in acute radiation effects

1.2.3.1 Controversy surrounding the proposed role of vascular damage in the acute lung radiation toxicity (radiation pneumonitis)

A rather old controversy exists in the lung, where it has been reported by Fuks *et al.* that radiation-induced endothelial apoptosis is responsible for the subsequent onset of radiation-induced pneumonitis in the lung [14]. There they showed that vascular endothelial cells in the lung underwent apoptosis ~ 6-8 hrs after clinically relevant radiation doses, and that administration of basic fibroblast

growth factor (bFGF) inhibited apoptotic death in endothelial cells. Administration of bFGF immediately before and after radiation exposure inhibited vascular endothelial apoptosis in mouse lung and subsequently protected the animals from the development of lethal radiation pneumonitis [14]. However, a conflicting report was published shortly thereafter, in direct response to the Fuks *et al.* report, that demonstrated the failure of bFGF to protect the lung from radiation-induced pneumonitis *via* the vascular endothelial apoptosis pathway [15]. Nothing more has been presented on this topic since then.

1.2.3.2 Controversy surrounding the proposed role of vascular damage in tumor cell death

Another recent debate has centered on the role of vascular endothelial apoptosis in the response of tumors to radiation therapy. It was reported that vascular endothelial apoptosis mediates tumor radio-sensitivity [16]. Briefly, it was shown that tumors implanted in mice deficient in acid sphingomyelinase or Bax (two pro-apoptotic genes purported to mediate vascular endothelial apoptosis) showed significant radio-resistance compared to their wild-type counterparts. It was therefore concluded that endothelial apoptosis regulates the tumor response to radiotherapy [16]. Again, this hypothesis was met with considerable controversy and discussion [17-20], and a conflicting report was subsequently published showing that the intrinsic tumor cell radio-sensitivity is the major determinant of the tumor response to radiation [21], not the intrinsic

radio-sensitivity of the tumor vasculature. Gerweck *et al.* altered the radio-sensitivity of repair-deficient tumor cells with the double-strand break repair gene, *DNA-PKcs*, which decreased the cell radio-sensitivity by a factor of ~1.5. If vascular damage was the determinant of tumor cell sensitivity, one would expect tumors with and without *DNA-PKcs* transfection to show a similar radiation response. They, however, did not. The ratio (± *DNA-PKcs* transfection) of growth delay was ~1.5 for all irradiation conditions [21].

1.2.3.3 Controversy surrounding the proposed role of vascular damage in the acute small intestine radiation toxicity (stem cell death and the gastrointestinal (GI) syndrome)

It has traditionally been assumed that the GI syndrome results from direct damage to stem cells leading to a depletion of differentiated epithelial cells and a complete loss of tissue structure and function at high doses. However, the GI syndrome has recently been suggested to be a direct consequence of an early (4 hrs) wave of apoptosis in the intestinal vascular endothelial cells [22]. These authors irradiated mice with single whole-body photon doses of 8-15 Gy, some of which were sufficient to cause death from the GI syndrome, and demonstrated that it was possible to change the mode of death from the GI syndrome to the bone marrow syndrome (in effect, producing about 3 Gy of radioprotection) when endothelial cell apoptosis was suppressed genetically by deletion of the gene for acid sphingomyelinase (a proapoptotic gene purported to mediate vascular

endothelial apoptosis), which controls endothelial cell apoptosis through a ceramide pathway [23-28], or pharmacologically by administration of basic fibroblast growth factor (bFGF). Immunohistochemistry showed that bFGF localizes to the lamina propria and not the epithelial cells, including the stem cells in the crypts [22]. Endothelial apoptosis was shown to be p53 independent. p53 (also known as 'tumor protein 53') is a transcription factor known to regulate the cell cycle. It has a role as a tumor suppressor and has many anti-cancer functions such as activating DNA repair proteins, initiating cell-cycle arrest during DNA repair and initiating apoptosis [29]. Endothelial apoptosis has, however, been shown to be acid sphingomyelinase dependent, where radiation activates acid sphinomyelinase in the plasma membrane, which generates ceramide by enzymatic hydrolysis of sphingomyelin. Ceramide then activates the apoptotic response through the mitochondrial system [25-28]. The precise mechanism of this proposed linkage between intestinal endothelial cell apoptosis and crypt stem cell depletion leading to the GI syndrome remains unproven [28, 30, 31], and it has been met with considerable controversy in the literature [32, 33].

Critics of this theory have countered using the argument that if microvascular apoptosis (and subsequent microvascular dysfunction) initiates intestinal crypt stem cell death, the mechanism would be hypoxic or ischemic death. The resulting intestinal crypt survival curves would initially be steep for well oxygenated cells after a single radiation dose, and then tend to be shallower for subsequent, fractionated doses from the resultant tissue hypoxia due to microvascular dysfunction. However, the published survival data that exist do not

show any effect due to tissue hypoxia [33-36]. Also, the rapid tissue repopulation due to surviving crypt stem cells following radiation exposure would be impossible with a disrupted capillary network [33]. Critics have also noted that bFGF (or other growth factors) has been reported to confer radioprotection [37-42] to the apoptosis-susceptible crypt epithelium [39, 43] through cell cycle delay in G1 [44] or stimulating epithelial proliferation [45]. Finally, Potten [46] has recently reported that although high levels of crypt epithelial apoptosis were observed at 4 and 10 hrs post-irradiation, little or no endothelial apoptosis was evident after using the same radiation doses and staining techniques reported by Paris *et al.* [22, 46]. Clearly, there is a need for novel irradiation techniques that will allow the direct testing of most, if not all, of these controversial hypotheses.

Time of death, or more specifically, mode of death following whole-body radiation exposure is not an adequate endpoint for radiation biology studies. We know from classical radiation biology experiments that the time of death due to the GI syndrome can be affected by the intrinsic radio-sensitivity of the hematopoietic bone marrow cells [47]. Mason *et al.* showed that intestinal stem cell survival was the same in mice that received either whole-body irradiation or just abdominal irradiation (shielded bone marrow). However, the LD_{50} (lethal dose in 50% of the population) shifted from ~20 Gy to ~16 Gy when the irradiation conditions were changed from total abdominal to whole-body irradiation conditions. Thus, the LD_{50} was shifted by ~ 4 Gy, which can be attributed to the influence of bone marrow sensitivity on time of death. Therefore, animal survival after large radiation doses (in the case of Paris *et al.*, ~15 Gy) is

not solely related to intestinal stem cell survival but, rather, depends on the combined influence of both intestinal and hematopoietic stem cell sensitivities [47]. Ambiguities are thus incorporated into the Paris *et al.* conclusions, because we know from the work of Mason *et al.* that time (and mode) of death can be influenced by multiple factors.

1.2.3.4 The need for a selective vascular irradiation technique as a tool for direct mechanistic studies into normal tissue radiation effects

Selective vascular irradiation techniques have been used by researchers to explore the role of vascular damage in CNS radiation toxicities. Specifically they were able to show that vascular damage was responsible for the onset of late necrosis in the rat spinal cord, whereas glial progenitor cell survival was unaffected by selective vascular irradiation [12, 13]. They exploited the blood-brain barrier to restrict a ^{10}B enriched compound (BSH) to the blood. Subsequent irradiation with thermal neutrons resulted in an elevated dose to the vascular endothelium (from the short range (5-9 μm) reaction products (α and ^{7}Li ions) released from the boron neutron capture reaction) relative to the simultaneous neutron beam dose delivered uniformly to the vessels and surrounding tissue. This technique will not work outside of the CNS, because BSH will diffuse from the blood stream into the surrounding tissues resulting in a uniform ^{10}B dose to both the vascular endothelium and surround tissues.

There is clearly a need for a generalized methodology for selective vascular irradiation to address the multiple controversies that exist for vascular damage in acute radiation effects as well as the unanswered questions regarding the role of radiation damage in the onset of late radiation effects. The specific methodology we employed for a generalized scheme to selectively irradiate the vascular endothelium is, in principle, similar to the CNS studies, but will be outlined at the end of this introduction and will be explained in detail in subsequent chapters.

1.2.4 The mouse small intestine: an ideal system for selective vascular irradiation studies

The mouse small intestine is an ideal system for selective vascular irradiation studies, because it exhibits both acute and late effects and has clinical relevance in that gastrointestinal tract sensitivity limits the amount of radiation that can be delivered to the abdominal region during cancer therapy. The stem cells that regenerate the epithelial lining of the small intestine are highly sensitive to radiation exposure [46, 48], and the dose response for stem cell death in the small intestine has been studied in great detail [34-36, 46, 48-51]. It is widely accepted that radiation targets the intestinal stem cells, but some researchers now think that vascular damage is the primary lesion leading to stem cell death. The small intestine has also been shown to have a late effect (fibrosis) [2, 3], and vascular damage may be involved with this process. The role of vascular

damage in the small intestine radiation toxicity is either highly controversial or unanswered.

1.2.4.1 Anatomy of the small intestine

The small intestine is a classic example of a stem cell-based, rapidly-renewing tissue. The small intestine is a tubular organ comprised of a monolayer of columnar epithelial cells, which surround a complex connective tissue and vascular network to form the familiar finger-like projections called "villi". Epithelial cells originate from within the crypts of Lieberkühn that reside at the base of villi (Figure 1-1). Epithelial cells differentiate as they migrate up the villus in a vertical fashion [46, 52, 53], where they ultimately perform their prescribed functions (secretion, absorption and protection against the gut microflora), die and slough off at the villus tip; the total transit time taking ~ 3-4 days. This continuous cell loss is perfectly balanced by cell regeneration from within the crypts. It has been estimated that some 250 cells reside in a crypt, and among those approximately 150 exhibit cell cycle times that are as rapid as any mammalian cell system (~12 hrs) [46]. Approximately 6-9 crypts service a single villus. This indicates that each villus loses between 1000 and 1400 cells per day. It is also known that each epithelial cell is continuously moving with a velocity of approximately one cell diameter per hour [46, 54].

Experiments have shown that vertical epithelial movement is restricted to a columnar structure with little or no horizontal movement or mixing between

neighboring columns [46, 52, 53, 55]. This implies that there is a strong cell-lineage organization to the epithelial structure, where cells of equal age move together as they differentiate and progress through their life cycles. Using tritiated thymidine to label cells in S-phase, experiments have defined and verified the epithelial cell migration velocity, and have identified the position from within the crypt where all cells in the columnar structure originate. This defines the position of "lineage ancestor stem cells" [46, 54, 56]. Tritiated thymidine studies have also been used to show the existence of a "proliferative zone", (where cells divide and mature as they migrate) beyond which cell division ceases, to ultimately yield a population of mature epithelial cells [46, 48, 57, 58].

These studies have thus shown that crypts contain a well defined set of cell lineages, which are supported by a subpopulation of immortal stem cells that exist in steady state at positions 4-5 (see Figure 1-1 for a description of crypt cell position numbering) within the crypt. Stem cells live above a population of protective Paneth cells that occupy positions 1-4 [46]. Each time a stem cell divides, one daughter cell remains as the "immortal" stem cell, while the other daughter moves to the next position within the crypt cell hierarchy. This daughter then begins the differentiation process to become either a Paneth cell or a functional epithelial cell. Early cell divisions take place within the "proliferative zone" as some cells begin to move laterally to maintain the 3-dimensional crypt structure and enter a cell lineage that may contain upwards of 6 defined generations (Figure 1-1). Each generation corresponds to the cells' physical location with the crypt structure, i.e. cells closer to the stem cells are 'younger'

than the cells above them. The functionality and architecture of this stem cell system was inferred from the radio-labeling of migrating epithelial cells.

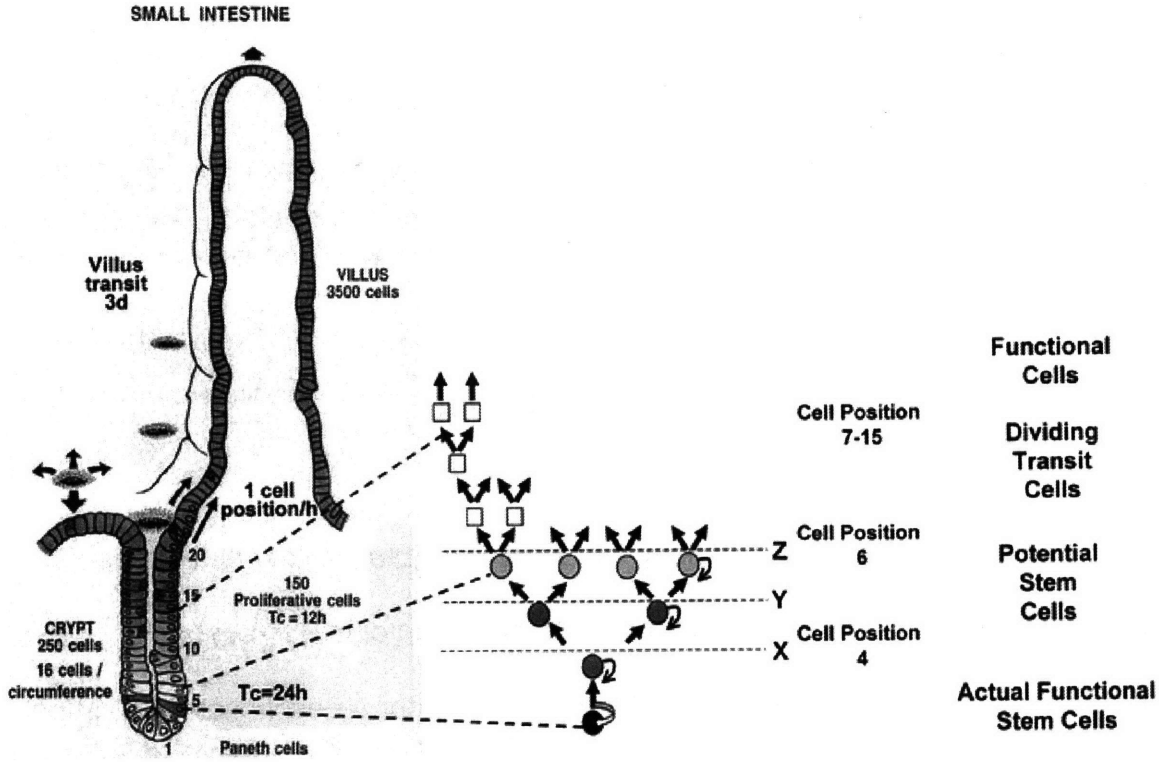

Figure 1-1. Schematic of small intestine architecture and stem cell dynamics. The delineation between 'actual and potential stem cells' and the dividing transit cells within the proliferative zone is thought to occur at or around positions X, Y and Z [46]. This figure was taken directly from reference 46 with permission from the publisher.

Specific stem cell markers do not currently exist. However, there has been much effort put towards the development of such markers to ultimately verify the proposed models [59, 60].

1.2.4.2 Acute radiation pathology of the small intestine

The small intestine is one of the most radiation sensitive tissues in the body, second only to the bone marrow, and exhibits a well defined set of acute effects. Despite being slightly less radio-sensitive than the bone marrow, radiation damage in the small intestine will manifest itself first because of the rapid functional cell migration and stem cell turnover time (total transit time from crypt to villus tip takes ~3-4 days). The radiation sensitivity of the small intestine is the dose limiting factor in the treatment of abdominal tumors with radiation therapy. In the mouse small intestine, a wave of apoptosis is observed in what are thought to be crypt stem cells [60] as early as 3-6 hrs after irradiation with doses as low as 0.01 Gy [46]. This effect saturates at ~ 1 Gy [61]. By 24 hrs post-irradiation, crypt epithelial apoptosis levels fall to control levels. The wave of radiation-induced apoptosis in crypts occurs almost primarily at crypt positions 4-5 and not in the rapidly proliferating cells in the higher positions [46], although apoptosis in higher positions may occur at later times [31]. There is no dependence on LET (liner energy transfer) or dose rate for crypt epithelial apoptosis, which implies that these cells do not undergo DNA repair processes [46]. This early wave of crypt epithelial apoptosis is known to be p53 dependent from experiments that have shown that p53 knockout mice (p53 -/-) exhibit suppressed epithelial apoptosis 4 hrs after irradiation [22, 46, 62]. Despite the apoptotic response of crypt stem cells after irradiation, there were no differences

in the dose response of crypt regeneration between wild-type and p53 knockout mice [62].

Higher radiation doses are postulated to deplete the first few generations of differentiated transit cells that still retain the ability to revert to fully-functional stem cells [46]. Individual crypts are not sterilized until all of the actual and potential stem cells are inactivated, which occurs at doses of about 8 Gy or higher. The survival of one or more clonogenic cells per crypt allows its regeneration. Doses above approximately 15 Gy sterilize virtually all of the crypt stem cells, resulting in complete loss of the intestinal villi and death from the gastrointestinal (GI) syndrome in about 4-5 days. When all of the crypt stem cells are killed due to radiation exposure, the delicate system of continuous loss and renewal is disrupted. Cells continue to be sloughed off from the tips of villi but are no longer being replaced. As a result, the villi become denuded, shorten and shrink. The gastrointestinal syndrome is characterized by the complete loss of tissue structure and function resulting in loss of appetite, diarrhea, bleeding and eventual bacterial infection from invading resident gut microflora [46, 63].

A quantitative measure of crypt stem cell survival has been developed and is known as the 'crypt microcolony assay' or 'crypt regeneration assay' [35, 51]. The technique has endured many developmental iterations to finally converge on a microscopic assay, where stem cell survival is quantitated 3-4 days after radiation exposure. Surviving stem cells will repopulate the functional epithelial cells by forming enlarged crypt-like foci that will eventually reconstruct the inner structure of the small intestine. The crypt regeneration assay involves exposing

mice to various radiation doses, sacrificing the animals, harvesting the small intestine at 3.5 days when the surviving stem cells have begun to regenerate the crypts, preparing intestinal cross-sections (fixation in 10% formalin, embedding in paraffin, cutting and staining with hematoxylin and eosin (H&E)) and scoring the number of regenerating crypt-like foci per intestinal circumference [51]. The number of regenerating crypts can then be plotted as a function of dose to generate survival curves (Figure 1-2), which typically display a broad shoulder and exponential decrease at high doses [46]. Various technical considerations must be made while scoring regenerating crypts to account for oblique tissue cuts and variations in crypt size relative to control crypts [64]. Criteria must also be established to define a healthy regenerating crypt, which include the presence of viable Paneth cells and contiguous crypt epithelial cells feeding a villus [64].

Given that the anatomy and radiation pathology of the small intestine is known in great detail and that a quantitative assay exists to measure the extent of radiation damage, this system is perfectly suited to explore the role of vascular radiation damage in radiation toxicities. This system is also particularly interesting because of the recent controversy that has developed regarding the role of vascular damage in the onset of acute radiation effects. Therefore, the small intestine was chosen for the proof-of-principle studies of the generalized methodology for selective vascular irradiation presented in this thesis.

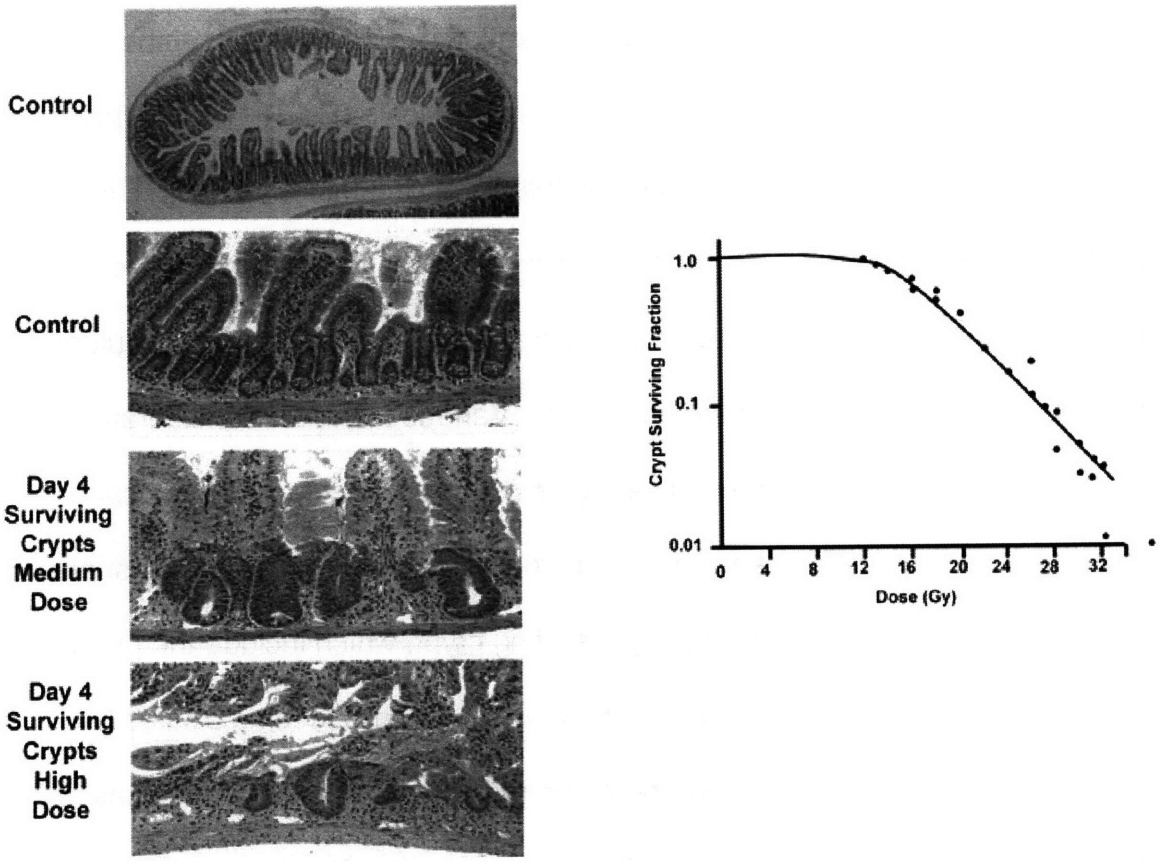

Figure 1-2. Intestinal crypt regeneration assay. Intestinal cross-sections are prepared to reveal individual crypt/villus units after H&E staining. Control sections display abundant (~80-100 crypts per circumference depending on mouse strain) crypt numbers, whereas crypt numbers begin to decrease as a function of dose (left). At right, plotting crypt surviving fraction (normalized to controls) as a function of dose will generate survival curves [46]. This figure was taken directly from reference 46 with permission from the publisher.

1.3 Project objectives

This project contributes to the greater understanding of the role of vascular damage in the onset of normal tissue radiation effects in general and in the small intestine in particular. A unique methodology for the selective irradiation of the vascular endothelium was developed in mice to explore the role of vascular radiation damage in the normal tissue radiation response. This allowed, for the first time, a direct measure of the role of microvascular damage in the normal tissue radiation response without the need for complicating factors such as growth factors or genetic manipulations (knockout mice). The intestinal crypt regeneration assay was used to measure the effect of selective vascular irradiation on intestinal crypt stem cell survival. Animal survival was used as an endpoint to ascertain the role of selective vascular irradiation in the onset of various early (acute) radiation syndromes. Vascular endothelial apoptosis was measured in the mouse small intestine after selective vascular irradiation or uniform external beam irradiation. This provided a resolution to the ongoing debate regarding the role of vascular radiation damage (specifically apoptosis) in the early radiation response in the mouse small intestine. Measurements were made on early inflammatory cytokine levels in the brain and small intestine after selective vascular irradiation or uniform external beam irradiation. This allowed, for the first time, a method to parse out the role of vascular radiation damage in the initiation of inflammatory signaling cascades, which may ultimately lead to the onset of late radiation effects (specifically, radiation-induced fibrosis in the small

intestine). All of the methodologies described in this thesis can be abstracted and/or modified for use in other normal tissues or in tumors.

1.4 Study design

Part 1: A unique methodology for the selective irradiation of the vascular endothelium outside of the central nervous system (CNS) was developed. This technique utilized the short range (5-9 μm) α and ^{7}Li particles released from boron-neutron capture reactions restricted to the blood stream of live mice. Novel ^{10}B-containing compounds (boronated Dextran-77 and boronated liposomes) were developed or modified for use in this methodology. Vascular dosimetry (as well as whole-body neutron dosimetry) was carefully considered. Monte-Carlo simulations were performed to determine the rate of dose drop-off as a function distance from the vessel lumen. Mouse biodistribution studies were performed for each compound to determine the ^{10}B concentrations in blood and normal tissue as a function of time post-injection. Preliminary mouse irradiation studies were conducted using the intestinal crypt regeneration assay and mouse survival as endpoints to measure the biological response after selective vascular and uniform irradiation conditions. The optimal compound (boronated liposomes) was chosen from these studies and was subsequently used for the rest of the project.

Part 2: Boronated liposomes were used in a study of the acute response in the mouse small intestine, which culminated in a publication in the Proceedings of

the National Academy of Sciences [63]. Rigorous dosimetry considerations are presented as well as full intestinal crypt survival curves and mouse survival data for neutron beam-only and selective vascular irradiation conditions. The main conclusions from this study are: **1.** The extra dose delivered by the ^{10}B-containing compound during neutron irradiation was fully restricted to the vascular endothelium. **2.** The compound itself does not leak from the vasculature. **3.** The added dose selectively delivered to the vascular endothelium does not cause enhanced crypt death beyond that produced by the neutron beam alone. Therefore, vascular damage (extra dose) does not contribute to the overall radiosesitivity of intestinal crypt stem cells. **4.** Conclusion 3 was extended and verified using an animal survival (mode of death) endpoint. The added radiation dose selectively delivered to the vascular endothelium did not cause a transition in the mode of death from the bone marrow syndrome to the GI syndrome when the neutron beam dose was brought just below the threshold for death from the GI syndrome. Thus, the uniform neutron beam dose to the crypts was solely responsible for this transition. The manuscript itself will serve as the main body of text for this part.

Part 3: The selective vascular irradiation methodology developed and tested in parts 1 and 2 was used in this part of the project to directly address the controversy regarding the role vascular endothelial apoptosis in the radiation-induced GI syndrome. The debate still exists largely due to the lack of experimental techniques to selectively irradiate one target cell population in order

to directly test these hypotheses. Instead, researchers indirectly inferred a vascular cause by administering various compounds (in this case growth factors) and using genetically modified animals (knockout mice). These conventional techniques may introduce unpredictable complications and influence the interpretation of the data. Thus, our technique provides a way to directly test the role of vascular endothelial apoptosis in the radiation-induced GI syndrome by allowing us to selectively elevate the dose to one target cell population, namely the vascular endothelium, while keeping all others relatively unharmed.

Vascular endothelial apoptosis was measured in irradiated mouse small intestine using uniform photon irradiation (x-rays and gamma rays), uniform neutron irradiation and the selective vascular irradiation methodology introduced earlier. Various tissue stains for apoptosis are presented as well as dose response data that show the incidence of apoptosis in the villus lamina propria as a function of vascular dose for 4 different irradiation modalities. These studies ultimately culminated in a publication in the International Journal of Radiation Oncology Biology and Physics [65]. The main conclusions from this study are: **1.** Vascular endothelial apoptosis did not occur at the level originally reported by Paris *et al.* [22] as the radiation dose crossed the threshold for death from the GI syndrome using x-rays, gamma rays, neutrons-only and selective vascular irradiation. Most significantly, the data Paris *et al.* presented using whole-body gamma irradiation could not be reproduced. **2.** Dual-fluorescence staining for apoptosis and tissue-resident leukocytes (white blood cells) identified the majority of the apoptotic bodies in these studies as apoptotic leukocytes. Thus,

vascular endothelial apoptosis is not causative in the radiation-induced GI syndrome, which is a conclusion that largely refutes the claim that radiation-induced endothelial apoptosis is the initiating lesion leading to stem cell death in the small intestine [14, 22, 30, 31, 66]. The manuscript itself will serve as the main body of text for this part.

Part 4: The selective vascular irradiation methodology was used to examine the early expression of inflammatory cytokines, which may lead to the onset of late radiation effects in the mouse small intestine. Tumor necrosis factor-α (TNF-α), intercellular adhesion molecule-1 (ICAM-1), interleukin-1 (IL-1), interleukin-6 (IL-6) and transforming growth factor-β (TGF-β) levels were measured in tissue following selective vascular irradiation and uniform whole-body irradiation using real-time polymerase chain reaction (real-time PCR) and DNA microarray analysis. Preliminary results indicate that ICAM-1 and TNF-α are upregulated early on in response to radiation exposure in both the uniform and selective vascular irradiation groups. The results show that there are differences between the neutrons-only and selective vascular irradiation groups. These results will serve as the foundation for future studies that will examine the role of vascular radiation damage in the onset of late radiation effects, namely fibrosis in the small intestine. This technique can also be applied to other late responding tissues such as the brain and even the lung.

References

1. Hall, E.J., Giaccia, A.J., *Radiobiology for Radiologist.* 6 ed. 2006: Lippincott Williams & Wilkins. 546.
2. Okunieff, P., T. Cornelison, M. Mester, W. Liu, I. Ding, Y. Chen, H. Zhang, J.P. Williams, and J. Finkelstein, *Mechanism and modification of gastrointestinal soft tissue response to radiation: role of growth factors.* Int J Radiat Oncol Biol Phys, 2005. **62**(1): p. 273-8.
3. Hopewell, J. and H.R. Withers, *Proposition: long-term changes in irradiated tissues are due principally to vascular damage in the tissues.* Med Phys, 1998. **25**(12): p. 2265-8.
4. Hauer-Jensen, M., L.M. Fink, and J. Wang, *Radiation injury and the protein C pathway.* Crit Care Med, 2004. **32**(5 Suppl): p. S325-30.
5. Barcellos-Hoff, M.H., *How tissues respond to damage at the cellular level: orchestration by transforming growth factor-{beta} (TGF-{beta}).* BJR Suppl, 2005. **27**: p. 123-7.
6. McBride, W.H., C.S. Chiang, J.L. Olson, C.C. Wang, J.H. Hong, F. Pajonk, G.J. Dougherty, K.S. Iwamoto, M. Pervan, and Y.P. Liao, *A sense of danger from radiation.* Radiat Res, 2004. **162**(1): p. 1-19.
7. Denham, J.W. and M. Hauer-Jensen, *The radiotherapeutic injury--a complex 'wound'.* Radiother Oncol, 2002. **63**(2): p. 129-45.
8. Morris, G.M., J.A. Coderre, A. Bywaters, E. Whitehouse, and J.W. Hopewell, *Boron neutron capture irradiation of the rat spinal cord: histopathological evidence of a vascular-mediated pathogenesis.* Radiat Res, 1996. **146**(3): p. 313-20.
9. Morris, G.M., J.A. Coderre, J.W. Hopewell, P.L. Micca, and C. Fisher, *Boron neutron capture irradiation of the rat spinal cord: effects of variable doses of borocaptate sodium.* Radiother Oncol, 1996. **39**(3): p. 253-9.
10. Morris, G.M., J.A. Coderre, J.W. Hopewell, P.L. Micca, M.M. Nawrocky, H.B. Liu, and A. Bywaters, *Response of the central nervous system to boron neutron capture irradiation: evaluation using rat spinal cord model.* Radiother Oncol, 1994. **32**(3): p. 249-55.
11. Morris, G.M., J.A. Coderre, E.M. Whitehouse, P. Micca, and J.W. Hopewell, *Boron neutron capture therapy: a guide to the understanding of the pathogenesis of late radiation damage to the rat spinal cord.* Int J Radiat Oncol Biol Phys, 1994. **28**(5): p. 1107-12.
12. Coderre, J.A., G.M. Morris, P.L. Micca, J.W. Hopewell, I. Verhagen, B.J. Kleiboer, and A.J. van der Kogel, *Late effects of radiation on the central nervous system: role of vascular endothelial damage and glial stem cell survival.* Radiat Res, 2006. **166**(3): p. 495-503.
13. Otsuka, S., J.A. Coderre, P.L. Micca, G.M. Morris, J.W. Hopewell, R. Rola, and J.R. Fike, *Depletion of neural precursor cells after local brain irradiation is due to radiation dose to the parenchyma, not the vasculature.* Radiat Res, 2006. **165**(5): p. 582-91.

14. Fuks, Z., R.S. Persaud, A. Alfieri, M. McLoughlin, D. Ehleiter, J.L. Schwartz, A.P. Seddon, C. Cordon-Cardo, and A. Haimovitz-Friedman, *Basic fibroblast growth factor protects endothelial cells against radiation-induced programmed cell death in vitro and in vivo.* Cancer Res, 1994. **54**(10): p. 2582-90.
15. Tee, P.G. and E.L. Travis, *Basic fibroblast growth factor does not protect against classical radiation pneumonitis in two strains of mice.* Cancer Res, 1995. **55**(2): p. 298-302.
16. Garcia-Barros, M., F. Paris, C. Cordon-Cardo, D. Lyden, S. Rafii, A. Haimovitz-Friedman, Z. Fuks, and R. Kolesnick, *Tumor response to radiotherapy regulated by endothelial cell apoptosis.* Science, 2003. **300**(5622): p. 1155-9.
17. Joiner, M., *New frontiers or red herrings in radiation oncology?* Lancet Oncol, 2004. **5**(1): p. 10.
18. Suit, H.D. and H. Willers, *Comment on "Tumor response to radiotherapy regulated by endothelial cell apoptosis" (I).* Science, 2003. **302**(5652): p. 1894; author reply 1894.
19. Abdulkarim, B. and E. Deutsch, *Endothelial-cell apoptosis and tumour response to radiotherapy.* Lancet Oncol, 2004. **5**(1): p. 9.
20. Folkman, J. and K. Camphausen, *Cancer. What does radiotherapy do to endothelial cells?* Science, 2001. **293**(5528): p. 227-8.
21. Gerweck, L.E., S. Vijayappa, A. Kurimasa, K. Ogawa, and D.J. Chen, *Tumor cell radiosensitivity is a major determinant of tumor response to radiation.* Cancer Res, 2006. **66**(17): p. 8352-5.
22. Paris, F., Z. Fuks, A. Kang, P. Capodieci, G. Juan, D. Ehleiter, A. Haimovitz-Friedman, C. Cordon-Cardo, and R. Kolesnick, *Endothelial apoptosis as the primary lesion initiating intestinal radiation damage in mice.* Science, 2001. **293**(5528): p. 293-7.
23. Haimovitz-Friedman, A., C.C. Kan, D. Ehleiter, R.S. Persaud, M. McLoughlin, Z. Fuks, and R.N. Kolesnick, *Ionizing radiation acts on cellular membranes to generate ceramide and initiate apoptosis.* J Exp Med, 1994. **180**(2): p. 525-35.
24. Haimovitz-Friedman, A., R.N. Kolesnick, and Z. Fuks, *Ceramide signaling in apoptosis.* Br Med Bull, 1997. **53**(3): p. 539-53.
25. Kolesnick, R. and Z. Fuks, *Ceramide: a signal for apoptosis or mitogenesis?* J Exp Med, 1995. **181**(6): p. 1949-52.
26. Kolesnick, R.N. and M. Kronke, *Regulation of ceramide production and apoptosis.* Annu Rev Physiol, 1998. **60**: p. 643-65.
27. Kolesnick, R. and Y.A. Hannun, *Ceramide and apoptosis.* Trends Biochem Sci, 1999. **24**(6): p. 224-5; author reply 227.
28. Kolesnick, R. and Z. Fuks, *Radiation and ceramide-induced apoptosis.* Oncogene, 2003. **22**(37): p. 5897-906.
29. Ventura, A., D.G. Kirsch, M.E. McLaughlin, D.A. Tuveson, J. Grimm, L. Lintault, J. Newman, E.E. Reczek, R. Weissleder, and T. Jacks, *Restoration of p53 function leads to tumour regression in vivo.* Nature, 2007. **445**(7128): p. 661-5.

30. Maj, J.G., F. Paris, A. Haimovitz-Friedman, E. Venkatraman, R. Kolesnick, and Z. Fuks, *Microvascular function regulates intestinal crypt response to radiation.* Cancer Res, 2003. **63**(15): p. 4338-41.
31. Ch'ang, H.J., J.G. Maj, F. Paris, H.R. Xing, J. Zhang, J.P. Truman, C. Cardon-Cardo, A. Haimovitz-Friedman, R. Kolesnick, and Z. Fuks, *ATM regulates target switching to escalating doses of radiation in the intestines.* Nat Med, 2005. **11**(5): p. 484-90.
32. Hendry, J.H., C. Booth, and C.S. Potten, *Endothelial cells and radiation gastrointestinal syndrome.* Science, 2001. **294**(5546): p. 1411.
33. Suit, H.D. and H.R. Withers, *Endothelial cells and radiation gastrointestinal syndrome.* Science, 2001. **294**(5546): p. 1411.
34. Withers, H.R., A.M. Chu, K.A. Mason, B.O. Reid, H.T. Barkley, Jr., and J.B. Smathers, *Response of jejunal mucosa to fractionated doses of neutrons or gamma-rays.* Eur J Cancer, 1974. **10**(4): p. 249-52.
35. Withers, H.R. and M.M. Elkind, *Radiosensitivity and fractionation response of crypt cells of mouse jejunum.* Radiat Res, 1969. **38**(3): p. 598-613.
36. Withers, H.R. and M.M. Elkind, *Dose-survival characteristics of epithelial cells of mouse intestinal mucosa.* Radiology, 1968. **91**(5): p. 998-1000.
37. Potten, C.S., J.A. O'Shea, C.L. Farrell, K. Rex, and C. Booth, *The effects of repeated doses of keratinocyte growth factor on cell proliferation in the cellular hierarchy of the crypts of the murine small intestine.* Cell Growth Differ, 2001. **12**(5): p. 265-75.
38. Khan, W.B., C. Shui, S. Ning, and S.J. Knox, *Enhancement of murine intestinal stem cell survival after irradiation by keratinocyte growth factor.* Radiat Res, 1997. **148**(3): p. 248-53.
39. Okunieff, P., M. Mester, J. Wang, T. Maddox, X. Gong, D. Tang, M. Coffee, and I. Ding, *In vivo radioprotective effects of angiogenic growth factors on the small bowel of C3H mice.* Radiat Res, 1998. **150**(2): p. 204-11.
40. Neta, R. and J.J. Oppenheim, *Radioprotection with cytokines--learning from nature to cope with radiation damage.* Cancer Cells, 1991. **3**(10): p. 391-6.
41. Potten, C.S., *Interleukin-11 protects the clonogenic stem cells in murine small-intestinal crypts from impairment of their reproductive capacity by radiation.* Int J Cancer, 1995. **62**(3): p. 356-61.
42. Booth, D., J.D. Haley, A.M. Bruskin, and C.S. Potten, *Transforming growth factor-B3 protects murine small intestinal crypt stem cells and animal survival after irradiation, possibly by reducing stem-cell cycling.* Int J Cancer, 2000. **86**(1): p. 53-9.
43. Houchen, C.W., R.J. George, M.A. Sturmoski, and S.M. Cohn, *FGF-2 enhances intestinal stem cell survival and its expression is induced after radiation injury.* Am J Physiol, 1999. **276**(1 Pt 1): p. G249-58.
44. Potten, C.S., D. Booth, and J.D. Haley, *Pretreatment with transforming growth factor beta-3 protects small intestinal stem cells against radiation damage in vivo.* Br J Cancer, 1997. **75**(10): p. 1454-9.
45. Farrell, C.L., J.V. Bready, K.L. Rex, J.N. Chen, C.R. DiPalma, K.L. Whitcomb, S. Yin, D.C. Hill, B. Wiemann, C.O. Starnes, A.M. Havill, Z.N.

Lu, S.L. Aukerman, G.F. Pierce, A. Thomason, C.S. Potten, T.R. Ulich, and D.L. Lacey, *Keratinocyte growth factor protects mice from chemotherapy and radiation-induced gastrointestinal injury and mortality.* Cancer Res, 1998. **58**(5): p. 933-9.

46. Potten, C.S., *Radiation, the ideal cytotoxic agent for studying the cell biology of tissues such as the small intestine.* Radiat Res, 2004. **161**(2): p. 123-36.
47. Mason, K.A., H.R. Withers, W.H. McBride, C.A. Davis, and J.B. Smathers, *Comparison of the gastrointestinal syndrome after total-body or total-abdominal irradiation.* Radiat Res, 1989. **117**(3): p. 480-8.
48. Potten, C.S., *Stem cells in gastrointestinal epithelium: numbers, characteristics and death.* Philos Trans R Soc Lond B Biol Sci, 1998. **353**(1370): p. 821-30.
49. Roberts, S.A., J.H. Hendry, and C.S. Potten, *Intestinal crypt clonogens: a new interpretation of radiation survival curve shape and clonogenic cell number.* Cell Prolif, 2003. **36**(4): p. 215-31.
50. Withers, H.R., J.T. Brennan, and M.M. Elkind, *The response of stem cells of intestinal mucosa to irradiation with 14 MeV neutrons.* Br J Radiol, 1970. **43**(515): p. 796-801.
51. Withers, H.R. and M.M. Elkind, *Microcolony survival assay for cells of mouse intestinal mucosa exposed to radiation.* Int J Radiat Biol Relat Stud Phys Chem Med, 1970. **17**(3): p. 261-7.
52. Winton, D.J., M.A. Blount, and B.A. Ponder, *A clonal marker induced by mutation in mouse intestinal epithelium.* Nature, 1988. **333**(6172): p. 463-6.
53. Winton, D.J. and B.A. Ponder, *Stem-cell organization in mouse small intestine.* Proc Biol Sci, 1990. **241**(1300): p. 13-8.
54. Kaur, P. and C.S. Potten, *Cell migration velocities in the crypts of the small intestine after cytotoxic insult are not dependent on mitotic activity.* Cell Tissue Kinet, 1986. **19**(6): p. 601-10.
55. Wong, M.H., J.R. Saam, T.S. Stappenbeck, C.H. Rexer, and J.I. Gordon, *Genetic mosaic analysis based on Cre recombinase and navigated laser capture microdissection.* Proc Natl Acad Sci U S A, 2000. **97**(23): p. 12601-6.
56. Qiu, J.M., S.A. Roberts, and C.S. Potten, *Cell migration in the small and large bowel shows a strong circadian rhythm.* Epithelial Cell Biol, 1994. **3**(4): p. 137-48.
57. Potten, C.S., C. Booth, and D.M. Pritchard, *The intestinal epithelial stem cell: the mucosal governor.* Int J Exp Pathol, 1997. **78**(4): p. 219-43.
58. Marshman, E., C. Booth, and C.S. Potten, *The intestinal epithelial stem cell.* Bioessays, 2002. **24**(1): p. 91-8.
59. Potten, C.S., G. Owen, and D. Booth, *Intestinal stem cells protect their genome by selective segregation of template DNA strands.* J Cell Sci, 2002. **115**(Pt 11): p. 2381-8.
60. Potten, C.S., C. Booth, G.L. Tudor, D. Booth, G. Brady, P. Hurley, G. Ashton, R. Clarke, S. Sakakibara, and H. Okano, *Identification of a*

putative intestinal stem cell and early lineage marker; musashi-1. Differentiation, 2003. **71**(1): p. 28-41.

61. Hendry, J.H., C.S. Potten, C. Chadwick, and M. Bianchi, *Cell death (apoptosis) in the mouse small intestine after low doses: effects of dose-rate, 14.7 MeV neutrons, and 600 MeV (maximum energy) neutrons.* Int J Radiat Biol Relat Stud Phys Chem Med, 1982. **42**(6): p. 611-20.
62. Merritt, A.J., T.D. Allen, C.S. Potten, and J.A. Hickman, *Apoptosis in small intestinal epithelial from p53-null mice: evidence for a delayed, p53-independent G2/M-associated cell death after gamma-irradiation.* Oncogene, 1997. **14**(23): p. 2759-66.
63. Schuller, B.W., P.J. Binns, K.J. Riley, L. Ma, M.F. Hawthorne, and J.A. Coderre, *Selective irradiation of the vascular endothelium has no effect on the survival of murine intestinal crypt stem cells.* Proc Natl Acad Sci U S A, 2006. **103**(10): p. 3787-92.
64. Potten, C.S., M. Rezvani, J.H. Hendry, J.V. Moore, and D. Major, *The correction of intestinal microcolony counts for variation in size.* Int J Radiat Biol Relat Stud Phys Chem Med, 1981. **40**(3): p. 321-6.
65. Schuller, B.W., A.B. Rogers, K.S. Cormier, K.J. Riley, P.J. Binns, R. Julius, M.F. Hawthorne, and J.A. Coderre, *No significant endothelial apoptosis in the radiation-induced gastrointestinal syndrome.* Int J Radiat Oncol Biol Phys, 2007. **68**(1): p. 205-10.
66. Cho, C.H., R.A. Kammerer, H.J. Lee, K. Yasunaga, K.T. Kim, H.H. Choi, W. Kim, S.H. Kim, S.K. Park, G.M. Lee, and G.Y. Koh, *Designed angiopoietin-1 variant, COMP-Ang1, protects against radiation-induced endothelial cell apoptosis.* Proc Natl Acad Sci U S A, 2004. **101**(15): p. 5553-8.

Chapter 2: Selective Irradiation of the Vascular Endothelium: Development of the ^{10}B Carrier.

2.1 Introduction

The tissue response to radiation exposure is a complicated sequence of events that involves many different cell types, i.e. vascular endothelium, epithelium, nerve cells, etc. It is desirable to analyze the response of each individual cell population to radiation exposure in order to elucidate the dynamic cell signaling processes that occur between the different cell types within the tissue architecture and then define the mechanism of radiation damage in the tissue of interest. Which cell types are involved? What is the initiating lesion? In what cell type does the lesion occur? These are the critical questions a radiation biologist hopes to answer, and, theoretically, the most direct way to answer these questions would be to selectively irradiate each cell type individually *in vivo* and then examine the tissue response to this selective cell damage. Conventional irradiation techniques do not allow for the selective irradiation of specific target cell populations within a complex organism, and thus it is difficult to reveal radiation damage mechanisms in various tissues.

Radiation damage in normal tissue is traditionally separated into 'early' (acute) and 'late' effects, where, for late effects, there may be a clinically 'silent' period before the damage manifests itself. Stem cell based, rapidly-renewing

tissues such as the small intestine, bone marrow and oral mucosa are classic examples of acutely responding tissues. It is generally accepted that damage to the regenerative stem cell populations is the initiating lesion leading to radiation effects in these tissues. Once the regenerative stem cell populations die due to radiation exposure, the loss of tissue structure and function is very quick to follow, usually within a few days or weeks after radiation exposure [1]. There is, however, a hypothesis that exists in the radiation biology community that claims that vascular damage, rather than direct stem cell damage, is the cause of acute radiation effects.

Late radiation effects typically occur in slowly proliferating tissues such as the lung, kidney, liver and CNS. Fibrosis, atrophy, vascular damage, neural damage and negative growth effects are the typical radiation-induced late effects, and they tend to develop months to years after radiation exposure [1]. Researchers now believe that vascular damage may be responsible for promoting the conditions required for late effects, namely chronic inflammation.

One of the more controversial topics in radiation biology today revolves around the mechanism of crypt stem cell death in the mouse small intestine. A recent report has suggested that apoptosis in the vascular endothelium is the initiating lesion in the eventual onset of the radiation-induced gastrointestinal (GI) syndrome [2]. The authors attempted to manipulate the microvasculature by creating a mouse lacking acid sphingomyelinase (*asmase -/-*), which is the enzyme responsible for initiating endothelial apoptosis through a ceramide pathway [3-8], and by administration of basic fibroblast growth factor (bFGF),

which was purported to selectively protect the vascular endothelium from radiation damage. They claimed that bFGF localizes to the lamina propria and not the epithelial cells, including the stem cells in the crypts [2]. However, it has already been shown that growth factors, including bFGF, are active outside of the vasculature and confer some radioprotective effect on the intestinal epithelium, either by stimulating stem cell proliferation, inhibiting cell-cycle progression or preventing radiation induced apoptosis [9-13]. Clearly, there is a need for improved irradiation modalities that will allow the selective irradiation of the vascular endothelium, which will ultimately allow a more direct and less complicated methodology to explore the role of vascular damage in the radiation-induced GI syndrome.

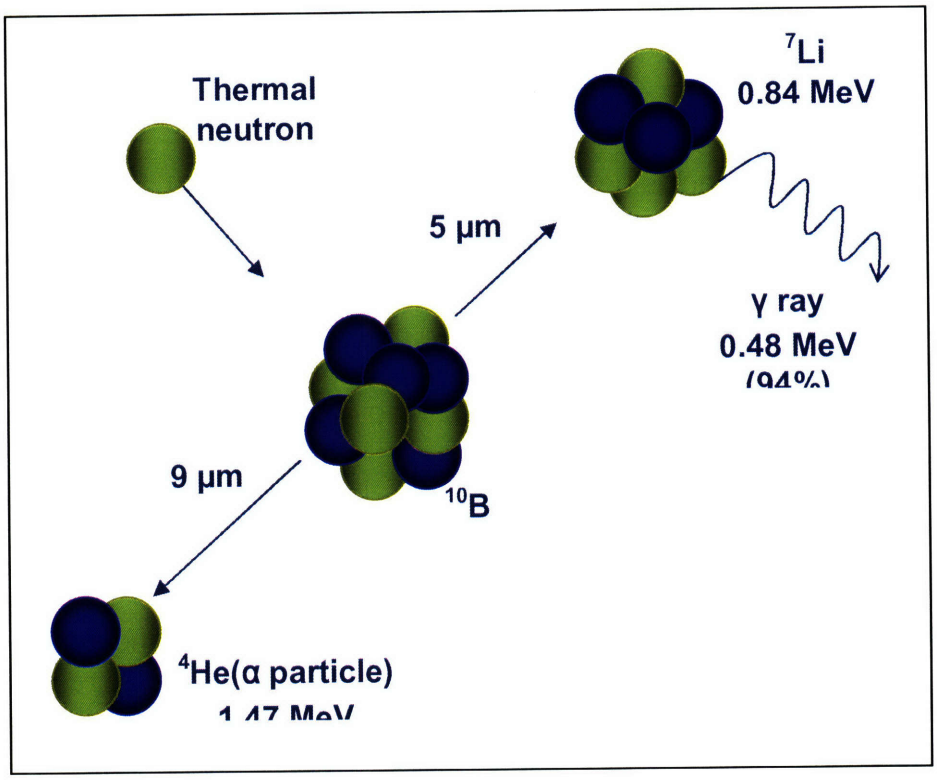

Figure 2-1. Schematic of the boron neutron capture reaction. ^{10}B will capture a thermal neutron and split into two densely ionizing α and ^{7}Li particles with energies of 0.84 and 1.47 MeV, respectively.

The boron-neutron capture (BNC) reaction (Figure 2-1) provides a unique tool for probing the mechanisms of radiation damage in both normal tissues and tumors. The stable minor isotope of boron, ^{10}B, exhibits a large thermal neutron capture cross section (3837 barns, 1 barn = 10^{-24} cm^2) and will readily capture thermal neutrons to form a metastable ^{11}B nucleus, which will rapidly split into two densely ionizing particles, α and ^{7}Li, with ranges in soft tissue of approximately 5 and 9 μm, respectively. If ^{10}B can be confined to the blood stream and coupled to external irradiation with thermal neutrons, the resultant BNC reactions will selectively elevate the dose to the vascular endothelium, as

the ranges of the BNC reaction products are roughly equivalent to the inner diameter of the smallest capillaries [14] (Figure 2-2). It would be impractical (and dangerous) to attempt this technique with a soluble radioisotope to achieve equivalent dose rates to what are attainable with the described BNC technique (more on this later in the chapter).

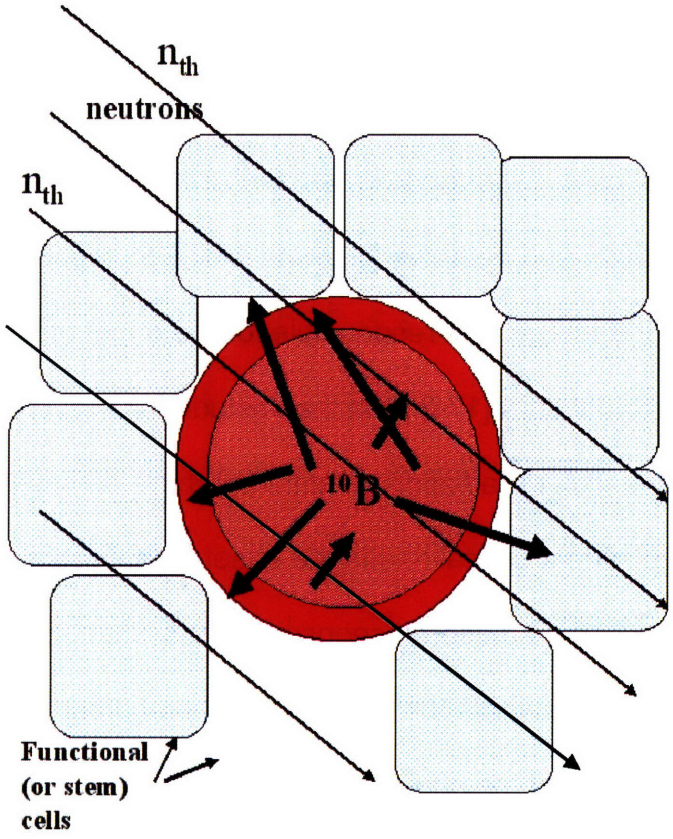

Figure 2-2. Schematic behind the selective vascular irradiation methodology. ^{10}B is confined to the blood stream (pink). The confined ^{10}B will capture the thermal neutrons delivered externally. The resultant BNC reactions will selectively elevate the dose to the vascular endothelium (red circle) while simultaneously keeping the surrounding functional cells (blue) at a lower dose.

The technique of selective vascular irradiation has been used in the central nervous system (CNS) using a ^{10}B containing compound, sulfhydryl boron hydride ($Na_2B_{12}H_{11}SH$, BSH), which does not cross the blood brain barrier. Thus, the problem of confining ^{10}B to the blood stream was solved without needing to engineer a new ^{10}B compound. The technique was used to test the hypothesis that radiation damage to the CNS vascular network initiates the late development of demyelination and white matter necrosis in CNS tissue. The exact mechanism of the late radiation damage onset in the CNS is not fully understood, but vascular endothelial cells, oligodendrocytes and astrocytes have been implicated in diffuse demyelination and necrosis following radiation exposure [15, 16]. It was shown that vascular damage was responsible for the onset of late (7 months) necrosis in the rat spinal cord [17-21]. In these studies, O-2A glial progenitor cells survived selective vascular irradiation conditions, which indicated that vascular radiation damage played a critical role in the onset of late radiation effects but had no effect on the early radiation response in that system. Similar studies were carried out in the rat brain where the loss of neural precursor cells was correlated with stem cell dose and not the added dose selectively delivered to the vasculature [22].

This same approach of selectively irradiating the vascular endothelium should, in theory, be possible outside of the CNS, but would not be possible using BSH. BSH has a molecular weight of only 350 daltons and has been shown in previous boron-neutron capture therapy (BNCT) studies (where this drug is primarily used) to uniformly equilibrate in non-CNS tissues [23]. In order

to develop a similar methodology for non-CNS tissues, a large ^{10}B containing compound must be used that is physically unable to diffuse out of the blood stream through the capillary pores. Macromolecules migrate out of the blood stream through the large-pore system of capillaries [24]. According to the pore theory of capillary permeability, capillaries should allow the transmigration of molecules of diameter up to ~500 Å [24-26]. It has also been estimated that the large-pore system occupies between 1-10% of the total pore surface area, which also includes a system of small-pores with diameter ~90 Å [24, 26]. Thus, the objective is to choose a boronated molecule that has a larger average diameter than the largest capillary pores.

Given the recent controversy surrounding the role of the vascular endothelial apoptosis in the onset of the radiation-induced GI syndrome, this tissue presented a good opportunity for a proof-of-principle study on the development of a new methodology where we could selectively irradiate the vascular endothelium in the mouse small intestine in a way similar to that already carried out in the CNS. However, this would entail the development of a new class of large boronated macromolecules. Chemists have already begun to develop very large boron containing compounds for use in BNCT. We thought it would then be fairly straight forward to adopt these boronated macromolecules for use in the technique we wished to develop. The search for a sufficiently large boronated molecule led us to the doctoral thesis work of Lars Gedda from Uppsala University (1997) in Sweden. There, he studied and developed novel ^{10}B containing compounds for use in BNCT. Specifically, he developed large

boronated dextran molecules, which he then conjugated to epidermal growth factor (EGF) to serve as a new BNCT agent against EGF receptor-rich tumors such as gliomas, squamous cell carcinomas and breast cancers [27]. We were able to reproduce the chemistry required to boronate dextran in large amounts, but unfortunately, this molecule proved toxic to our mice during biodistribution and crypt regeneration pilot studies. Large doses of dextran have been shown to cause immediate histamine release in rats, which may be the cause of the acute dextran toxicity [28-30]. Our search then led us to the BNCT compound development efforts from the laboratory of M. Frederick Hawthorne of the Department of Chemistry at UCLA (now at University of Missouri). There, he was developing a new class of boronated compounds, which were subsequently incorporated into liposomes [31, 32]. We were able to achieve very high ^{10}B concentrations in blood, with very low (undetectable) amounts in the surrounding normal tissues. There was also no detectable mouse toxicity associated with the boronated liposomes. These boronated liposomes now serve as the foundation of the selective vascular irradiation studies that form the core of this project.

This chapter will serve to describe, in detail, the selective vascular irradiation methodology from the development and characterization of a sufficiently large ^{10}B carrier through to its preliminary usage in mice. A careful consideration of the associated vascular dosimetry will be made. Data from the very first intestinal crypt regeneration and mouse survival studies using boronated dextran will be presented, along with evidence for the dextran toxicity in mice. Upon finishing the chapter, the reader should have a strong grasp of the

methodological details associated with the compound development, vascular dosimetry and the crypt regeneration and mouse survival assays.

2.2 Materials and Methods

2.2.1 Boronated dextran synthesis

A large ^{10}B enriched compound was developed for use in the selective vascular irradiation experiments. The initial compound is a type of cross-linked polysaccharide known as a dextran. Dextrans are high molecular weight polysaccharides consisting of D-glucose subunits linked primarily through 1,6 α-glycosidic bonds. The degree of cross-linking can be varied by the presence of 1,3 or 1,4 bonds. A dextran with a molecular weight of 77,000 daltons (Dextran 77, ~125 Å), to which 40-50 BSH molecules have been covalently attached, has been reported [27]. This dextran is similar in size to serum albumin (67,500 daltons), where one of its functions is the regulation of colloidal osmotic pressure of blood. In fact, solutions of dextrans in the 70,000-75,000 dalton range have been used as substitutes for blood plasma. The published procedure has been used (although slightly modified) to produce boronated dextran (^{10}B enriched) (Figure 2-3) in large quantity. The complete procedure is as follows:

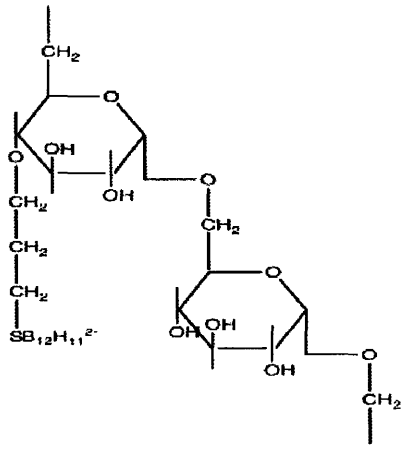

Figure 2-3. Final structure of boronated dextran after allylation at a hydroxyl group with subsequent addition of BSH to the terminal double bond [27].

Allylation of Dextran

1. Set a water bath to 40°C. Set a mineral-oil bath to 60°C with constant stirring to ensure proper thermal circulation. Allow the temperature to stabilize.
2. Weigh out 2 g of Dextran 77, place in a 50 ml vessel and add 10 ml of 40°C water. Leave in the 40°C water bath.
3. Weigh out 0.5 g of NaOH (sodium hydroxide) in a 10 ml tube and add 5 ml of 40°C water. Leave in the 40°C water bath.
4. Weigh out 20 mg of $NaBH_4$ (sodium borohydride) and keep in the weighing boat/paper.
5. Add the NaOH solution and $NaBH_4$ to a reaction flask (50 ml, tear-drop or round-bottom), washing the $NaBH_4$ off the boat.

6. Add the dextran solution to the reaction flask.
7. Add 2.5 ml of allyl bromide.
8. Add a stir bar, immerse the reaction flask in the 60°C mineral-oil bath and stir for 3 hrs.
9. When finished, pour solution into weighed beaker/flask and add 150 ml of cold isopropanol. White precipitate will form (this is the allyl-dextran).
10. Leave in the refrigerator overnight.
11. Decant off the isopropanol.
12. Dissolve the precipitate in small amount (~ 5 ml) of warm water.
13. Add another 150 ml of cold isopropanol and leave in the refrigerator overnight.
14. Decant off the isopropanol, and dissolve the precipitate again in a small amount of warm water.
15. Add another 150 ml of cold isopropanol and leave in the refrigerator overnight.
16. Lyophilize in weighed tube and store at -70°C.
17. Weigh the tube to determine the amount of allyl-dextran present.

Boronating the Allyl-dextran

1. Add together 20 mg of ^{10}B enriched sulhydryl boron hydride (BSH), 20 mg of $(NH_4)_2S_2O_8$ (ammonium persulfate) and 20 mg of the allylated dextran in 200 µl water.

2. Stir at 50°C for 2 hrs.

Purification (separation of boronated dextran from unbound BSH)

1. Use NAP-5 sephadex size-exclusion columns (Amersham Biosciences).
2. Add the 200 µl sample to the column. Allow the sample to fully enter the column before proceeding.
3. Add 300 µl of distilled water. Allow this to fully enter the column before proceeding.
4. Elute with 850 µl of distilled water and collect in a weighed container.
5. Lyophilize and store at -70°C.
6. Weigh the tube to determine the amount of boronated dextran present.

Proton nuclear magnetic resonance (p-NMR) spectra were obtained to verify the chemical structure of allyl-dextran. Since the addition of BSH to the terminal double bond of the allyl-group is a fairly straight forward chemical reaction, the positive identification of allyl-dextran was assumed to ultimately indicate that the final product will be boronated dextran (Figure 2-4). These spectra were obtained and analyzed at the Department of Chemistry's Instrumentation Facility (DCIF) with the assistance of Sejal Patel (Ph.D. (2004), Department of Chemistry, MIT). A saturated solution of allyl-dextran was made with NMR-grade heavy water (D_2O). Spectra were obtained using a 500 MHz system, and samples were spun to maintain magnetic field uniformity.

A. Dextran

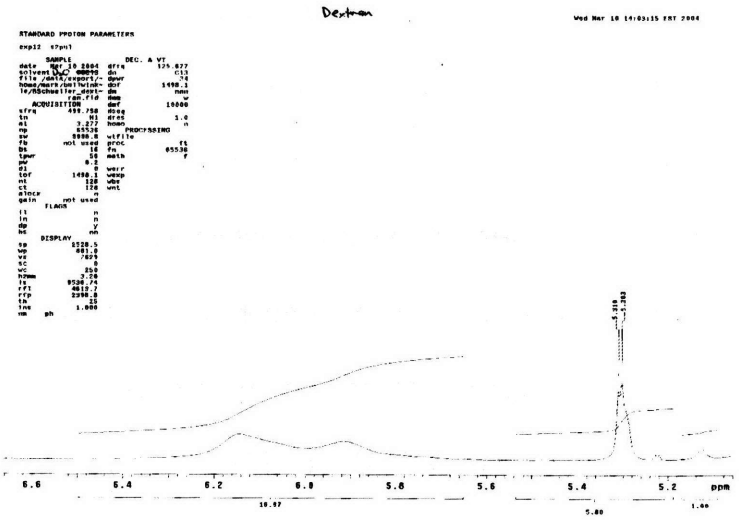

B. Allyl-Dextran

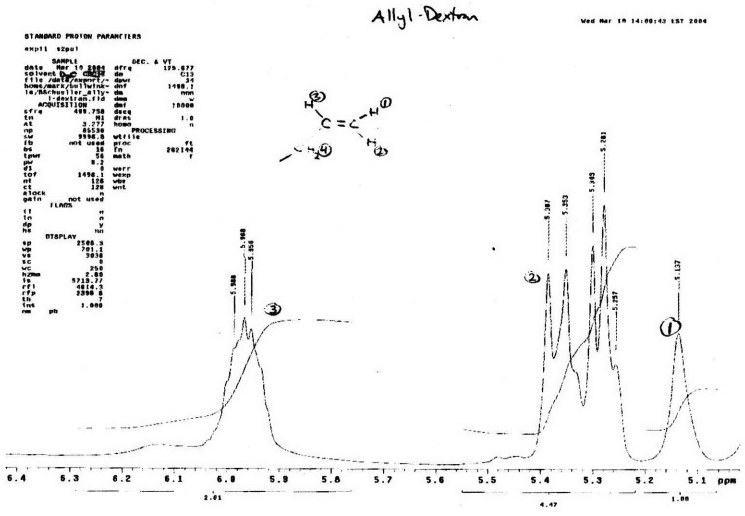

Figure 2-4. p-NMR spectra on dextran or allyl-dextran. (A) Dextran alone shows no signature in the allyl region. (B) Allyl-dextran exhibits the p-NMR allyl structure. The handwritten numbers correspond to the specific location of each proton in the group.

The solubility of the boronated dextran was high, which allowed the injection of sufficient amounts of ^{10}B for use in the selective vascular irradiation studies. Boronated dextran was solubilized in phosphate buffered saline to a final concentration between 20-80 mg boronated dextran/ml. Prompt gamma neutron activation analysis (PGNAA, described in the next section) of a 20 mg/ml boronated dextran solution indicated a ^{10}B concentration of 2000 µg ^{10}B/ml, which means the boronated dextran contained approximately 100 µg ^{10}B/mg. This number agrees nearly exactly with Gedda [27].

2.2.2 ^{10}B Quantification: Prompt Gamma Neutron Activation Analysis

Neutron activation analysis (NAA) is a technique that has been developed to determine the elemental composition of a material by measuring the decay products emanating from the material after irradiation with neutrons. Each elemental isotope has a characteristic decay signature. Therefore, the elemental composition of a material can be ascertained by measuring this unique decay signature. Prompt gamma neutron activation analysis (PGNAA) is a special case of NAA where characteristic gamma rays are instantaneously emitted from the sample following neutron activation and can thus be measured during the neutron irradiation process.

PGNAA has been utilized to quantitate the amount or concentration of ^{10}B in a material. As described earlier, ^{10}B will readily capture a thermal neutron and

spontaneously fission into two densely ionizing α and ^{7}Li particles. The ^{7}Li ion is emitted in an excited state and will undergo subsequent relaxation to emit a 478 keV photon in 94% of decay events. This photon can then be used as the characteristic decay signature for ^{10}B [33]. The Nuclear Reactor Laboratory at MIT operates a dedicated PGNAA facility on the 4DH3 thermal neutron port in the MIT reactor. This facility was built and optimized for ^{10}B quantification by Kent Riley [34, 35]. In his method, a collimated thermal neutron beam is directed at a sample containing an unknown quantity of ^{10}B. Gamma rays emitted following thermal neutron capture in hydrogen and ^{10}B and are detected by a liquid nitrogen-cooled high-purity germanium detector coupled to an appropriate spectrometer. The system is calibrated by plotting the ratio of ^{10}B to hydrogen counts (B/H ratio) as a function of known ^{10}B concentrations in liquid samples of National Institutes of Standards and Technology (NIST) certified boric acid (unenriched). Therefore, the ^{10}B concentration in an unknown sample can be easily calculated by measuring its B/H ratio. The practical detection limit of this system is roughly 1 μg ^{10}B/g in samples of only a few hundred milligrams.

2.2.3 Mouse*-Dextran biodistribution

Dextrans of varying molecular weight have been used to measure the permeability of the rat intestine [24, 36], where electron microscopy was used to

* All animal procedures were reviewed and approved by the Committee on Animal Care at the Massachusetts Institute of Technology and were conducted according to the principles outlined in the Guide for the Care and Use of Laboratory Animals prepared by National Institute of Laboratory Resources of the National Research Council.

visualize the location of individual dextran molecules after lead staining. Individual 75,000 dalton dextran molecules were observed to pass through fenestrae and channels of the endothelium and migrate to the pericapillary space and the basement membrane, but the vast majority (initial plasma concentration) remained in the blood vessel lumen. The 75,000 dalton dextran was still in the blood plasma at 24 hrs post-injection. This study indicated that the leakage of the boronated dextran out of the vessels into the perivascular space was negligible.

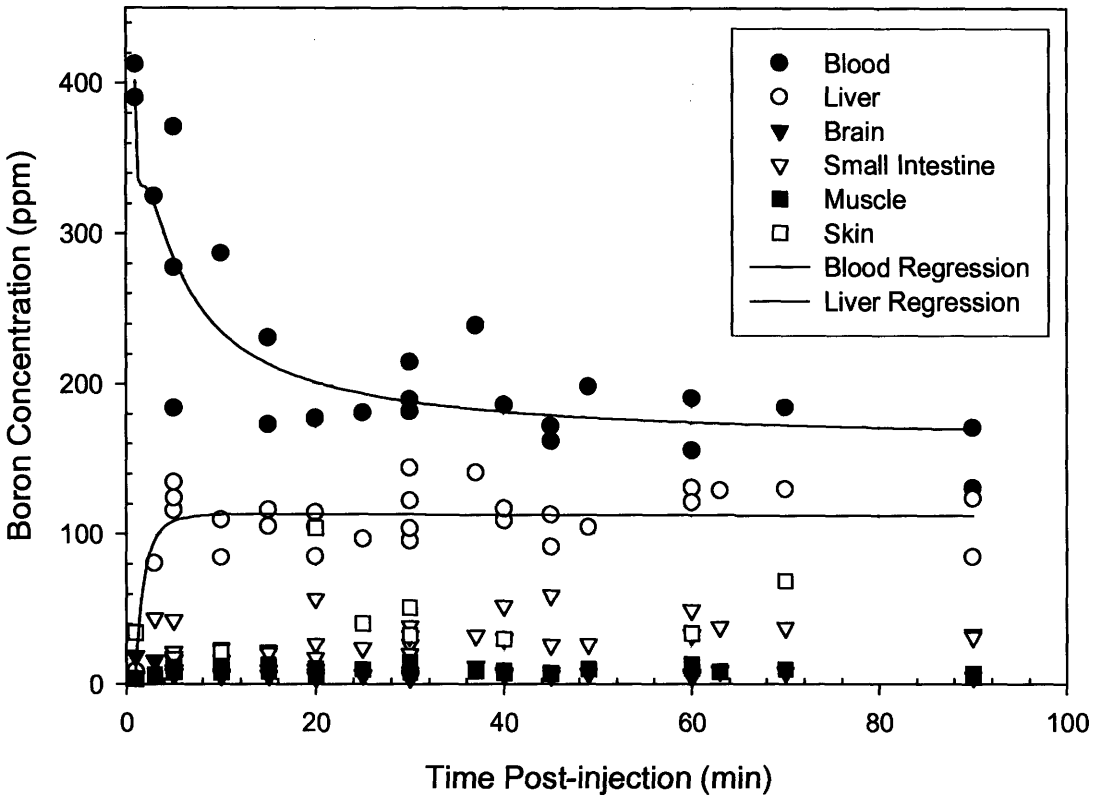

Figure 2-5. Mice (n=24) received 0.1 ml of a boronated dextran solution containing 8 mg ^{10}B/ml via the retro-orbital sinus and were sacrificed at time points out to 90 minutes post-injection. All of the individual values are shown.

Since the radiation dosimetry critically depends on the ^{10}B concentration in blood and tissue at the time of neutron irradiation, a mouse-dextran biodistribution study was carried out to determine the ^{10}B concentration in blood, small intestine, liver, brain, muscle and skin as a function of time-post injection in 8-12 week old female BALB/c mice. Mice were briefly anesthetized under isoflourane and injected with 0.1 ml of varying concentrations of boronated dextran *via* the retro-orbital sinus. Mice were then humanely killed at various time points post-injection, and various tissues were subsequently harvested for boron analysis by PGNAA. Figure 2-5 shows the results of the biodistribution study after a 0.1 ml injection of an 8 mg ^{10}B/ml boronated dextran solution.

Biodistribution studies in mice show a classic biphasic clearance pattern with half-lives of roughly 10 and 60 minutes, respectively. The overall objective was achieved with this compound in that very high blood-boron concentrations (>150 ppm) were measured with relatively low boron concentrations (~30 ppm) in the surrounding normal tissues. The data are completely consistent with the presumed intravascular localization of the compound. Boron concentrations in liver are considerably higher than the other normal tissues, which can be attributed to the relatively high blood content in that particular organ [37]. The liver also acts somewhat as a 'filter', which may also add to the high boron concentrations observed.

The initial biodistribution experiments showed very high blood-boron concentrations with long clearance half-lives, but the manner in which the mice responded to the dextran injections foreshadowed the eventual failure of the

compound as a boron delivery agent. Preliminary vascular dose calculations (the details of which will be covered later) indicated that in order to maximize the dose delivered to vascular endothelial cells relative to the surrounding parenchymal cells, a blood-boron concentration of >100 μg ^{10}B/g at the time of irradiation was desirable. Within the plateau region of the blood-boron clearance curve (Figure 2-5, >30 minutes), a 0.1 ml injection of the 8 mg ^{10}B/ml boronated dextran solution produced blood-boron concentrations in excess of 150 μg ^{10}B/ml. However, injection of boronated dextran at this concentration proved to be too toxic for the mice and would not be suitable for longer term experiments: 5/5 mice died within 24 hours. This small survival experiment was performed in response to obvious acute toxicities (shallow, rapid breathing, delay in coming out of anesthesia) during the biodistribution experiments. Subsequent injections of boronated dextran, diluted to 4 mg ^{10}B/ml, resulted in the deaths of 2/5 mice within 24 hours. The remaining survivors lost 20% of their body weight within a 3 day period. Even further dilution to 2 mg ^{10}B/ml yielded a better mouse response: all mice survived with minimal weight loss. At this dilution, a biodistribution study and PGNAA boron analysis showed 41.6 ± 11.3, 37.1 ± 6.2, 7.1 ± 2.7, 2.2 ± 0.5 and 3.9 ± 0.9 μg ^{10}B/g in blood, liver, small intestine, muscle and skin, respectively, at 30 min post-injection. The boron content in the brain was below the detection limit for the PGNAA system. These concentrations were sub-optimal, but were ultimately used for the subsequent intestinal crypt regeneration and mouse survival studies in order to avoid unwanted mouse deaths due to the dextran toxicities at higher concentrations. Due to logistical reasons associated

with the neutron irradiations along with the behavior of the blood-boron clearance curve, 30 minutes post-injection was chosen as the starting point for the irradiations.

2.2.4 Neutron irradiation, crypt regeneration and mouse survival

2.2.4.1 Neutron irradiation facilities

The fission converter neutron beam (FCB) irradiation facility at the MIT reactor is a state-of-the-art irradiation facility, which has been optimized for human irradiations during cancer treatment using boron neutron capture therapy (BNCT) [38-40]. A specific mouse irradiation geometry (described later) has been developed to allow uniform neutron penetration, which is optimal for these studies. Neutrons are delivered at epithermal energy (average energy 2 keV) to maximize beam penetration into tissue. The thermal neutron flux peaks inside the mouse after neutron thermalization (energy loss *via* collission) during passage through Lucite shielding material and mouse tissue. This results in a uniform dose distribution as a function of depth through the mouse body. Whole-body irradiations are possible, because the endpoints in the following studies are short compared to the onset of the bone marrow and gastrointestinal radiation syndromes. The facility is equipped with an automated dose monitoring and control system to precisely administer the desired dose.

2.2.4.2 Epithermal neutron beam dosimetry

Whole-body mouse irradiations were carried out in the epithermal neutron beam at the MIT reactor (MITR) as previously described [41]. Mice were irradiated in a Lucite holder designed to immobilize unanesthetized mice by all four feet such that the abdomens were presented to the 16-cm-diameter horizontal epithermal beam [41]. Unless specifically noted, all doses quoted are physical absorbed doses to which no weighting factors have been applied. Absorbed doses ranging from 3.2 ± 0.2 to 10.0 ± 0.7 Gy were administered with irradiations lasting from 6 to 20 min. The epithermal neutrons were thermalized by 1.5 cm of Lucite, consisting of the 0.5 cm thick mouse holder and an additional 1.0 cm sheet of Lucite placed between the holder and the beam aperture. The mouse bodies were centered at a depth of 2.5 cm. Photon and fast neutron absorbed dose rates were measured using paired ionization chambers with walls of graphite and tissue equivalent A-150 plastic. The absorbed dose from neutron capture in ^{10}B and nitrogen was determined using the measured difference in the activation of bare and Cd-covered gold foils and kerma coefficients of 8.66×10^{-8} and 7.88×10^{-12} Gy cm^2, respectively. A uniform nitrogen concentration of 3.5% by weight was applied for tissue and boron concentrations measured in the biodistribution studies were used to determine the absorbed doses in the blood and vessel wall [38].

The total absorbed dose rate in the epithermal neutron beam was 0.57 ± 0.04 Gy min^{-1} at a depth of 2.5 cm and was comprised of 77% low-linear energy

transfer (LET) photons and 23% high-LET radiations, which are principally protons arising from thermal neutron capture in nitrogen. The relative uncertainty on the neutron beam doses was 2.2%, which includes only the statistical uncertainty in the beam monitor counts and variations of approximately 1 mm in positioning of the irradiation jig along the center of the beam central axis. The additional absorbed dose rate from the ^{10}B capture reactions was 3.3 ± 0.18 cGy min^{-1} per μg ^{10}B present.

2.2.4.3 Selective vascular irradiation dosimetry

The boron neutron capture reactions in the boronated dextran groups occur, by design, only within the vessel lumen. This creates a non-uniform dose distribution in which the dose delivered to the vascular endothelium is less than the boron dose absorbed in the blood volume within the lumen. Rydin *et al.* quantified this effect of vessel geometry on the dose absorbed in an endothelial cell from boron neutron capture reactions restricted to the lumen of a blood-filled capillary relative to the boron dose absorbed in the blood [42]. According to this model, when ^{10}B is restricted to the lumen, the boron dose absorbed in the capillary wall is 1/3 of the boron dose absorbed in the blood, given a capillary wall thickness of 0.25 μm, which is considered representative for the mice used in this study. The total physical absorbed dose in the vascular endothelium is the sum of the external beam dose and the vascular-specific boron dose. The vascular-specific boron dose is calculated as:

$$D_V = (1/3)\ ((8.66 \times 10^{-12}\ \text{cGy cm}^2/\text{ppm})(\Phi)(^{10}\text{B [ppm]}))$$

$$\Phi = \text{Thermal neutron flux } [(\text{cm}^2\ \text{s})^{-1}]$$

The total absorbed dose rate in the vascular endothelial cells, with boronated dextran in the blood at the time of neutron irradiation, was estimated as the sum of the whole-body neutron beam absorbed dose rate plus 1/3* of the ^{10}B absorbed dose rate in the blood. The additional absorbed dose rate in the microvasculature coming from boron neutron capture reactions in the blood was 1.1 ± 0.06 cGy min^{-1} per μg ^{10}B, which includes the geometrical factor of 1/3 [42]. The higher ^{10}B concentration in the blood associated with the boronated dextran allowed the dose to the vascular endothelial cells to be increased, while holding all other parameters constant. Thus, the total absorbed dose rate in the microvasculature was 1.01 ± 0.05 Gy min^{-1} (a factor of 1.8 greater than the neutron beam dose) with a boron concentration of 42 ± 11 μg ^{10}B/g in the blood. The stated uncertainties on the microvascular absorbed dose rates include the uncertainty in the neutron beam dosimetry as well as the uncertainty in the blood-boron concentration at the time of irradiation. The calculated dose separation is shown in Figure 2-6.

* n.b. - This geometrical factor of 1/3 will range from 1/3-1/5 depending on variations in capillary size (diameter and wall thickness). Even if a factor of 1/5 is used in the vessel dose calculations, the resulting vessel doses are still high enough so as not to affect any of the conclusions presented in this thesis.

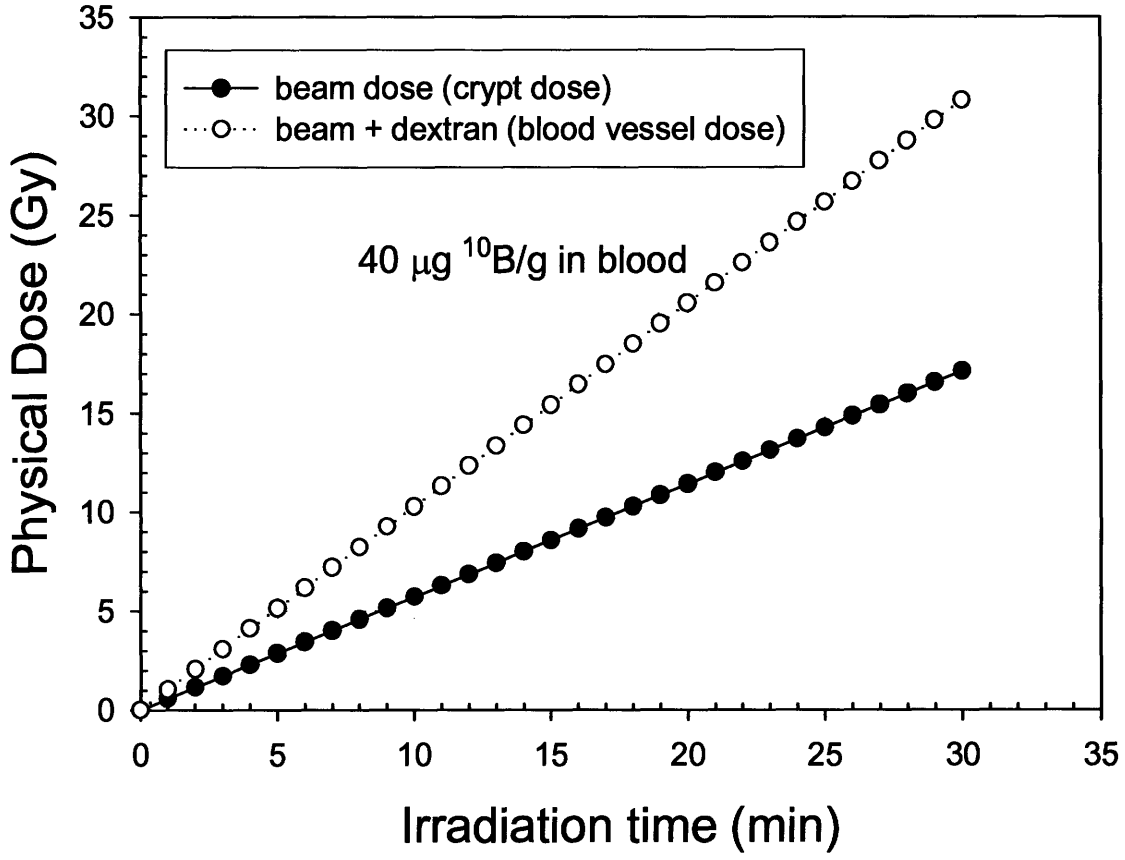

Figure 2-6. Calculated doses delivered to the crypts (neutron beam-only, closed circles) and the vascular endothelial cells (open circles). The line separation demonstrates the concomitant vascular dose associated with the external neutron beam dose with boronated dextran in the blood. The dose rate to the vasculature is 1.8 times the dose rate to the crypts.

2.2.4.4 Intestinal crypt regeneration assay

The intestinal crypt regeneration assay was used to measure the effect of radiation exposure on the survival of intestinal crypt stem cells. Mice were

irradiated with either the neutron beam alone, or after a 0.1 ml retro-orbital injection of a 2 mg ^{10}B/ml boronated dextran solution, to doses from 0-10 Gy. Mice were then sacrificed 84 ± 1 hrs (3.5 days) after irradiation by asphyxiation in a carbon dioxide atmosphere or inhalation overdose of isoflourane. The mouse abdomen was neatly dissected to fully expose the digestive tract. The small intestine was carefully removed so as not to damage the delicate tissue. A 5 cm section of the jejunum (middle 5 cm of the middle third of the small intestine measured from stomach to caecum) was ultimately harvested. The gut contents were carefully expressed, and the lumen was washed with a 10% formalin solution with the careful use of a syringe and needle. The segment of jejunum was then further cut into approximately ten 0.5 cm segments, immersed in 10% formalin fixative for 24-48 hours and processed for histology♦ by embedding the sections vertically in paraffin to generate circular cross sections when cut. Sections (3-6 μm thick) were taken from the paraffin tissue blocks. They were de-paraffinized and stained with hematoxilin & eosin (H&E) to reveal the tissue structure. Stained tissue slides were visualized under a visible light microscope using 100-400X magnification to clearly show the structure of regenerating crypts. The criteria used for scoring a regenerating crypt were 10 or more contiguous epithelial cells and at least one viable Paneth cell [43-45]. No size correction factor was applied as the average crypt size in all irradiation groups was the same [46]. All slides were scored by a single, blinded observer.

♦ Most paraffin embedding and tissue staining in this project was performed in the histology laboratory of MIT's Division of Comparative Medicine by Kathleen Cormier under the advisement of Prashant Nambiar, PhD (no longer at MIT) or Arlin Rogers, PhD (current DCM pathologist). Histology work was also carried out at an outside laboratory, MassHistology (Worcester, MA), as needed.

The numbers of regenerating crypts as a function of neutron beam dose are plotted in Figure 2-7. The neutron beam-only crypt regeneration data are in good agreement with the results of Gueulette et al. [47] in the same mouse (female BALB/c) using the same irradiation jig and geometry in the same epithermal neutron beam. The neutron beam plus boronated dextran line is shifted to the left relative to the neutron beam-only line. This implies that there was enhanced crypt death per unit neutron beam dose due to the presence of the boronated dextran in the blood. The additional dose selectively delivered to the vasculature thus resulted in enhanced crypt death. This strongly suggested that radiation damage in the vascular endothelial cells contributed to stem cell loss in the small intestine and the ultimate development of the radiation-induced GI syndrome.

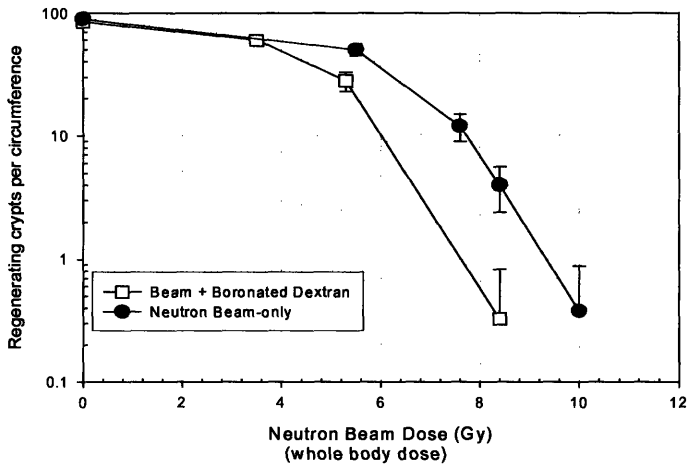

Figure 2-7. Crypt regeneration as a function of neutron beam dose for neutron beam-only or neutron + boronated dextran irradiations. The neutron beam + boronated dextran line is shifted to the left, which implies that vascular damage plays a role in the radiation-induced GI syndrome. Four mice per point, 4 intestinal cross-sections scored per mouse.

2.2.4.5 Mouse survival following whole-body neutron irradiation

A mouse survival endpoint was used to determine the mode of death following whole-body neutron beam irradiation either alone or in the presence of boronated dextran only in the blood (0.1 ml retro-orbital injection of a 2 mg ^{10}B/ml boronated dextran solution). The objective of this study was to bring the neutron beam dose right up to the transition from a bone marrow to a GI syndrome induced death and then selectively add dose to the vasculature to see if the mode of death changed from the bone marrow syndrome to the GI syndrome. In mice, the GI syndrome will occur within 4-5 days following large doses (>13 Gy photons), whereas the bone marrow syndrome will occur within 7-14 days following lower radiation doses. If the transition were to occur, it could be concluded that vascular damage plays a critical role in the radiation-induced GI syndrome.

Groups of 11-13 female BALB/c mice received whole-body neutron beam doses of 8.3 Gy in the presence or absence of boronated dextran in the blood. Mice were allowed to live beyond the usual 3.5 day endpoint for the crypt regeneration assay to allow the various radiation syndromes time to develop. Mice were monitored daily for overall health and were sacrificed upon entering a moribund state. One must be diligent in performing such experiments, as the mouse must be sacrificed right before it dies to both obtain a valid data point and avoid any undo pain and suffering for the animal. A plot of percent survival versus number of days post-irradiation is shown in Figure 2-8. It is clear that the

group that received neutron irradiation with boronated dextran in the blood, overall, died sooner than the group irradiated with the neutron beam alone.

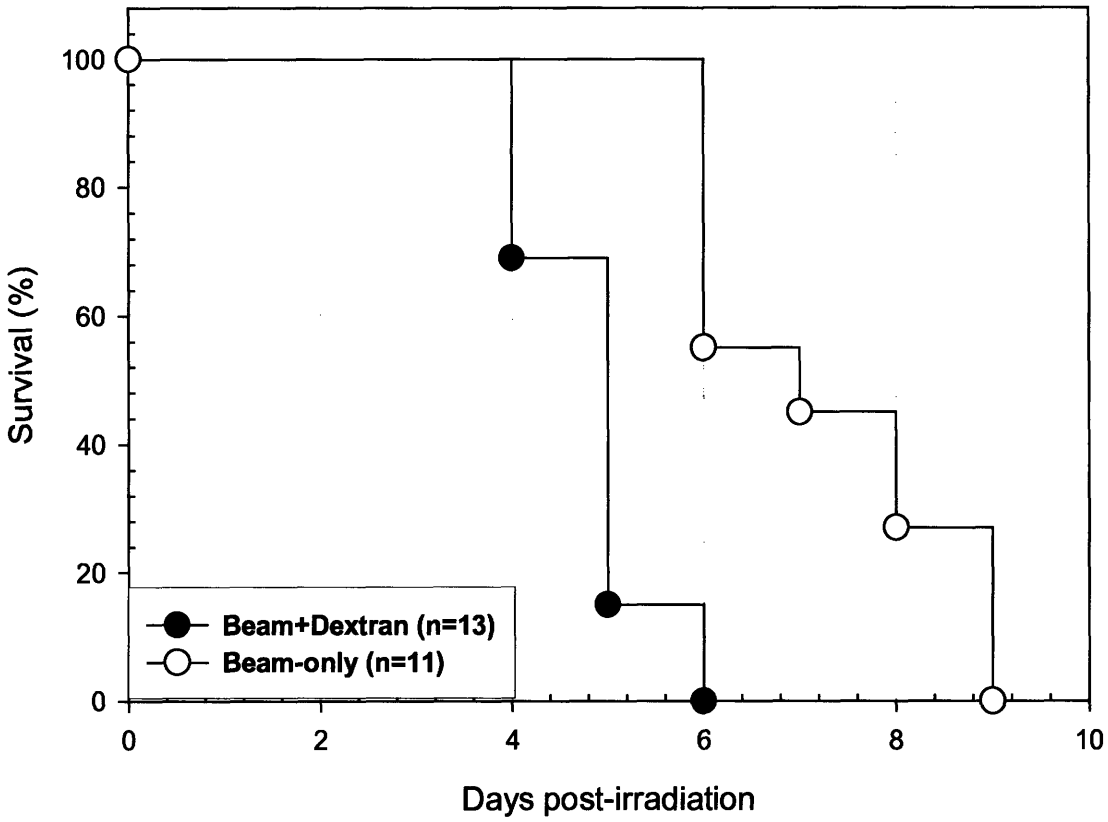

Figure 2-8. Mouse survival after whole-body neutron beam irradiation (8.3 Gy) in the presence or absence of boronated dextran in the blood.

Time of death is often times insufficient to determine the exact cause of death. We know from classical radiation biology experiments that the time of death due to the GI syndrome can be affected by the intrinsic radio-sensitivity of the hematopoietic bone marrow cells [48]. Mason *et al.* showed that intestinal stem cell survival was the same in mice that received either whole-body

irradiation or just abdominal irradiation. However, the LD_{50} (lethal dose in 50% of the population) shifted from ~20 Gy to ~16 Gy when the irradiation conditions were changed from total abdominal to whole-body irradiation conditions. Thus, the LD_{50} was shifted by ~ 4 Gy, which can be attributed to the influence of bone marrow sensitivity on time of death. Therefore, animal survival after large radiation doses is not solely related to intestinal stem cell survival but, rather, depends on the combined influence of both intestinal and hematopoietic stem cell sensitivities [48].

Femur and small intestine samples were harvested from the mice at the point of sacrifice and were subsequently prepared for histology. Femurs were decalcified in a formic acid and 10% formalin solution for 12-24 hrs, after which they were immediately transferred to a 10% formalin fixation solution. Femurs were then embedded in paraffin in a horizontal fashion to reveal the bone marrow when cut. Longitudinal sections (3-6 μm think) were taken from the paraffin tissue blocks and stained with H&E to reveal the bone and bone marrow structure. Small intestine samples were harvested and prepared in an identical manner to what has already been described in Section 2.2.4.4. Histological images from the described survival experiments are shown in Figure 2-9.

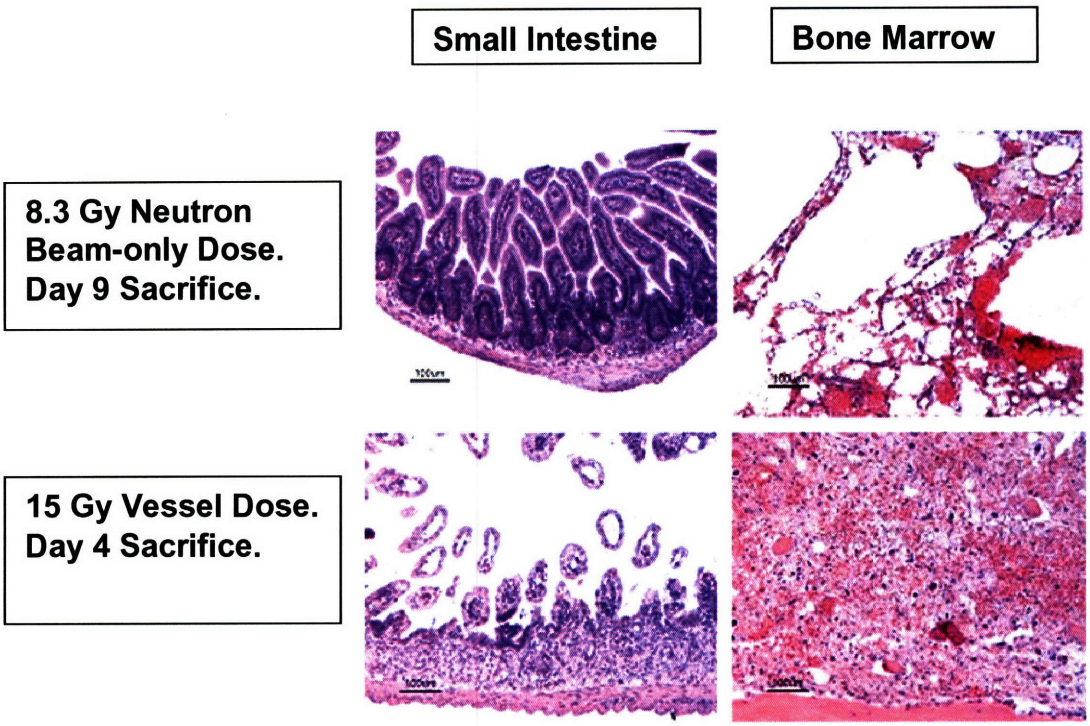

Figure 2-9. Representative H&E stained small intestine and bone marrow sections from mice that received epithermal neutron beam irradiation in the presence or absence of boronated dextran in the blood. The top row of images was taken from a mouse sacrificed 9 days after neutron irradiation. The bottom row of images was taken from a mouse sacrificed 4 days after a neutron beam dose of 8.3 Gy with boronated dextran in the blood (blood vessel dose = 15 Gy). Scale bars = 100 μm.

Figure 2-9 clearly shows the mode of death for animals subjected to each irradiation condition (neutron beam-only or neutrons + boronated dextran in the blood) in the animal survival experiments. It was determined from these experiments that the transition point for death from the bone marrow syndrome to the GI syndrome occurs between 8.3 – 9.0 Gy (neutron beam-only dose; see Figure 3-4). Therefore, the images in the top row of Figure 2-9 show a mouse that was given a dose very close to this transition point. It is clear from the

histology that this mouse died from the radiation-induced bone-marrow syndrome, as the gut was well on the way to recovery while the bone marrow was severely depleted and showed extensive necrosis of the matrix with widespread hemorrhaging. In contrast, the images in the bottom row of Figure 2-9 are from a mouse uniformly irradiated to the same dose as the mouse in the top row (8.3 Gy) but with a substantially higher dose delivered to the microvasculature from the boronated dextran restricted to the blood stream. This mouse obviously died of the GI syndrome. One can see that the familiar crypt-villus structure of the small intestine was completely destroyed. As a result, this mouse could no longer absorb nutrients from the intestinal lumen and probably died from a bacterial infection due to the invading gut microflora. Even though the bone marrow from this mouse was also severely depleted, this mouse ultimately succumbed to the GI syndrome, as a GI syndrome induced death will occur more rapidly than a bone marrow syndrome induced death. Therefore, it seemed evident at the time that radiation damage in the vascular endothelium was playing a critical role in the development of the radiation-induced GI syndrome, because the added dose selectively delivered to the vascular endothelium from the boronated dextran was able to cause a transition in the mode of death from the bone marrow syndrome to the GI syndrome.

2.2.4.6 Selective vascular irradiation dosimetry revisited

One potential concern that arose during the course of developing the selective vascular irradiation methodology was the potential for direct crypt irradiation from α-particles coming from the blood vessels adjacent to the crypts. The 9 μm range of the alpha particle released from the boron neutron capture reaction is sufficient to reach and kill crypt stem cells if the blood vessel is within 9 μm of a crypt. It was believed at the time that, if this were to occur, the added crypt dose due to direct α-particle irradiation would be negligible compared to the neutron beam dose and would not cause enhanced stem cell death. Nevertheless, more quantitative studies were needed to ensure that any observed physiological change was due to the dose to the vasculature and not the potential added dose from α-particles escaping from within blood vessels. Figure 2-10 shows staining for a vascular specific marker, CD31, used to visualize the complex network of blood vessels around crypts. CD31 plays an important role in tissue regeneration and is typically expressed on endothelial cells, platelets, lymphocytes and neutrophils among other cell types.

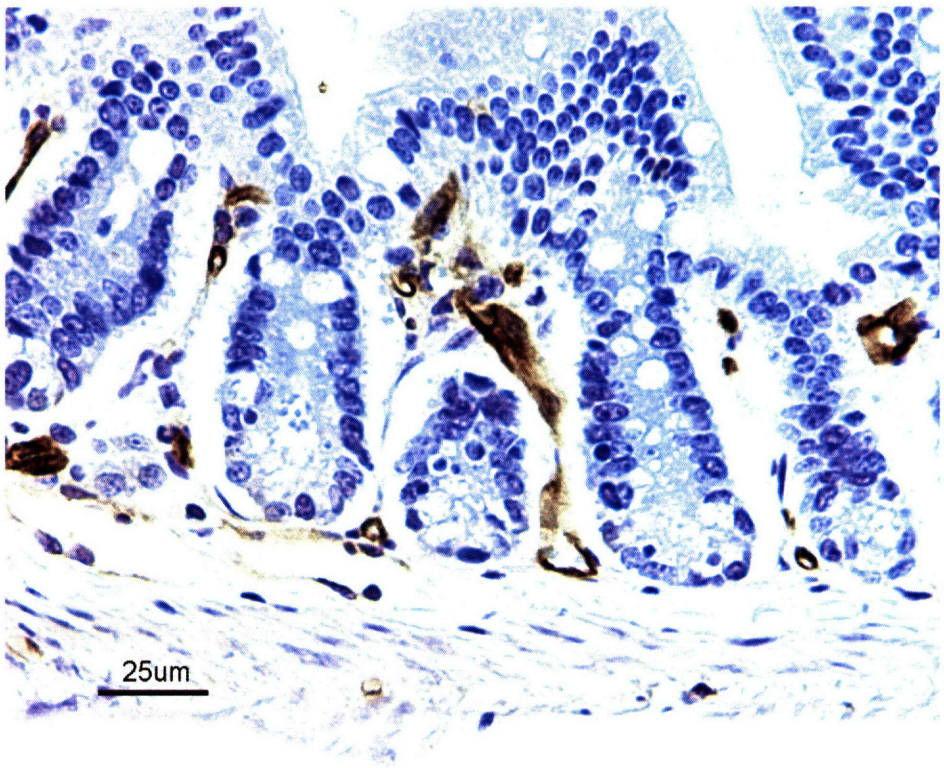

Figure 2-10. CD31 staining for blood vessels (brown) with a hematoxylin counterstain (blue). Scale bar = 25 μm.

Three qualitative arguments were initially made to show how any direct α-particle irradiation of crypts would have a negligible effect on the overall physiological response when compared to the neutron beam doses delivered during the selective vascular irradiation experiments. They are: 1) The spatial relationship between intestinal crypts and blood vessels in CD31 stained sections (cf. Figure 2-10) was measured. Of 515 crypts counted, 60% had a blood vessel within ~10 μm. 2) Particles emitted from boron neutron capture reactions in the blood will have an isotropic distribution in space. The available surface area (solid angle) for α-particle interaction on the crypt surface will be small. Thus, only a small percentage of those α-particles released beyond the lumen of the

blood vessel will contribute to the overall crypt dose. 3) The exact positions of the stem cells within a crypt are still unknown, although labeling studies indicate that cell positions 4-5 probably contain the regenerative stem cells [45]. It is also necessary to keep in mind that intestinal crypts are three dimensional structures. Crypts contain 16 cells assembled into an annulus at each position [49]. Thus, in order to completely inactivate a crypt's proliferative capacity, all 48 cells at positions 4-6 must be killed. Since there will only be a few crypt cells within 9 μm of a blood vessel, the probability of killing all of the cells in the annulus subtended by postitions 4-6 is very low. These arguments were supplemented by more quantitative considerations through actual modeling and simulation (Monte Carlo methods).

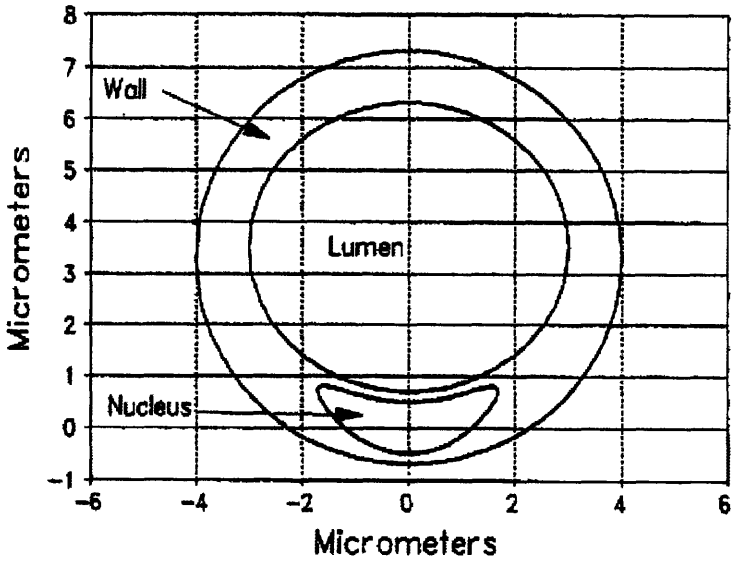

Figure 2-11. Input geometry for an endothelial cell used to calculate the α-particle dose gradient beyond the vessel lumen [53].

Extensive quantitative studies have already been performed to address the problem of vascular dose during BNCT or use of intravascular radiation sources [14, 50-54]. Specifically, various computational techniques were developed to quantify absorbed dose in endothelial cells during BNCT [52, 53]. A Monte Carlo based particle tracking program was developed by David E. Charlton *et al.* [52, 53] to quantify the dose to an endothelial cell nucleus for the various ^{10}B distributions typically seen in BNCT. This program was obtained from D. E. Charlton by personal request. Charlton's program proved useful, because the input parameters that defined the cell geometry could be manipulated to allow one to restrict ^{10}B to the vessel lumen and vary the capillary size, which would perfectly model the unique ^{10}B distribution and dosimetry problems in this project.

The program uses the standard Monte Carlo technique where the origins of ions produced by the boron neutron capture reactions are placed at random within an interaction volume, which in this case is the blood vessel lumen (Figure 2-11). As the source ions will be emitted isotropically, their angular directions can be determined using Monte Carlo methods [53]. To determine if an ion will traverse the endothelial cell nucleus, the simultaneous equations are solved for the ion track and nuclear surface, which are given by:

Ion Track: $(x-x_1)/\cos\alpha = (y-y_1)/\cos\beta = (z-z_1)/\cos\gamma$

(where x_1, y_1, z_1 are the coordinates for the ion's origin; α, β, γ are the directional angles; x, y, z are the track coordinates)

Nuclear Surface: $(x^2/a^2)+ [(y-(x^2/w^2))^2/b^2] + (z^2/c^2) = 1$

(where a,b,c are ellipsoidal radii, and w is an adjustable parameter to control the nuclear curvature)

To calculate the α-particle dose gradient as a function of distance from the edge of the blood vessel lumen, the input parameters used to define the geometry of the endothelial cell were adjusted such that the endothelial cell nucleus could be moved at defined intervals away from the vessel lumen and used as a dosimeter. By keeping the lumen dimensions constant, increasing the thickness of the capillary wall to 8μm, and moving the cell nucleus from the edge of the lumen to the outer wall in small increments, it became possible to use the absorbed dose to the nucleus as an indicator of the dose gradient as a function of distance from the vessel lumen. The simulation was run to mimic the highest neutron beam dose delivered in the selective vascular irradiation studies, which would serve as an upper limit for the α-particle dose gradient outside of the vessel lumen. The specific input data are shown in Table 2-1 below:

Table 2-1: Simulation Input Data

Nuclear radii (μm):	1.7, 0.5, 2.5
Radii of lumen (μm):	3.0, 2.8
Radius of capillary (μm)	11.0
Distance from nucleus to lumen:	variable
Distance from nucleus to outer wall:	variable
Distortion factor (w):	2.0
Number of cells per run:	60,000
Neutron fluence (n/cm^2):	5.7 x 10^{12}

Concentrations:	^{14}N (g/100g)	^{10}B (μg/g)
Lumen	2.9	40 or 110
Cytoplasm	1.7	0
Nucleus	1.7	0
External	1.7	0

Running the simulation was a fairly straight forward process. The specific steps taken in the running of these simulations are outlined in Table 2-2 below:

Table 2-2: Mechanics of the Simulations

- Keep the lumen dimensions constant.
- Keep [^{10}B] in lumen constant.
- Keep the neutron fluence constant.
- Keep the nuclear dimensions constant.
- Increase the capillary wall thickness to 8 μm
- Vary the nucleus-to-lumen distance (0.0, 0.2, 0.5, 1.0, 2.0, 3.0, 4.0, 5.0, 6.0, 7.0 μm).
- Run the simulation to calculate the absorbed dose in the nucleus as a function of distance from the vessel lumen.

The results of the dose gradient simulations are shown in Figure 2-12 below:

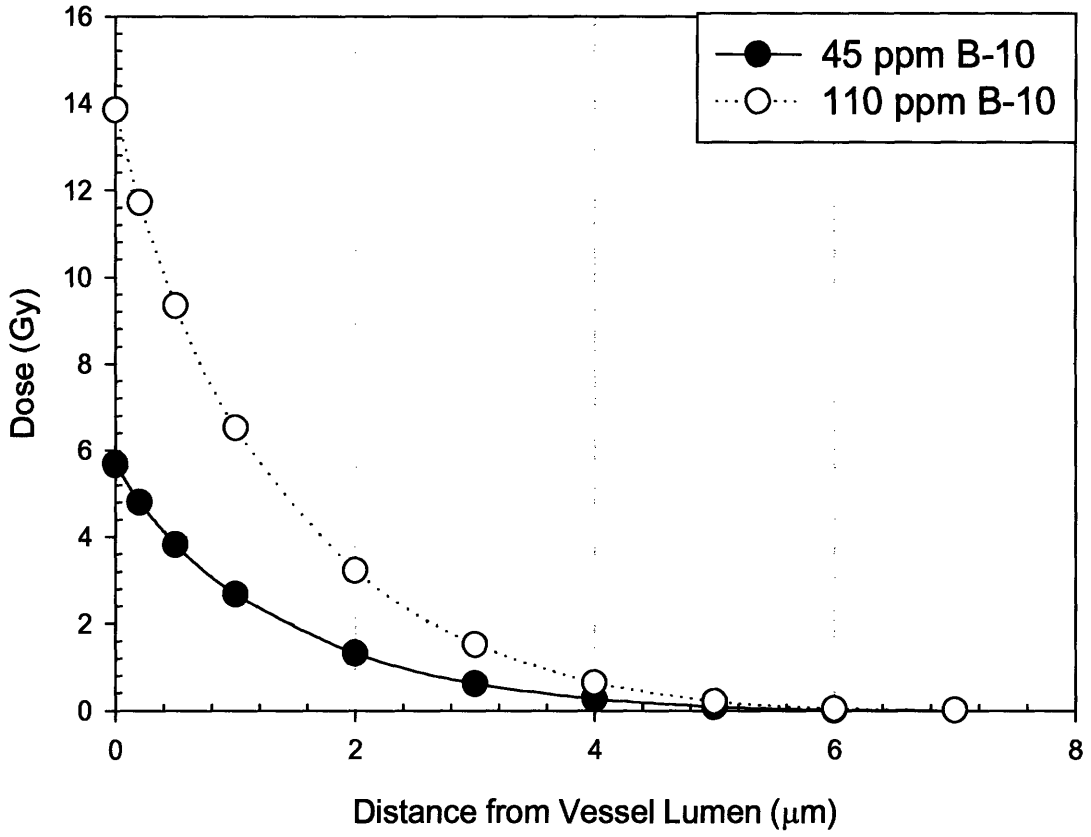

Figure 2-12. *α*-particle dose as a function of distance from the vessel lumen.

The dose gradient shown in Figure 2-12 shows a nearly $1/r^2$ behavior as the distance between the nucleus and vessel lumen was steadily increased. At a distance of just 2 μm from the vessel lumen, the dose was only 25% of the dose at the luminal wall, and at a distance of just 7 μm from the vessel lumen, the dose was nearly zero. Thus, these quantitative calculations coupled with the

qualitative arguments outlined above led to the ultimate conclusion that the α-particle dose contribution to the crypt stem cells was negligible, and that the probability of all cells in the proliferative annulus subtended by positions 4-6 receiving a lethal dose from particles originating within the vessel lumen was vanishingly small.

2.3 Discussion: failure of dextran, transition to liposomes

The ultimate objective of this period in the project was to find a ^{10}B delivery agent that could supply sufficiently large blood-boron concentrations (>100 ppm) at the time of neutron irradiation (30 min post-injection) without leaking from the vasculature or being overtly toxic. Boronated dextran could satisfy the requirement to deliver sufficiently large blood-boron concentrations, but it failed from the standpoint of its overt mouse toxicity and possible leakage due to this inherent toxicity (increased vascular permeability following anaphylaxis reactions). The 8 mg ^{10}B/ml injection solution of boronated dextran was able to supply blood-boron concentrations in excess of 150 ppm at 30 min post-injection, but the mice did not survive longer than 24 hrs. To cope with this undesired toxicity, the injection solution concentration had to be reduced to a point where the mice could tolerate it; this concentration was ultimately 2 mg ^{10}B/ml. Because of this compromise, the blood-boron concentration 30 min post-injection fell from >150 ppm to ~ 40 ppm. This low blood-boron concentration would not be sufficient to achieve the desired dose separation (ideally a factor of

3 greater than the neutron beam dose) between the whole-body epithermal neutron beam dose and the concomitant vascular dose. All of the data presented in this chapter were gathered using an injection solution concentration of 2 mg ^{10}B/ml. Although it seemed from the data gathered using boronated dextran that the vasculature played a role in intestinal crypt stem cell death and the eventual development of the radiation-induced GI syndrome, the overt dextran toxicity led us to question the validity of our data. What effect could dextran have on vascular permeability? Can we be sure that the dextran is not leaking? Are the observed effects in the crypt regeneration and animal survival assays due to damage to the vasculature or boronated dextran leakage out of the blood into the surrounding tissues? These questions could not readily be answered. At that point, the possible conclusions one could draw from the data were tenuous at best.

A search of the literature revealed that high concentrations of dextran administered to rats or isolated mast cells cause a massive histamine release, and in the case of the *in vivo* rat studies, high doses of dextran ultimately led to anaphylactic edema [28-30]. Edema is defined as the increased secretion of fluid into the tissue interstitium or impaired fluid removal causing tissue swelling. The rat experiments showed an increase in anaphylactic edema in the foot and skin following localized dextran injections in the respective tissues. The conclusions from these studies could explain the acute boronated dextran toxicity observed in the mice at the higher injection concentrations given systemically. The most pertinant study, however, was from Haraldsson *et al.* where they were able to

show that histamine release increases capillary permeability in a calcium-dependent manner [55]. A possible sequence of events leading to animal toxicity could be that the high systemic doses of dextran caused massive histamine release leading to increased capillary permeability and subsequent lethal anaphylactic edema. The lower dextran injection doses could potentially avoid lethal anaphylactic reactions but still maintain increased vascular permeability. Therefore, one could suspect that the observed effects in the crypt regeneration and mouse survival assays were the result of boronated dextran leakage from blood vessels and not the result of vascular damage. The added boron dose to the intestinal crypts from the leakage of boronated dextran out of the blood could cause both the enhanced crypt death seen in the crypt regeneration assay (Figure 2-7) and the transition from a bone marrow syndrome induced death to a GI syndrome induced death as seen in the mouse survival assay (Figures 2-8 & 2-9). Because of both the animal toxicity and possibility of boron leakage associated with the boronated dextran, a new, more reliable compound was needed that would allow us to escape most of these pressing questions.

When the validity of boronated dextran came into question, a collaboration was established with M.F. Hawthorne of the Department of Chemistry and Biochemistry at UCLA (now at University of Missouri), a leading authority on boron chemistry. The Hawthorne group has been developing novel ^{10}B containing compounds for use in BNCT for many years. They have developed a set of novel boron compounds that can be readily incorporated into liposomes [31, 32]. Figure 2-13 shows both of the new boron compounds that have been

developed as well as a schematic picture of a liposome. Liposomes with the *nido*-carborane anion species, $K^+[nido\text{-}7\text{-}CH_3(CH_2)_{15}\text{-}7,8\text{-}C_2B_9H_{11}]^{1-}$ (MAC),

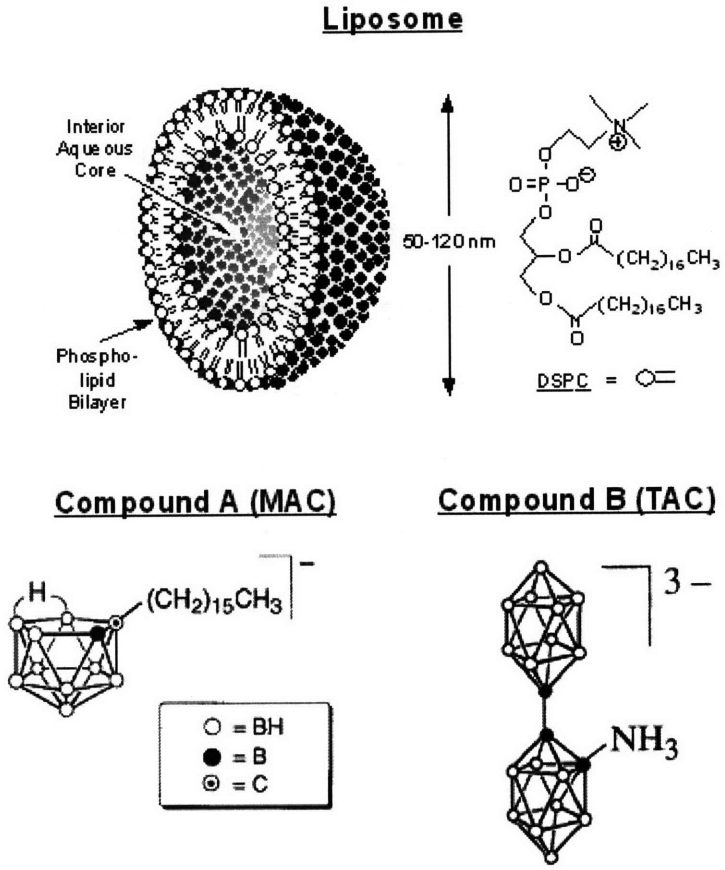

Figure 2-13. Liposomes have been prepared with the boronated compounds, MAC and TAC, incorporated into the lipid bilayer and aqueous core, respectively. DSPC = distearoylphosphatidylcholine.

embedded in the lipid bilayer have been prepared [32] as well as liposomes with the water-soluble polyhedral borane anion derivative $[B_{20}H_{17}NH_3]^{3-}$ (TAC)

dissolved in the aqueous core [31]. Liposomes with MAC in the lipid bilayer and TAC in the aqueous core have also been prepared [56].

Liposomes 69 nm in diameter with MAC incorporated into the lipid bilayer were prepared by the Hawthorne group and sent to the Coderre group. This was the first batch* of liposomes tested by the Coderre group. Boron analysis of the MAC liposome preparation using PGNAA yielded an initial ^{10}B concentration of 260 μg ^{10}B/ml. It was determined that the mice could endure a retro-orbital injection volume of 0.2 ml, which delivered an injected ^{10}B dose of 2.6 mg ^{10}B/kg body weight. For an initial MAC liposome biodistribution study, 10 female BALB/c mice were each injected with 0.2 ml of the liposome solution *via* the retro-orbital sinus and were then sacrificed 30 minutes post-injection for boron analysis using PGNAA. The blood-boron concentration at 30 minutes post-injection was 32.5 ± 3.5 μg ^{10}B/g (mean ± SD). This blood-boron concentration is consistent with complete intravascular localization of the MAC liposomes. Assuming the blood content in a mouse is ~7% of its body weight, the injected boron dose would result in a theoretical blood-boron concentration of ~ 35 μg ^{10}B/g. More proof of complete intravascular localization of the MAC liposomes came from the gross ^{10}B concentration in the small intestine. The boron concentration in the small intestine at 30 minutes post-injection was actually below the detection limit for the prompt gamma neutron activation analysis system. Fluorescently labeled (Rhodamine-DHPE) liposomes (MAC, unenriched) were also used to show complete vascular localization in tissue (Figure 2-14). The ^{10}B concentration in

* n.b. - Subsequent batches of boronated liposomes had slightly different average diameters and ^{10}B concentrations. Independent boron analyses and biodistribution studies were performed for each batch (e.g., Chapter 3 uses a different batch and presents different biodistribution data).

liver was ~ 8 μg ^{10}B/g, which was anticipated due to the high blood content of liver. There was no apparent mouse toxicity associated with any of the injections as judged by body weight and condition.

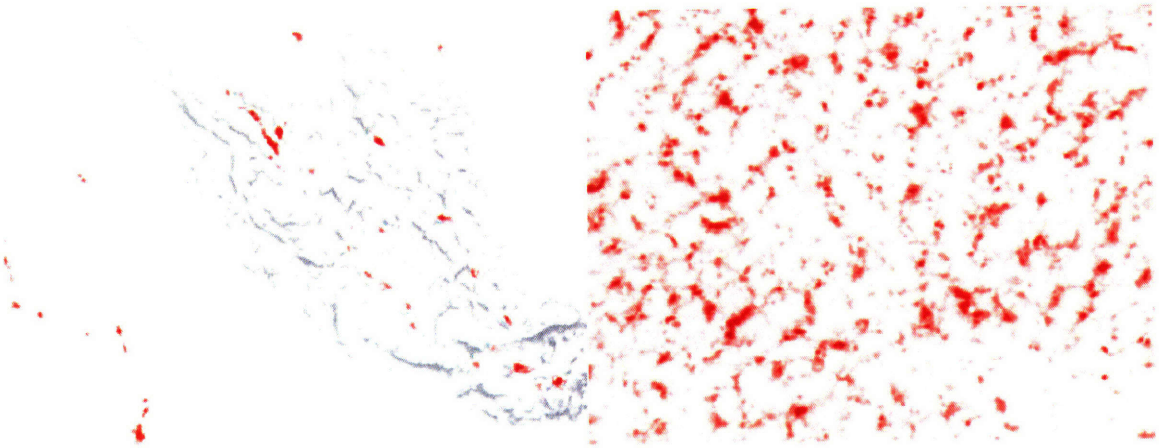

Figure 2-14. Visible light image (left) of an unstained frozen section (10 μm thick) of a mouse villus (grey) superimposed on a fluorescence image (red) of the same villus following a 0.2 ml retro-orbital injection of fluorescently labeled lipsomes. An adjacent fluorescent villus without visible light overlay is shown on the left side of the image. Fluorescence image (red) of the liver from the same mouse (right). Complete vascular localization of the liposomes is suggested in the small intestine (left, intense fluorescence in the region of high vascular density). Intense fluorescence in the liver is due to very high vascular density (right).

The initial biodistribution studies using the MAC liposome solution were intended to quickly ascertain whether there was any apparent boron leakage or acute mouse toxicity. However, the MAC liposome solution produced a relatively low blood-boron concentration (roughly the same as boronated dextran) and

would not be sufficient for further radio-biological studies. Thus, a liposome formulation with a much higher ^{10}B concentration was needed. Liposomes 75 nm in diameter with MAC in the lipid bilayer and TAC in the aqueous interior were prepared by the Hawthorne group and sent to the Coderre group. This liposome solution contained 1482 μg ^{10}B/ml as determined by PGNAA, and a 0.2 ml injection volume delivered an injected ^{10}B dose of 14.8 mg ^{10}B /kg body weight. Twenty four female BALB/c mice were injected with 0.2 ml of the MAC+TAC liposome solution *via* the retro-orbital sinus for biodistribution and animal toxicity studies. At 30 minutes post-injection the blood-boron concentration was 127 ± 25 μg ^{10}B/g (n=9). Between 60 and 90 minutes post-injection, the blood-boron concentration was 108 ± 14 μg ^{10}B/g (n=10). For all time-points the ^{10}B concentrations in small intestine and skin were below the PGNAA detection limit, which was indicative of complete intravascular localization of the liposomes. Boron concentrations in liver were ~ 80 μg ^{10}B/g. Finally, the 0.2 ml MAC+TAC injection volume produced no apparent toxic side effects as judged by body weight and condition over a 1 week period (n=5).

Very high blood-boron concentrations with no apparent mouse toxicities were thus achievable with the new MAC+TAC liposome formulations. Blood-boron concentrations of 127 ± 25 μg ^{10}B/g allowed the dose absorbed in the microvasculature to be increased by a factor of >3 relative to the concomitant neutron beam dose delivered to the rest of the body (crypt stem cells in particular). Thus, the epithermal neutron beam dose could be maintained well below the threshold for detectable crypt depletion of ~ 5-6 Gy, while also

simultaneously delivering a dose to endothelial cells well above this threshold. Thus, the objective of adequate dose separation between the neutron beam dose and the simultaneous dose to the vasculature was achieved with no detectable mouse toxicity using the liposome solutions. These liposome formulations served as the foundation of the radio-biological studies that form the core of this thesis, which will be described in detail in the following chapters.

References

1. Hall, E.J., Giaccia, A.J., *Radiobiology for Radiologist.* 6 ed. 2006: Lippincott Williams & Wilkins. 546.
2. Paris, F., Z. Fuks, A. Kang, P. Capodieci, G. Juan, D. Ehleiter, A. Haimovitz-Friedman, C. Cordon-Cardo, and R. Kolesnick, *Endothelial apoptosis as the primary lesion initiating intestinal radiation damage in mice.* Science, 2001. **293**(5528): p. 293-7.
3. Haimovitz-Friedman, A., C.C. Kan, D. Ehleiter, R.S. Persaud, M. McLoughlin, Z. Fuks, and R.N. Kolesnick, *Ionizing radiation acts on cellular membranes to generate ceramide and initiate apoptosis.* J Exp Med, 1994. **180**(2): p. 525-35.
4. Haimovitz-Friedman, A., R.N. Kolesnick, and Z. Fuks, *Ceramide signaling in apoptosis.* Br Med Bull, 1997. **53**(3): p. 539-53.
5. Kolesnick, R. and Z. Fuks, *Ceramide: a signal for apoptosis or mitogenesis?* J Exp Med, 1995. **181**(6): p. 1949-52.
6. Kolesnick, R.N. and M. Kronke, *Regulation of ceramide production and apoptosis.* Annu Rev Physiol, 1998. **60**: p. 643-65.
7. Kolesnick, R. and Y.A. Hannun, *Ceramide and apoptosis.* Trends Biochem Sci, 1999. **24**(6): p. 224-5; author reply 227.
8. Kolesnick, R. and Z. Fuks, *Radiation and ceramide-induced apoptosis.* Oncogene, 2003. **22**(37): p. 5897-906.
9. Potten, C.S., *Interleukin-11 protects the clonogenic stem cells in murine small-intestinal crypts from impairment of their reproductive capacity by radiation.* Int J Cancer, 1995. **62**(3): p. 356-61.
10. Potten, C.S., D. Booth, and J.D. Haley, *Pretreatment with transforming growth factor beta-3 protects small intestinal stem cells against radiation damage in vivo.* Br J Cancer, 1997. **75**(10): p. 1454-9.
11. Okunieff, P., M. Mester, J. Wang, T. Maddox, X. Gong, D. Tang, M. Coffee, and I. Ding, *In vivo radioprotective effects of angiogenic growth factors on the small bowel of C3H mice.* Radiat Res, 1998. **150**(2): p. 204-11.
12. Neta, R. and J.J. Oppenheim, *Radioprotection with cytokines--learning from nature to cope with radiation damage.* Cancer Cells, 1991. **3**(10): p. 391-6.
13. Khan, W.B., C. Shui, S. Ning, and S.J. Knox, *Enhancement of murine intestinal stem cell survival after irradiation by keratinocyte growth factor.* Radiat Res, 1997. **148**(3): p. 248-53.
14. Rydin, R.A., O.L. Deutsch, and B.W. Murray, *The effect of geometry on capillary wall dose for boron neutron capture therapy.* Phys Med Biol, 1976. **21**(1): p. 134-8.
15. Calvo, W., J.W. Hopewell, H.S. Reinhold, and T.K. Yeung, *Time- and dose-related changes in the white matter of the rat brain after single doses of X rays.* Br J Radiol, 1988. **61**(731): p. 1043-52.

16. Hopewell, J.W., *Late radiation damage to the central nervous system: a radiobiological interpretation.* Neuropathol Appl Neurobiol, 1979. **5**(5): p. 329-43.
17. Morris, G.M., J.A. Coderre, A. Bywaters, E. Whitehouse, and J.W. Hopewell, *Boron neutron capture irradiation of the rat spinal cord: histopathological evidence of a vascular-mediated pathogenesis.* Radiat Res, 1996. **146**(3): p. 313-20.
18. Morris, G.M., J.A. Coderre, J.W. Hopewell, P.L. Micca, and C. Fisher, *Boron neutron capture irradiation of the rat spinal cord: effects of variable doses of borocaptate sodium.* Radiother Oncol, 1996. **39**(3): p. 253-9.
19. Morris, G.M., J.A. Coderre, J.W. Hopewell, P.L. Micca, M.M. Nawrocky, H.B. Liu, and A. Bywaters, *Response of the central nervous system to boron neutron capture irradiation: evaluation using rat spinal cord model.* Radiother Oncol, 1994. **32**(3): p. 249-55.
20. Morris, G.M., J.A. Coderre, E.M. Whitehouse, P. Micca, and J.W. Hopewell, *Boron neutron capture therapy: a guide to the understanding of the pathogenesis of late radiation damage to the rat spinal cord.* Int J Radiat Oncol Biol Phys, 1994. **28**(5): p. 1107-12.
21. Coderre, J.A., G.M. Morris, P.L. Micca, J.W. Hopewell, I. Verhagen, B.J. Kleiboer, and A.J. van der Kogel, *Late effects of radiation on the central nervous system: role of vascular endothelial damage and glial stem cell survival.* Radiat Res, 2006. **166**(3): p. 495-503.
22. Otsuka, S., J.A. Coderre, P.L. Micca, G.M. Morris, J.W. Hopewell, R. Rola, and J.R. Fike, *Depletion of neural precursor cells after local brain irradiation is due to radiation dose to the parenchyma, not the vasculature.* Radiat Res, 2006. **165**(5): p. 582-91.
23. Kraft, S.L., P.R. Gavin, C.W. Leathers, C.E. DeHaan, W.F. Bauer, D.L. Miller, R.V. Dorn, 3rd, and M.L. Griebenow, *Biodistribution of boron in dogs with spontaneous intracranial tumors following borocaptate sodium administration.* Cancer Res, 1994. **54**(5): p. 1259-63.
24. Simionescu, N., M. Simionescu, and G.E. Palade, *Permeability of intestinal capillaries. Pathway followed by dextrans and glycogens.* J Cell Biol, 1972. **53**(2): p. 365-92.
25. Renkin, E.M., *Transport of Large Molecules across Capillary Walls.* Physiologist, 1964. **60**: p. 13-28.
26. Grotte, G., *Passage of dextran molecules across the blood-lymph barrier.* Acta Chir Scand Suppl, 1956. **211**: p. 1-84.
27. Gedda, L., P. Olsson, J. Ponten, and J. Carlsson, *Development and in vitro studies of epidermal growth factor-dextran conjugates for boron neutron capture therapy.* Bioconjug Chem, 1996. **7**(5): p. 584-91.
28. Hanahoe, T.H., *Effects of calcium on dextran anaphylactoid oedema in the rat.* Br J Pharmacol, 1972. **44**(2): p. 314-6.
29. Foreman, J.C. and J.L. Mongar, *Effect of calcium on dextran-induced histamine release from isolated mast cells.* Br J Pharmacol, 1972. **46**(4): p. 767-9.

30. Moodley, I., J.L. Mongar, and J.C. Foreman, *Histamine release induced by dextran: the nature of the dextran receptor.* Eur J Pharmacol, 1982. **83**(1-2): p. 69-81.
31. Feakes, D.A., K. Shelly, C.B. Knobler, and M.F. Hawthorne, *Na3[B20H17NH3]: synthesis and liposomal delivery to murine tumors.* Proc Natl Acad Sci U S A, 1994. **91**(8): p. 3029-33.
32. Feakes, D.A., K. Shelly, and M.F. Hawthorne, *Selective boron delivery to murine tumors by lipophilic species incorporated in the membranes of unilamellar liposomes.* Proc Natl Acad Sci U S A, 1995. **92**(5): p. 1367-70.
33. Fairchild, R.G., D. Gabel, B.H. Laster, D. Greenberg, W. Kiszenick, and P.L. Micca, *Microanalytical techniques for boron analysis using the 10B(n,alpha)7Li reaction.* Med Phys, 1986. **13**(1): p. 50-6.
34. Riley, K.J., *Improved boron 10 quantification via PGNAA and ICP-AES.* 1997. p. 230 p.
35. Riley, K.J., Harling, O.K., *An improved prompt gamma neutron activation analysis facility using a focused diffracted neutron beam.* Meth. Phys. Rev. B, 1998. **143**: p. 414-421.
36. Simionescu, N. and G.E. Palade, *Dextrans and glycogens as particulate tracers for studying capillary permeability.* J Cell Biol, 1971. **50**(3): p. 616-24.
37. Dellenback, R.J. and G.H. Muelheims, *Red blood cell volume and distribution before and after bleed-out in the rat.* Am J Physiol, 1960. **198**: p. 1177-80.
38. Riley, K.J., P.J. Binns, and O.K. Harling, *Performance characteristics of the MIT fission converter based epithermal neutron beam.* Phys Med Biol, 2003. **48**(7): p. 943-58.
39. Riley, K.J., P.J. Binns, and O.K. Harling, *A state-of-the-art epithermal neutron irradiation facility for neutron capture therapy.* Phys Med Biol, 2004. **49**(16): p. 3725-35.
40. Riley, K.J., P.J. Binns, S.J. Ali, and O.K. Harling, *The design, construction and performance of a variable collimator for epithermal neutron capture therapy beams.* Phys Med Biol, 2004. **49**(10): p. 2015-28.
41. Gueulette, J., P.J. Binns, B.M. Coster, X.Q. Lu, S.A. Roberts, and K.J. Riley, *RBE of the MIT Epithermal Neutron Beam for Crypt Cell Regeneration in Mice.* Radiat Res, 2005. **164**(6): p. 805-9.
42. Rydin, R.A., O.L. Deutsch, and B.W. Murray, *The effect of geometry on capillary wall dose for boron neutron capture therapy.* Phys. Med. Biol., 1976. **21**: p. 134 - 138.
43. Withers, H.R., J.T. Brennan, and M.M. Elkind, *The response of stem cells of intestinal mucosa to irradiation with 14 MeV neutrons.* Br J Radiol, 1970. **43**(515): p. 796-801.
44. Withers, H.R. and M.M. Elkind, *Microcolony survival assay for cells of mouse intestinal mucosa exposed to radiation.* Int J Radiat Biol Relat Stud Phys Chem Med, 1970. **17**(3): p. 261-7.

45. Potten, C.S., *Radiation, the ideal cytotoxic agent for studying the cell biology of tissues such as the small intestine.* Radiat Res, 2004. **161**(2): p. 123-36.
46. Potten, C.S., M. Rezvani, J.H. Hendry, J.V. Moore, and D. Major, *The correction of intestinal microcolony counts for variation in size.* Int J Radiat Biol Relat Stud Phys Chem Med, 1981. **40**(3): p. 321-6.
47. Gueulette, J., P.J. Binns, B.M. De Coster, X.Q. Lu, S.A. Roberts, and K.J. Riley, *RBE of the MIT epithermal neutron beam for crypt cell regeneration in mice.* Radiat Res, 2005. **164**(6): p. 805-9.
48. Mason, K.A., H.R. Withers, W.H. McBride, C.A. Davis, and J.B. Smathers, *Comparison of the gastrointestinal syndrome after total-body or total-abdominal irradiation.* Radiat Res, 1989. **117**(3): p. 480-8.
49. Marshman, E., C. Booth, and C.S. Potten, *The intestinal epithelial stem cell.* Bioessays, 2002. **24**(1): p. 91-8.
50. Akabani, G., J.W. Poston, Sr., and W.E. Bolch, *Estimates of beta absorbed fractions in small tissue volumes for selected radionuclides.* J Nucl Med, 1991. **32**(5): p. 835-9.
51. Akabani, G. and J.W. Poston, Sr., *Absorbed dose calculations to blood and blood vessels for internally deposited radionuclides.* J Nucl Med, 1991. **32**(5): p. 830-4.
52. Charlton, D.E., *Energy deposition in small ellipsoidal volumes by high-LET particles: application to thermal neutron dosimetry.* Int J Radiat Biol, 1991. **59**(3): p. 827-42.
53. Charlton, D.E. and B.J. Allen, *Monte Carlo calculations of ion passages through brain endothelial nuclei during boron neutron capture therapy.* Int J Radiat Biol, 1993. **64**(6): p. 739-47.
54. Kitao, K., *A method for calculating the absorbed dose near interface from 10B(n, alpha)7Li reaction.* Radiat Res, 1975. **61**(2): p. 304-15.
55. Haraldsson, B., U. Zackrisson, and B. Rippe, *Calcium dependence of histamine-induced increases in capillary permeability in isolated perfused rat hindquarters.* Acta Physiol Scand, 1986. **128**(2): p. 247-58.
56. Watson-Clark, R.A., M.L. Banquerigo, K. Shelly, M.F. Hawthorne, and E. Brahn, *Model studies directed toward the application of boron neutron capture therapy to rheumatoid arthritis: boron delivery by liposomes in rat collagen-induced arthritis.* Proc Natl Acad Sci U S A, 1998. **95**(5): p. 2531-4.

Chapter 3: Selective Irradiation of the Vascular Endothelium has no Effect on the Survival of Murine Intestinal Crypt Stem Cells*

3.1 Introduction

Radiation-induced changes seen in normal tissues are traditionally separated into early and late effects. Stem cell-based, rapidly-renewing normal tissues such as the bone marrow and the intestinal epithelium are early-responding tissues where the time courses of the radiation syndromes are directly related to the turnover time of the differentiated functional cell compartments. The intestinal stem cells reside in the crypts of Lieberkühn at the base of the finger-like villi that comprise the intestinal epithelium. Epithelial cells differentiate as they migrate up the crypt and the villus and are eventually sloughed off at the tip into the intestinal lumen: the transit time taking approximately 3-4 days. In the mouse small intestine, a wave of apoptosis is observed, in what are thought to be crypt stem cells [1], as early as 3-6 hrs after irradiation with doses as low as 0.01 Gy [2]. This effect saturates at about 1 Gy. Higher doses are postulated to deplete the first few generations of differentiated transit cells that still retain the ability to revert to fully-functional stem cells [2]. Individual crypts are not sterilized until all of the actual and potential stem cells

* Schuller, B.W., P.J. Binns, K.J. Riley, L. Ma, M.F. Hawthorne, and J.A. Coderre, *Selective irradiation of the vascular endothelium has no effect on the survival of murine intestinal crypt stem cells.* Proc Natl Acad Sci U S A, 2006. **103**(10): p. 3787-92.

are inactivated, which occurs at doses of about 8 Gy or higher. The crypt microcolony assay measures the survival of the last individual potential stem cells within each crypt [3]. This assay involves counting the number of regenerating crypt-like foci per intestinal circumference at 3-4 days post-irradiation. The survival of one or more clonogenic cells per crypt allows its regeneration. Doses above approximately 15 Gy sterilize virtually all of the crypt stem cells, resulting in complete loss of the intestinal villi and death from the GI syndrome in about 4-5 days. It has traditionally been assumed that the gastrointestinal (GI) syndrome results from the direct killing of the rapidly growing stem cells, depletion of the differentiated parenchymal cells and subsequent loss of tissue function [2, 4].

The GI syndrome has, however, recently been suggested to be a direct consequence of an early (4 hrs) wave of apoptosis in the intestinal vascular endothelial cells [5]. These authors irradiated mice with single whole-body photon doses of 15 Gy, sufficient to cause death from the GI syndrome, and demonstrated that it was possible to change the mode of death from the GI syndrome to the bone marrow syndrome (in effect, producing about 3 Gy of radioprotection) when endothelial cell apoptosis was suppressed genetically by deletion of the gene for acid sphingomyelinase, which controls endothelial cell apoptosis through a ceramide pathway, or pharmacologically by administration of basic fibroblast growth factor. The precise mechanism of this proposed linkage between intestinal endothelial cell apoptosis and crypt stem cell depletion leading to the GI syndrome remains unproven [6-8].

An approach for the selective irradiation of the vascular endothelium that allows mechanistic studies into the role of endothelial cell damage in normal tissue radiation responses [9-12] has been applied in this report to crypt stem cell loss in the mouse small intestine. The method is based on the short-ranged (5-9 μm) alpha and lithium particles released from the neutron capture reaction in the stable minor isotope of boron: ^{10}B. When the ^{10}B was restricted to the blood by incorporation into liposomes that could not diffuse into the surrounding tissues, absorbed dose in the microvasculature was increased relative to the uniform dose delivered by the neutron beam to the rest of the body. It is reported here that for both intestinal crypt stem cell survival and mode of death, there were no differences between the groups that were irradiated with the neutron beam alone and those that received the same beam dose and a substantially higher dose selectively delivered to the microvasculature.

3.2 Materials and Methods

3.2.1 Boron analysis

The boron concentration in liquid or solid samples was determined using the prompt gamma neutron activation analysis (PGNAA) facility at the MIT reactor [13]. This spectroscopic technique measures the prompt gamma ray emitted by the recoiling ^{7}Li nucleus following neutron capture in ^{10}B using a high purity germanium detector. The system was calibrated using National Institute of

Standards and Technology (NIST) certified boric acid, and has a detection limit of approximately 1 μg for ^{10}B. All stated uncertainties on ^{10}B measurements represent 1 standard deviation.

3.2.2 Liposomes

Two different ^{10}B-containing liposome formulations were used for these studies. Liposomes containing the amphipathic *nido*-carborane anion species, K^+ [*nido*-7-$CH_3(CH_2)_{15}$-7,8-$C_2B_9H_{11}$]$^{1-}$ (MAC), embedded in the lipid bilayer were prepared as previously described [14]. The water-soluble $[B_{20}H_{17}NH_3]^{3-}$ (TAC) polyhedral borane anion derivative can be incorporated into the interior of the liposome [15]. Liposomes with MAC in the lipid bilayer and TAC in the interior (MAC+TAC) were prepared as described [16]. All boron compounds were enriched in the ^{10}B isotope to >98%. The liposome formulations had a mean vesicle diameter between 70 and 90 nm and contained 24 mg total lipid/ml. The MAC and the MAC+TAC liposome injection solutions were sterilized by passage through a 0.22 μm filter before use and contained 540 $\pm$ 27 μg ^{10}B/ml and 1580 $\pm$ 79 μg ^{10}B/ml, respectively.

3.2.3 Animals and animal procedures

Female BALB/c mice, 8-12 weeks of age, were maintained in a 12-hour light/dark cycle and given food and water *ad libitum*. All procedures were

reviewed and approved by the Committee on Animal Care at the Massachusetts Institute of Technology and were conducted according to the principles outlined in the *Guide for the Care and Use of Laboratory Animals* prepared by the Institute of Laboratory Animal Resources, National Research Council.

3.2.4 Biodistribution studies

The ^{10}B dose distribution is directly related to the ^{10}B concentrations in tissues at the time of irradiation. Liposome biodistribution studies were carried out to determine the amount of ^{10}B in blood, liver, skin and small intestine as a function of time post-injection. Twenty BALB/c mice were injected with 0.2 ml of the MAC liposome solution (108 μg ^{10}B) *via* the retro orbital sinus while under brief isofluorane anesthesia. Five mice were killed by inhalation overdose of either isofluorane or carbon dioxide at each of 4 time points (15, 30, 45 and 60 min) after injection. Blood was drawn directly from the heart. The boron concentrations in blood and samples of skin (pinna), liver and small intestine were measured using PGNAA. Eight mice received 0.2 ml of the MAC+TAC liposome solution (316 μg ^{10}B) and were killed at 30 min post-injection for boron analysis.

The boronated amino acid, *p*-boronophenylalanine (BPA), was used to provide a uniform boron distribution in blood and tissues for a positive control experiment. Previous studies have shown that BPA distributes relatively uniformly from blood into normal tissues at 2-3 hrs post injection [17]. The BPA

was solubilized for injection as the fructose complex at a concentration of ~83 mg BPA/ml [18]. Five mice received a single injection of BPA (0.2 ml; 812 mg ^{10}B) into the retro-orbital sinus and were killed at 2 hrs post-injection for boron analysis.

3.2.5 Neutron beam irradiation

Whole-body mouse irradiations were carried out in the epithermal neutron beam at the MIT reactor (MITR) as previously described [19]. Mice were irradiated in a Lucite holder designed to immobilize unanesthetized mice by all four feet such that the abdomens were presented to the 16-cm-diameter horizontal epithermal beam [19]. Unless specifically noted, all doses quoted in this paper are physical absorbed doses to which no weighting factors have been applied. Absorbed doses ranging from 3.2 ± 0.2 to 10.0 ± 0.7 Gy were administered with irradiations lasting from 6 to 20 min. The epithermal neutrons were thermalized by 1.5 cm of Lucite, consisting of the 0.5 cm thick mouse holder and an additional 1.0 cm sheet of Lucite placed between the holder and the beam aperture. The mouse bodies were centered at a depth of 2.5 cm. Photon and fast neutron absorbed dose rates were measured using paired ionization chambers with walls of graphite and tissue equivalent A-150 plastic. The absorbed dose from neutron capture in ^{10}B and nitrogen was determined using the measured difference in the activation of bare and Cd-covered gold foils and kerma coefficients of 8.66×10^{-8} and 7.88×10^{-12} Gy cm^2, respectively. A

uniform nitrogen concentration of 3.5% by weight was applied for tissue and boron concentrations measured in the biodistribution studies were used to determine the absorbed doses in the blood and vessel wall [20].

3.2.6 Vascular dose calculations

The boron neutron capture reactions in the liposome groups occur, by design, only within the vessel lumen. This creates a non-uniform dose distribution in which the dose delivered to the vascular endothelium is less than the boron dose absorbed in the blood volume within the lumen. Rydin, *et al.* quantified this effect of vessel geometry on the dose absorbed in an endothelial cell from boron neutron capture reactions restricted to the lumen of a blood-filled capillary relative to the boron dose absorbed in the blood [21]. According to this model, when ^{10}B is restricted to the lumen, the boron dose absorbed in the capillary wall is 1/3 of the boron dose absorbed in the blood, given a capillary wall thickness of 0.25 μm, which is considered representative for the mice used in this study. The total physical absorbed dose in the vascular endothelium is the sum of the external beam dose and the vascular-specific boron dose.

3.2.7 Crypt regeneration assay

The intestinal crypt microcolony assay [3] was used to quantify the effects of the different absorbed dose distributions delivered to the microvasculature and

to the intestinal crypt stem cells. This assay has several advantages such as a steep dose response relationship and independence from the dose to adjacent normal tissues. Based on its sensitivity, it has been used to quantify the different biological effects of clinical fast neutron therapy beams differing in radiation quality by no more than about 10% [22]. In the studies reported here, mice received whole-body neutron beam irradiation either without administered boron, 30 ± 5 min after a 0.2 ml liposome injection or 2 hrs after injection of BPA. The mice were killed 84 ± 1 h after irradiation, and a 5 cm section of the jejunum was removed, cut into 0.5 cm segments and placed into 10% formalin fixative for 24-48 hrs. After fixation, the intestine sections were embedded vertically in paraffin to generate cross-sections when cut and then stained with hematoxylin and eosin (H&E). The numbers of regenerating crypts per circumference were counted using at least four sections per mouse and 4 mice per dose point. The criteria used for scoring a regenerating crypt were 10 or more contiguous epithelial cells and at least one Paneth cell [2, 3]. No correction factor was applied, as the average crypt size in all irradiated groups was the same. A single, blinded observer scored all slides.

3.2.8 Survival studies

Mouse survival experiments were carried out at whole-body epithermal neutron beam absorbed doses of 5.7 ± 0.4, 7.5 ± 0.5, 8.3 ± 0.6, 9.0 ± 0.6 and 10.0 ± 0.7 Gy. At the three lowest doses, groups of 8-12 mice received either

beam-only irradiation or irradiation together with boronated liposomes in the blood. The MAC liposomes were used for the 5.7 Gy dose level, and the MAC+TAC liposomes were used for both the 7.5 and 8.3 Gy dose levels. No boronated liposomes were administered for the 9.0 and 10.0 Gy dose levels. Mice were weighed daily following irradiation and killed upon entering a moribund state. Intestine and femur samples were harvested for histology to ascertain the likely mode of death.

3.3 Results

3.3.1 Biodistribution

The variation in the blood-boron concentration between 15 and 60 min after injection of the MAC liposome preparation is shown in Fig. 3-1. At 30 min post-injection, the boron concentration in blood was found to be 45 ± 7 μg ^{10}B/g. The ^{10}B concentrations in liver, skin and small intestine were 18 ± 2 μg ^{10}B/g, 3.7 ± 0.2 μg ^{10}B/g and 0.6 ± 1.0 μg ^{10}B/g, respectively. The low boron concentrations observed in the skin and intestine are most likely due to the blood content of the tissue samples analyzed. Thirty minutes post-injection was chosen as the time of irradiation based on both the boron biodistribution as well as logistical reasons associated with the reactor

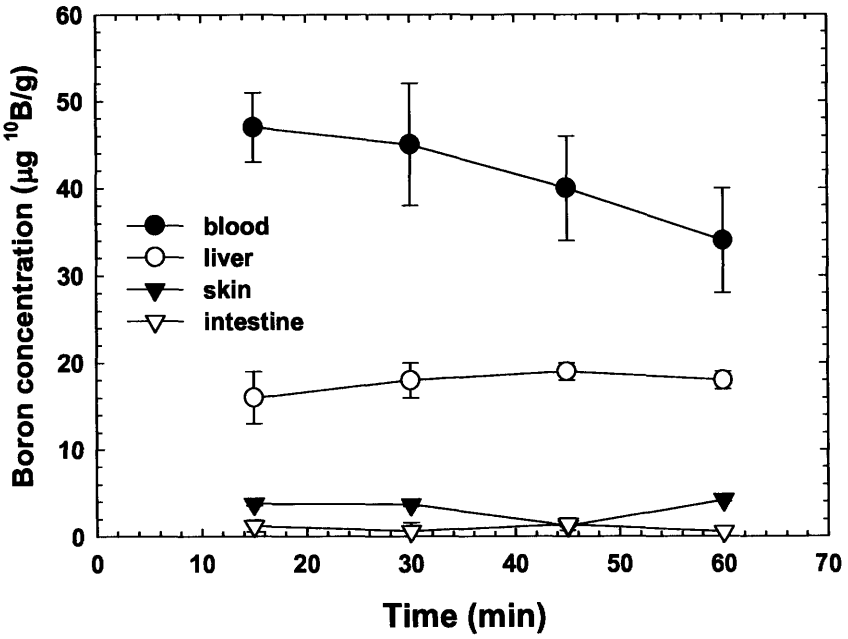

Figure 3-1. ^{10}B concentrations in blood and tissues as a function of time following injection of 0.2 ml of the MAC liposome preparation into the retro-orbital sinus. Points represent the mean ± SD; 5 mice per time point.

irradiations. The MAC+TAC liposome solution was used to provide a higher blood-boron concentration. Eight additional mice received a 0.2 ml injection of the MAC+TAC liposome preparation and were killed at 30 min post-injection. The ^{10}B concentrations in blood, liver and small intestine were 118 ± 12 μg ^{10}B/g, 61 ± 3 μg ^{10}B/g and 0.54 ± 0.49 μg ^{10}B/g, respectively. As expected, the blood-boron concentration scaled proportionately with the increased boron content in the MAC+TAC liposome solution. The boron concentration in the small intestine was below the PGNAA detection limit, as was the case for the MAC liposomes.

A 2-hr post-injection time point was chosen for the BPA biodistribution study to allow the boron to equilibrate from the blood into the normal tissues.

The ^{10}B concentrations in blood and small intestine were 13.7 ± 4.6 and 13.0 ± 3.6 μg ^{10}B/g, respectively (n = 5).

3.3.2 Dosimetry

The total absorbed dose rate in the epithermal neutron beam was 0.57 ± 0.04 Gy min^{-1} at a depth of 2.5 cm and was comprised of 77% low-linear energy transfer (LET) photons and 23% high-LET radiations, which are principally protons arising from thermal neutron capture in nitrogen. The relative uncertainty on the neutron beam doses was 2.2%, which includes only the statistical uncertainty in the beam monitor counts and variations of approximately 1mm in positioning of the irradiation jig along the center of the beam central axis. The additional absorbed dose rate from the ^{10}B capture reaction was 3.3 ± 0.18 cGy min^{-1} per μg ^{10}B present.

The total absorbed dose rate in the vascular endothelial cells, with boronated liposomes in the blood at the time of neutron irradiation, was estimated as the sum of the whole-body neutron beam absorbed dose rate plus 1/3 of the ^{10}B absorbed dose rate in the blood (Table 3-1). The additional absorbed dose rate in the microvasculature coming from boron neutron capture reactions in the blood was 1.1 ± 0.06 cGy min^{-1} per μg ^{10}B, which includes the geometrical factor of 1/3 [21]. The higher ^{10}B concentration in the blood associated with the MAC+TAC liposomes allowed the dose to the vascular endothelial cells to be increased, while holding all other parameters constant.

Thus, the total absorbed dose rate in the microvasculature was 1.08 ± 0.09 Gy min^{-1} or 1.90 ± 0.16 Gy min^{-1} with 45 ± 7 or 118 ± 12 μg ^{10}B/g in the blood, respectively. The stated uncertainties on the microvascular absorbed dose rates include the uncertainty in the neutron beam dosimetry as well as the uncertainty in the blood-boron concentration at the time of irradiation.

3.3.3 Intestinal crypt regeneration assay

The numbers of regenerating crypts per intestinal cross section as a function of the physical absorbed doses from the epithermal neutron beam are shown in Fig. 3-2 for the four experimental groups (epithermal neutron beam only, irradiation with either the MAC or the MAC+TAC liposomes in the blood, or the BPA positive control). The crypt regeneration data points for the two groups that received liposome injections and beam doses above 6 Gy were within 1 standard deviation of the exponential fit to the beam-only dose response data (Fig. 3-2) despite the presence of 45 ± 7 or 118 ± 12 μg ^{10}B/g in the blood and estimated endothelial cell doses that were 2 or 3 times higher than the whole-body beam doses (Table 3-1). Regression fits of the beam-only and the beam plus liposome data in the linear region of the dose response relationship indicate that absorbed doses of 7.3 ± 0.6 Gy (beam- only), 7.2 ± 0.6 Gy (beam + MAC),

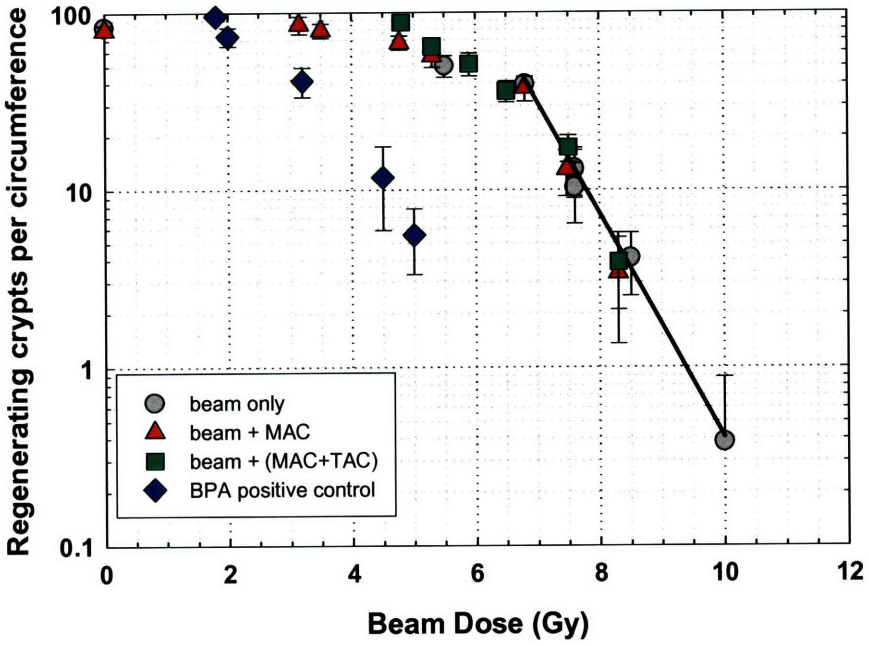

Figure 3-2. Number of regenerating crypts per intestinal circumference as a function of neutron beam dose 84 ± 1 hours after whole-body irradiation in the presence or absence of boronated liposomes in the blood or with a uniform ^{10}B distribution using BPA. The triangles and squares represent irradiation conditions where the dose to the microvasculature was increased, relative to the rest of the mouse, by a factor of 2 or 3, respectively. Points represent the mean ± SD of at least 16 jejunal cross sections, 4 sections from each of 4 mice.

and 7.1 ± 0.6 Gy (beam + (MAC+TAC)) were required to reduce crypt stem cell survival to the level of 20 regenerating crypts per circumference. The added absorbed dose selectively delivered to the vascular endothelial cells in the beam plus liposome groups did not contribute to intestinal crypt stem cell depletion. Liposome injections with no neutron irradiation had no effect on crypt regeneration numbers compared to the non-treated controls.

Table 3-1: Beam doses, total blood doses, and endothelial cell doses used in the survival experiments.

Beam-only dose (Gy)	^{10}B in blood[1] (μg ^{10}B/g)	Total blood dose[2] (Gy)	Endothelial cell dose[3] (Gy)
5.7 ± 0.4	45 ± 7	20.9 ± 1.0	10.8 ± 0.9
7.5 ± 0.5	118 ± 12	60.1 ± 5.7	25.0 ± 2.0
8.3 ± 0.6	118 ± 12	66.5 ± 6.3	27.7 ± 2.2
9.0 ± 0.6	0	9.0 ± 0.6	9.0 ± 0.6
10.0 ± 0.7	0	10.0 ± 0.7	10.0 ± 0.7

[1] MAC liposomes or MAC+TAC liposomes were used to produce 45 ± 7 or 118 ± 12 μg ^{10}B/g in the blood, respectively.

[2] Total blood dose (Gy) = beam dose + ^{10}B dose to the blood

[3] Endothelial cell dose (Gy) = beam dose + (1/3)(^{10}B dose to the blood)

The data shown in Fig. 3-2 are in good agreement with the published data of Gueulette in the same mouse (BALB/c) using the same irradiation jig and geometry in the same neutron beam [19]. In that study, the MITR epithermal neutron beam was shown to have a relative biological effectiveness of 1.5 ± 0.04, relative to 6 MV photons, for the crypt regeneration endpoint [19]. Thus, the neutron beam absorbed doses of 3.2-10.0 Gy used here, which are a mix of high- and low-LET radiations, correspond to photon-equivalent doses of 4.8-15.0 Gy for the crypt survival endpoint. Fig. 2 shows that there were less than 10 regenerating crypts per circumference for an absorbed dose of 8.3 Gy (12.5 Gy

photon-equivalent), which is consistent with this dose being near the threshold for a GI death.

The number of regenerating crypts per intestinal cross section following neutron irradiation in the presence of a uniform ^{10}B concentration in blood and intestine, as delivered by BPA, is also shown in Fig. 3-2. The intent of this BPA positive control experiment was to estimate the sensitivity of the crypt regeneration assay for the detection of potential ^{10}B diffusion out of the vessels. The presence of ~13 μg ^{10}B/g in both blood and intestine increased the physical absorbed dose rate by 75%, or by an additional 0.43 Gy min^{-1}. The BPA positive control dose response curve is shifted significantly to the left when plotted *versus* the beam dose (Fig. 3-2). Based on these data, we estimate that the crypt regeneration assay could detect the effect of the added ^{10}B dose from as little as 2 μg ^{10}B/g outside the vessels, which represents less than 2% "leakage" of the MAC+TAC blood-boron concentration.

Even with all ^{10}B restricted to the vessel lumen, the ranges of the alpha and lithium particles (9μm and 5μm) are such that some dose will be absorbed outside of the vessel wall. Monte Carlo simulations show that the ^{10}B dose gradient outside the vessel drops off steeply. For example, for the 8.3 Gy beam dose with the MAC+TAC liposomes (118 μg ^{10}B/g in the blood: Table 3-1) the absorbed ^{10}B dose to the blood inside the vessel lumen is 58.2 Gy. Outside the vessel, at distances of 2, 5 and 7 μm from the vessel wall, the ^{10}B dose component is 3.0, 0.2 and 0.005 Gy, respectively. However, the crypt microcolony assay results (Fig. 3-2) indicate that this potential penetration of the

particle dose outside the vessel had no detectable effect on the crypt stem cell survival.

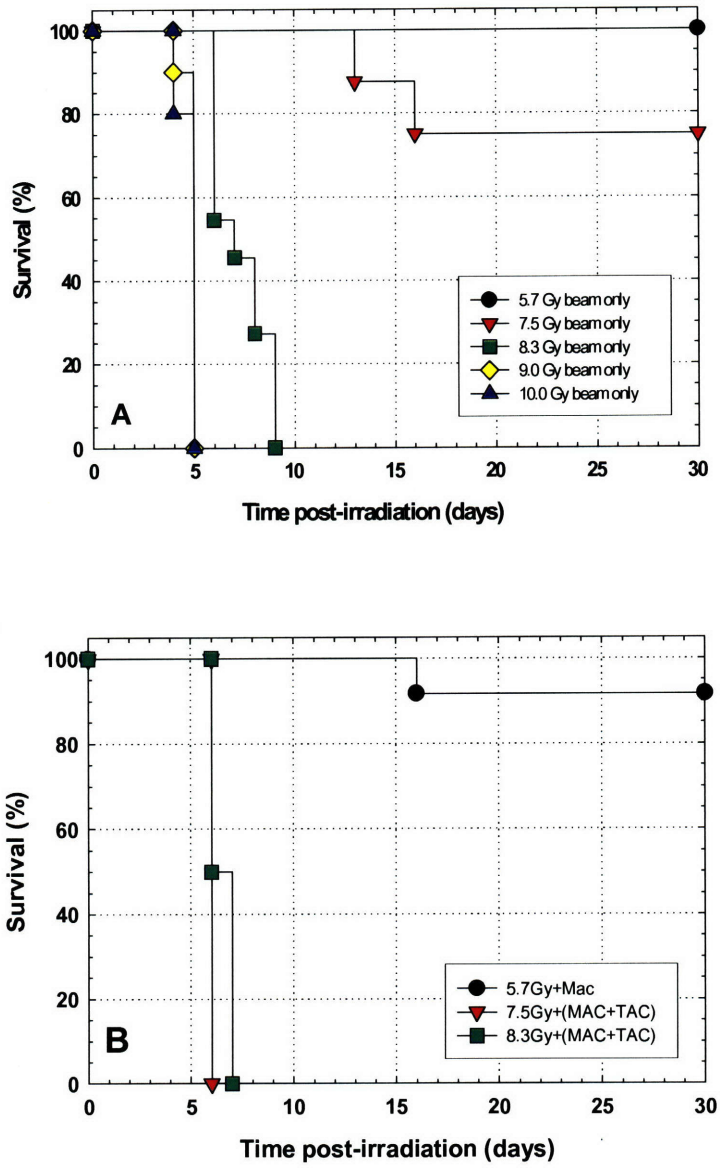

Figure 3-3. A. Mouse survival after whole-body neutron beam-only irradiations. B. Mouse survival after whole-body neutron irradiation with boronated liposomes present in the blood. The microvascular absorbed doses were 10.8 ± 0.9 (MAC), 25.0 ± 2.0 (MAC+TAC) and 27.7 ± 2.2 Gy (MAC+TAC), respectively.

3.3.4 Mouse survival

Figure 3-3A shows the survival of the beam-only groups as a function of time after whole-body neutron beam irradiation. All mice (n=12) given 5.7 Gy and 8 of 10 mice given 7.5 Gy lived beyond 30 days, indicating that these beam doses were below the LD_{50} for death from a bone marrow syndrome. At neutron beam doses of 8.3, 9.0 and 10.0 Gy, all mice (n=28 total) died within 4-9 days (Fig. 3-3A). Figure 4 shows H&E-stained histological sections of small intestine (jejunum) and bone marrow from mice in the 8.3 and 9.0 Gy beam-only groups that were killed 9 and 5 days after irradiation, respectively. The intestinal mucosa was well on the way to recovery in the mouse that received the 8.3 Gy beam-only dose, whereas the intestinal epithelium was severely denuded in the mouse that received the 9.0 Gy beam-only dose, which is indicative of death from the GI syndrome. The bone marrow was severely depleted and showed extensive necrosis of the matrix and widespread hemorrhaging in both mice. Thus, the histopathology from the neutron beam-only irradiation groups indicates that the transition from a bone marrow death to a GI syndrome-induced death occurs at a whole-body absorbed dose between 8.3 and 9.0 Gy.

Figure 3-3 B shows the survival of the beam plus liposome groups as a function of time after whole-body neutron beam irradiation with boronated liposomes in the blood. The estimated total absorbed doses in the vascular endothelial cells were 2 or 3 times higher than the whole-body absorbed doses received by the crypt stem cells (Table 3-1). In the 5.7 Gy + MAC group, 11 of 12

mice lived beyond 30 days, whereas all mice (n=10) in the 7.5 Gy + (MAC+TAC) group and all mice (n=8) in the 8.3 Gy + (MAC+TAC) group died within 6-7 days. Figure 3-4 shows H&E-stained small intestine (jejunum) and bone marrow sections from a mouse in the 8.3 Gy + (MAC+TAC) group killed 7 days after irradiation. The intestinal mucosa recovered, whereas the bone marrow was severely

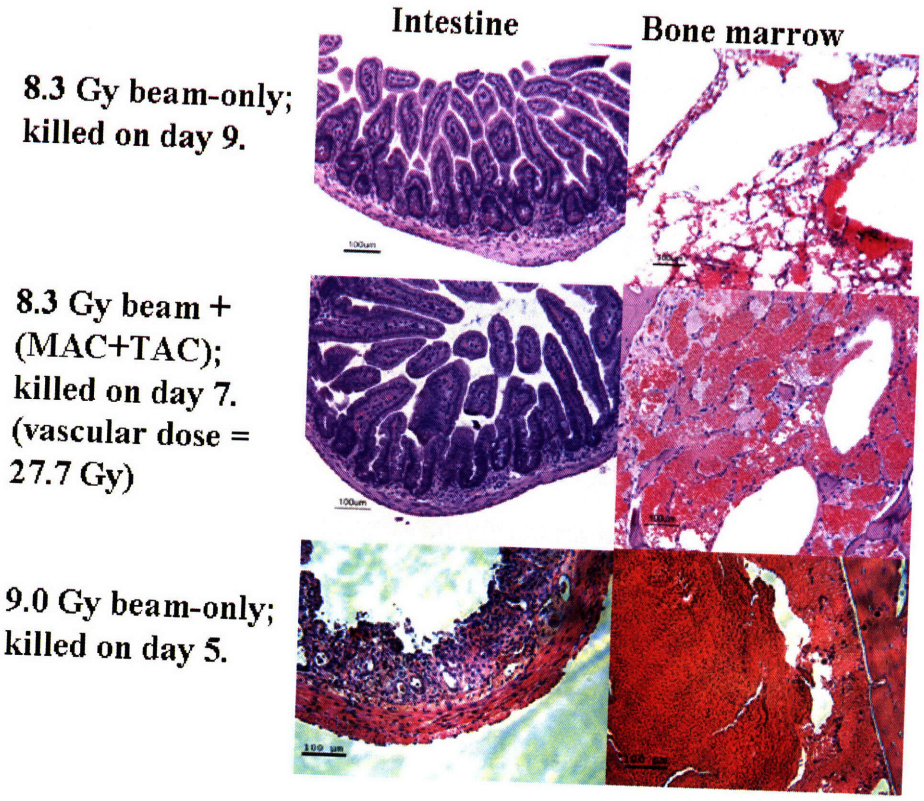

Figure 3-4. Histopathology in small intestine and bone marrow after whole-body neutron beam-only absorbed doses of 8.3 ± 0.6 or 9.0 ± 0.6 Gy. Also shown are tissues from a mouse in the 8.3 Gy + (MAC+TAC) liposomes group where the calculated absorbed dose to the endothelial cells was 27.7 ± 2.2 Gy.

depleted, indicating that this mouse died from the bone marrow syndrome despite a physical absorbed dose in the microvasculature that exceeded 27 Gy.

The 7.5 Gy beam-only and 7.5 Gy + (MAC+TAC) groups show considerably different survival times (Fig. 3-3), yet the mode of death was the same in both groups, namely, bone marrow depletion. The very high (> 50 Gy) absorbed dose in the blood (see Table 3-1) in the presence of the MAC+TAC liposomes contributed enough dose to the bone marrow to cause a rapid death from the bone marrow syndrome. The exact mechanism of liposome-mediated delivery of boron into the bone marrow is under investigation.

3.4 Discussion

The cellular and sub-cellular events that eventually lead to the breakdown of tissue structure and function are initiated at the time of irradiation. Our ability to preferentially increase the absorbed dose to the vascular endothelial cells allows direct testing of the role played by microvascular damage in the subsequent development of normal tissue damage. We have established that whole-body neutron beam-only doses of approximately 9.0 Gy represent the threshold for death from the GI syndrome. Our approach was to use neutron beam doses below the 9.0 Gy threshold for the GI syndrome in combination with boronated liposomes in the blood. The additional short-ranged boron neutron capture dose in the blood selectively increased the total absorbed dose in the microvasculature to values as high as 27.7 Gy, while the dose to the crypts remained below 9.0 Gy.

Despite these extremely high doses to the microvasculature, the crypt microcolony assay and histopathological confirmation of the mode of death indicated that all observed radiation effects in the small intestine could be attributed to the whole-body neutron beam dose: the added dose to the microvasculature was inconsequential. This leads us to the conclusion that damage to the intestinal microvasculature is not causative in the loss of stem cell function and the eventual depopulation of the intestinal lining that characterizes the gastrointestinal syndrome.

The role of microvascular *versus* parenchymal cell damage has long been a matter of considerable debate for late effects [23-25]. In recent years, it has become clear that the overall tissue response to radiation damage includes a complex interaction between the different cell types present that begins immediately after the radiation insult and persists throughout the clinically silent period until the expression of the late effect months or even years later. Radiation has been shown to result in the activation of a number of early-response cytokines which act through diverse signaling pathways [26]. This continuous cascade of cytokines has been proposed to induce a chronic inflammatory phase, which is in turn followed by late stromal alterations such as fibrosis [27]. Radiation injury has also been likened to a "complex wound" where persistent damage to the vascular endothelium results in eventual dysregulation of the coagulation system, which in turn causes a chronic inflammatory response leading to fibrotic changes [28]. Despite the increased understanding of the molecular responses in tissue to radiation exposure, questions still remain as to

which cell population(s) are the critical targets that initiate these signaling pathways, due in large part to the lack of experimental techniques for selectively irradiating potential target populations to test these hypotheses.

The present study is similar in concept to previous work by us that addressed the role of vascular damage in the development of both subacute and late effects in the central nervous system [9, 10]. In those studies, the blood brain (or spinal cord) barrier was used to keep a low molecular weight boron compound ($Na_2B_{12}H_{11}SH$, or BSH) within the lumen of the blood vessels during neutron irradiation. In the spinal cord study [10], an *in vivo/in vitro* assay for O-2A glial progenitor cells showed that, following uniform irradiation with the neutron beam alone, the glial progenitor population was severely depleted at 1 week and remained so until the development of white matter necrosis and limb paralysis at 6 months post-irradiation. In contrast, the glial progenitor population remained at high levels at all times following the irradiation with the neutron beam plus BSH in the blood. Both irradiation conditions were iso-effective for white matter necrosis [29]. The conclusion from that study was that damage to the vascular endothelium was the primary event leading to white matter necrosis [10]. In the rat brain study [9], at 30 days post-irradiation, the loss of neural precursor cells and their progeny was shown to correlate with the absorbed dose in the brain parenchyma (the beam dose) and was not affected by the selective irradiation of the microvasculature [9]. The results in the rat brain parallel what we report here for the acute loss of mouse intestinal crypt stem cells: the effect is direct and not mediated by the vascular dose.

The mixed high- and low-LET nature of the physical absorbed doses in the microvasculature reported here complicates a direct comparison to the low-LET doses used by Paris *et al.*, [5]. However, a biological weighting factor has been measured for BSH in the rat spinal cord using the myeloparesis endpoint [29], where white matter necrosis has been shown to be directly related to vascular damage [11, 12]. BSH in the CNS produces the same ^{10}B distribution pattern as the liposomes in the intestine in the current study: the ^{10}B is restricted to the vessel lumen. The weighting factor derived in the rat spinal cord for BSH is 0.46 and converts the ^{10}B physical dose absorbed in the blood into a photon-equivalent dose to the vasculature [29]. Application of the BSH weighting factor to the liposome ^{10}B blood doses (Table 3-1) generates estimated photon equivalent doses to the intestinal vasculature of 7.0, 24.2 and 26.8 Gy. In addition, the vasculature also received the non-specific beam dose. Clearly, the upper range of the doses delivered to the vasculature in the beam plus liposome irradiations reported here are significantly higher than the 8-15 Gy photon dose range used in the Paris *et al.* study [5].

The proof-of- principle results described here suggest that our technique for selective vascular irradiation could be useful in other non-CNS tissues such as the lung, where the role of vascular endothelial cell apoptosis as the initiating event in the development of lethal radiation pneumonitis in the mouse is a matter of debate [30, 31]. This approach could also play an important role in studies of the molecular mechanisms leading to late fibrosis in tissues such as the lung, the gastrointestinal tract or the kidney. Understanding the mechanisms which

regulate both early and late normal tissue radiation responses may have important implications and applications in the development of radiation protectors or treatments for radiation exposures.

Acknowledgements

This research was performed in part under appointment to the U.S. Department of Energy Nuclear Engineering and Health Physics Fellowship Program (BWS), and by the Innovations in Nuclear Infrastructure and Education Program (contract No. DE-FG07-02ID14420), both sponsored by the U.S. Department of Energy's Office of Nuclear Energy, Science and Technology. Additional support was provided by NIH Grant 1R01 CA97342-01A2 (MFH), the Westaway Family Memorial Fund at MIT (JAC) and by the MIT Center for Environmental Health Sciences NIEHS ES002109 (JAC).

References

1. Potten, C.S., C. Booth, G.L. Tudor, D. Booth, G. Brady, P. Hurley, G. Ashton, R. Clarke, S. Sakakibara, and H. Okano, *Identification of a putative intestinal stem cell and early lineage marker; musashi-1.* Differentiation, 2003. **71**(1): p. 28-41.
2. Potten, C.S., *Radiation, the ideal cytotoxic agent for studying the cell biology of tissues such as the small intestine.* Radiat. Res., 2004. **161**(2): p. 123-36.
3. Withers, H.R. and M.M. Elkind, *Microcolony survival assay for cells of mouse intestinal mucosa exposed to radiation.* Int. J. Radiat. Biol. Relat. Stud. Phys. Chem. Med., 1970. **17**(3): p. 261-7.
4. Hornsey, S., *The effectiveness of fast neutrons compared with low LET radiation on cell survival measured in the mouse jejunum.* Radiat Res, 1973. **55**(1): p. 58-68.
5. Paris, F., Z. Fuks, A. Kang, P. Capodieci, G. Juan, D. Ehleiter, A. Haimovitz-Friedman, C. Cordon-Cardo, and R. Kolesnick, *Endothelial apoptosis as the primary lesion initiating intestinal radiation damage in mice.* Science, 2001. **293**(5528): p. 293-7.
6. Ch'ang, H.J., J.G. Maj, F. Paris, H.R. Xing, J. Zhang, J.P. Truman, C. Cardon-Cardo, A. Haimovitz-Friedman, R. Kolesnick, and Z. Fuks, *ATM regulates target switching to escalating doses of radiation in the intestines.* Nat. Med., 2005. **11**(5): p. 484-90.
7. Maj, J.G., F. Paris, A. Haimovitz-Friedman, E. Venkatraman, R. Kolesnick, and Z. Fuks, *Microvascular function regulates intestinal crypt response to radiation.* Cancer Res, 2003. **63**(15): p. 4338-41.
8. Kolesnick, R. and Z. Fuks, *Radiation and ceramide-induced apoptosis.* Oncogene, 2003. **22**(37): p. 5897-906.
9. Otsuka, S., J.A. Coderre, P.L. Micca, G.M. Morris, J.W. Hopewell, R. Rola, and J.R. Fike, *Depletion of Neural Precursor Cells Following Local Brain Irradiation is due to Radiation Dose to the Parenchyma not the Vasculature.* Radiat. Res., 2006. **165**: p. (in press).
10. van der Kogel, A.J., B.J. Kleiboer, I. Verhagen, G.M. Morris, J.W. Hopewell, and J.A. Coderre, *White matter necrosis of the spinal cord: Studies on glial progenitor survival and selective vascular irradiation*, in *Radiation Research 1895-1995: Volume 2: Congress Lectures, Proceedings of the 10th International Congress of Radiation Research, Wurzburg , Germany,* U. Hagen, et al., Editors. 1996, H. Sturtz, AG: Wurzburg. p. 769-772.
11. Morris, G.M., J.A. Coderre, A. Bywaters, E. Whitehouse, and J.W. Hopewell, *Boron neutron-capture irradiation of the rat spinal-cord - Histopathological evidence of a vascular-mediated pathogenesis.* Radiat. Res., 1996. **146**: p. 313-320.
12. Morris, G.M., J.A. Coderre, E.M. Whitehouse, P. Micca, and J.W. Hopewell, *Boron neutron capture therapy - A guide to the understanding*

of the pathogenesis of late radiation damage to the rat spinal cord. Int. J. Radiat. Oncol. Biol. Phys., 1994. **28**: p. 1107 - 1112.
13. Riley, K. and O. Harling, *An improved prompt gamma neutron activation analysis facility using a focused diffracted neutron beam.* Nucl. Instrum. Meth. Phys. Res. B, 1998. **143**: p. 414-421.
14. Feakes, D.A., K. Shelly, and M.F. Hawthorne, *Selective boron delivery to murine tumors by lipophilic species incorporated in the membranes of unilamellar liposomes.* Proc. Nat. Acad. Sci., USA, 1995. **92**: p. 1367 - 1370.
15. Feakes, D., K. Shelly, C. Knobler, and M. Hawthorne, *Na3[B20H17NH3]: Synthesis and Liposomal Delivery to Murine Tumors.* Proc. Natl. Acad. Sci. USA, 1994. **91**(8): p. 3029-3033.
16. Watson-Clark, R.A., M.L. Banquerigo, K. Shelly, M.F. Hawthorne, and E. Brahn, *Model studies directed toward the application of boron neutron capture therapy to rheumatoid arthritis: boron delivery by liposomes in rat collagen-induced arthritis.* Proc. Natl. Acad. Sci. USA, 1998. **95**(5): p. 2531-4.
17. Coderre, J.A. and G.M. Morris, *The radiation biology of boron neutron capture therapy.* Radiat. Res., 1999. **151**(1): p. 1-18.
18. Coderre, J.A., T.M. Button, P.L. Micca, C.D. Fisher, M.M. Nawrocky, and H.B. Liu, *Neutron capture therapy of the 9L rat gliosarcoma using the p-boronophenylalanine-fructose complex.* Int. J. Radiat. Oncol. Biol. Phys., 1994. **30**(3): p. 643-52.
19. Gueulette, J., P.J. Binns, B.M. Coster, X.Q. Lu, S.A. Roberts, and K.J. Riley, *RBE of the MIT Epithermal Neutron Beam for Crypt Cell Regeneration in Mice.* Radiat Res, 2005. **164**(6): p. 805-9.
20. Riley, K.J., P.J. Binns, and O.K. Harling, *Performance characteristics of the MIT fission converter based epithermal neutron beam.* Phys. Med. Biol., 2003. **48**(7): p. 943-58.
21. Rydin, R.A., O.L. Deutsch, and B.W. Murray, *The effect of geometry on capillary wall dose for boron neutron capture therapy.* Phys. Med. Biol., 1976. **21**: p. 134 - 138.
22. Gueulette, J., M. Octave-Prignot, B.M. De Costera, A. Wambersie, and V. Gregoire, *Intestinal crypt regeneration in mice: a biological system for quality assurance in non-conventional radiation therapy.* Radiother Oncol, 2004. **73 Suppl 2**: p. S148-54.
23. Withers, H.R., L.J. Peters, and H.D. Kogelnik, *The pathobiology of late effects of radiation.*, in *Radiation Biology in Cancer Research*, R.E. Meyn and H.R. Withers, Editors. 1980, Raven Press: New York. p. 439-448.
24. Calvo, W., J.W. Hopewell, H.S. Reinhold, and T.K. Yeung, *Time- and dose-related changes in the white matter of the rat brain after single doses of X rays.* Brit. J. Radiol., 1988. **61**: p. 1043 - 1052.
25. Hopewell, J. and H.R. Withers, *Proposition: long-term changes in irradiated tissues are due principally to vascular damage in the tissues.* Med. Phys., 1998. **25**(12): p. 2265-8.

26. Rubin, P., C.J. Johnston, J.P. Williams, S. McDonald, and J.N. Finkelstein, *A perpetual cascade of cytokines postirradiation leads to pulmonary fibrosis.* Int. J. Radiat. Oncol. Biol. Phys., 1995. **33**(1): p. 99-109.
27. Okunieff, P., T. Cornelison, M. Mester, W. Liu, I. Ding, Y. Chen, H. Zhang, J.P. Williams, and J. Finkelstein, *Mechanism and modification of gastrointestinal soft tissue response to radiation: role of growth factors.* Int. J. Radiat. Oncol. Biol. Phys., 2005. **62**(1): p. 273-8.
28. Denham, J.W. and M. Hauer-Jensen, *The radiotherapeutic injury--a complex 'wound'.* Radiother. Oncol., 2002. **63**(2): p. 129-45.
29. Morris, G.M., J.A. Coderre, J.W. Hopewell, P.L. Micca, M.M. Nawrocky, H.B. Liu, and A. Bywaters, *Response of the central nervous system to boron neutron capture irradiation: Evaluation using rat spinal cord model.* Radiother. Oncol., 1994. **32**: p. 249 - 255.
30. Fuks, Z., R.S. Persaud, A. Alfieri, M. McLoughlin, D. Ehleiter, J.L. Schwartz, A.P. Seddon, C. Cordon-Cardo, and A. Haimovitz-Friedman, *Basic fibroblast growth factor protects endothelial cells against radiation-induced programmed cell death in vitro and in vivo.* Cancer Res., 1994. **54**(10): p. 2582-90.
31. Tee, P.G. and E.L. Travis, *Basic fibroblast growth factor does not protect against classical radiation pneumonitis in two strains of mice.* Cancer Res., 1995. **55**(2): p. 298-302.

Chapter 4: No Significant Endothelial Apoptosis in the Radiation Induced Gastrointestinal Syndrome*

4.1 Introduction

Microvascular *versus* parenchymal cell damage as the initiating event in radiation-induced normal tissue side effects has long been a matter of considerable debate. For late effects, the demonstration of a continuous cytokine signaling cascade throughout the latent period [1], together with reports that late effects could be modified pharmacologically [2], contributed to the current understanding that late-appearing changes are not necessarily the inevitable consequence of damage to a single target cell population, but, rather, the overall tissue response to the initial radiation damage [3]. Acute damage in rapidly-proliferating normal tissues has historically been assumed to be a direct result of the radiation inactivation of the stem cell populations supporting these tissues. The radiation-induced gastrointestinal (GI) syndrome is characterized by massive depletion of the intestinal epithelial lining leading to death in ~5-10 days, which reflects the functional lifetime of the differentiated epithelial cells. Recently, it was proposed that an early (4 hrs post-irradiation) wave of apoptosis in murine intestinal microvascular endothelial cells was the initiating event leading to the GI syndrome [4], a hypothesis which remains controversial [5-7].

---

* Schuller, B.W., A.B. Rogers, K.S. Cormier, K.J. Riley, P.J. Binns, R. Julius, M.F. Hawthorne, and J.A. Coderre, *No significant endothelial apoptosis in the radiation-induced gastrointestinal syndrome.* Int J Radiat Oncol Biol Phys, 2007. **68**(1): p. 205-10.

To directly test the role of vascular damage in the response of tissues to irradiation, we introduced a method for selective irradiation of the vascular endothelium that entails whole-body irradiation with low-energy neutrons in the presence of ^{10}B-labeled compounds that remain in the blood. The short-ranges (5-9 μm) of the alpha and lithium particles released following neutron-capture by ^{10}B in the blood result in a >3-fold higher radiation dose absorbed in the microvasculature. Using the blood brain barrier to restrict a low-molecular weight boron compound to the blood, we showed that vascular damage was the critical factor in the subsequent development of late damage (white matter necrosis) in the rat spinal cord [8]. However, it was the direct brain dose, and not the vascular dose, that correlated with a subacute (30 days) effect (loss of neural precursor cells) in the rat brain [9].

To address the role of vascular damage in tissues not protected by the blood brain barrier, we used the selective vascular irradiation approach with boron-loaded liposomes [10]. In the mouse small intestine, we showed that the significantly higher doses selectively delivered to the vascular endothelium (a) did not cause any additional loss of murine intestinal crypts, and (b) did not increase the incidence of death from the GI syndrome, beyond that produced by the neutron beam alone [10]. Here, we use the selective vascular irradiation methodology to address the hypothesis that early endothelial cell apoptosis is the cause of the GI syndrome.

4.2 Materials and Methods

4.2.1 Boronated liposomes

The ^{10}B-containing liposome formulations used for the mouse intestine studies were prepared as previously described [10, 11]. The liposome formulations had a mean vesicle diameter between 70 and 90 nm and contained 24 mg total lipid/ml. Boron concentrations of ~1580 μg ^{10}B/ml were determined by prompt gamma neutron activation analysis for the liposome injection solution.

4.2.2 Irradiation conditions and dosimetry

All animal protocols were approved by the MIT Committee on Animal Care and were conducted according to the principles outlined in the *Guide for the Care and Use of Laboratory Animals* prepared by the Institute of Laboratory Animal Resources, National Research Council. Unanesthetized mice received whole-body irradiation with 250 kVp x-rays, ^{137}Cs gamma rays or epithermal neutrons at dose rates of 2.5 Gy/min, 0.69 Gy/min and 0.57 Gy/min respectively that were measured using separate graphite- and A-150 plastic-walled ionization chambers. Absorbed dose in tissue using the epithermal neutron beam was comprised of 77% low-linear energy transfer (LET) photons and 23% high-LET reaction products, primarily protons produced in tissue by thermal neutron capture in nitrogen. In all irradiations, the dose to the blood vessels was assumed to be

equivalent to the whole-body dose and hence the dose to the crypt cells except for those performed in the neutron beam following the injection of liposomes containing boron. Under these irradiation conditions, the blood vessels received an additional dose resulting from secondary charged particles (alpha particle and lithium ion) produced in the blood following the capture of thermal neutrons by boron. The dose to the capillary wall from the presence of boron in the blood was determined from thermal neutron flux measurements performed in a nylon mouse phantom with bare and cadmium covered Au activation foils. The thermal neutron flux was multiplied by the weight fraction of boron in the blood of the mice, measured in previous biodistribution studies, a kerma coefficient of 8.66×10^{-8} Gy cm^2 and a geometry factor of 1/3. The geometry factor accounts for the non-uniform distribution of traversals in the capillary wall from the secondary charged particles that only emanate from the vessel lumen. The geometry factor varies depending upon both the diameter and wall thickness of the capillary [12, 13]. Based upon previous studies for a 8 μm-diameter capillary with a wall thickness of 0.25 μm, a geometrical reduction factor of 1/3 was considered appropriate [12] and the additional absorbed dose rate in the blood vessel wall from the ^{10}B capture reaction was 1.1 ± 0.06 cGy min^{-1} per μg $^{10}B/g$ present in the blood [10]. Irradiations began 30 ± 5 min after injection of the boronated-liposome solution (0.2 ml, retro-orbital sinus) when the ^{10}B blood concentration, measured in previous biodistribution studies [10], was 118 ± 12 μg $^{10}B/g$. Thus, for the selective vascular irradiation group, the whole-body dose rate from the neutron

beam was 0.57 Gy/min while the concurrent dose rate to the endothelial cells in all vessels was 1.9 Gy/min, a factor of 3.3 higher.

4.2.3 Histology and TUNEL staining

Intestinal (jejunum) sections were stained by the terminal deoxynucleotidyl transferase biotin-dUTP nick end labeling (TUNEL) method at an outside laboratory (Mass Histology, Worcester, MA) using a commercial kit (Dead End Colorimetric TUNEL System; Promega, Madison, WI). Positive tissue controls (irradiated thymus) and negative antibody controls (irrelevant mouse IgG replacing the primary antibody) were included in all TUNEL staining experiments. Jejunal sections were scored for all TUNEL-positive nuclei in the lamina propria of the villi using 50 villi per mouse and three mice per data point, with the following exceptions. The 250 kVp x-ray, BALB/c points contain only 1 mouse per point; the C57Bl/6 12 and 16 Gy ^{137}Cs contain 6 mice per point and represent two independent experiments.

4.2.4 Fluorescence immunohistochemistry

Unstained formalin-fixed paraffin-embedded jejunal sections were deparaffinized and subjected to heat-induced epitope retrieval in a commercial rice steamer for 20 min in pH 6 citrate buffer (DAKO Cytomation, Carpinteria, CA) followed by benchtop cooling. All remaining steps were performed as

described elsewhere [14] on an automated i6000 immunostainer (Biogenex, San Ramon, CA). Primary antibodies were sequentially labeled, with a biotin blocking step between markers. Apoptotic cells were labeled with rabbit monoclonal anti-caspase-3 antibody specific for the cleaved (activated) fragment (Cell Signaling Technologies, Beverly, MA), followed by goat anti-rabbit secondary antibody conjugated with Alexa Fluor 488 (Molecular Probes / Invitrogen, Eugene, OR). Endothelium was labeled with Meca-32 (rat anti-mouse anti-plasmalemma vesicle-associated protein; Developmental Studies Hybridoma Bank, University of Iowa, Iowa City, IA) followed by biotinylated secondary antibody, and then visualized by incubation with streptavidin-Cy3 (Amersham). Rat anti-mouse common leukocyte antigen (CD45, Ly5; BD Biosciences, San Jose, CA) was labeled as described for Meca-32. Nuclei were counterstained blue by mounting slides with antifade Vectashield plus DAPI (Vector Laboratories, Burlingame, CA). Positive tissue controls (a chemotherapeutic-treated mouse xenograft) and negative antibody controls (irrelevant mouse IgG replacing the primary activated caspase-3 antibody) were included in all immunofluorescence staining experiments. Fluorescent images were captured with a Zeiss Axioskop 2 system and individual panels merged in Adobe Photoshop. In order to overcome the problem of tissue autofluorescence at the fluorescein excitation maximum of ~490Å, we evaluated photomicrographs taken through a long-pass emission filter, which permitted the passage of all light >515Å following excitation at 450-490 Å. By this method, autofluorescence appeared as yellow due to the combined emission of red and green wavelengths, whereas Alexa Fluor 488-labeled cells

emitted only green light with an excitation maximum of 519 Å. In agreement with prior experience and published results, autofluorescence was particularly intense in formalin-fixed red blood cells (RBCs) within blood vessels. We eliminated bright autofluorescence through color subtraction. The more diffuse pale tissue autofluorescence was eliminated by thresholding techniques.

4.3 Results

The number of TUNEL-positive nuclei per villus showed no dose response between 1 and 33 Gy for either BALB/c or C57Bl/6 mice using four different irradiation modalities as shown in Fig. 4-1a. The doses expressed on the x-axis of Fig. 4-1a are to the blood vessels which, except for the selective vascular irradiation group (neutrons + liposomes), are equivalent to the whole-body doses. All irradiation groups represented in Fig. 4-1a include data above the dose thresholds for death from the GI syndrome (as judged by histology on bone marrow and intestine), which are: 8.3-9.0 Gy for the neutrons only [10]; ~ 9-10 Gy

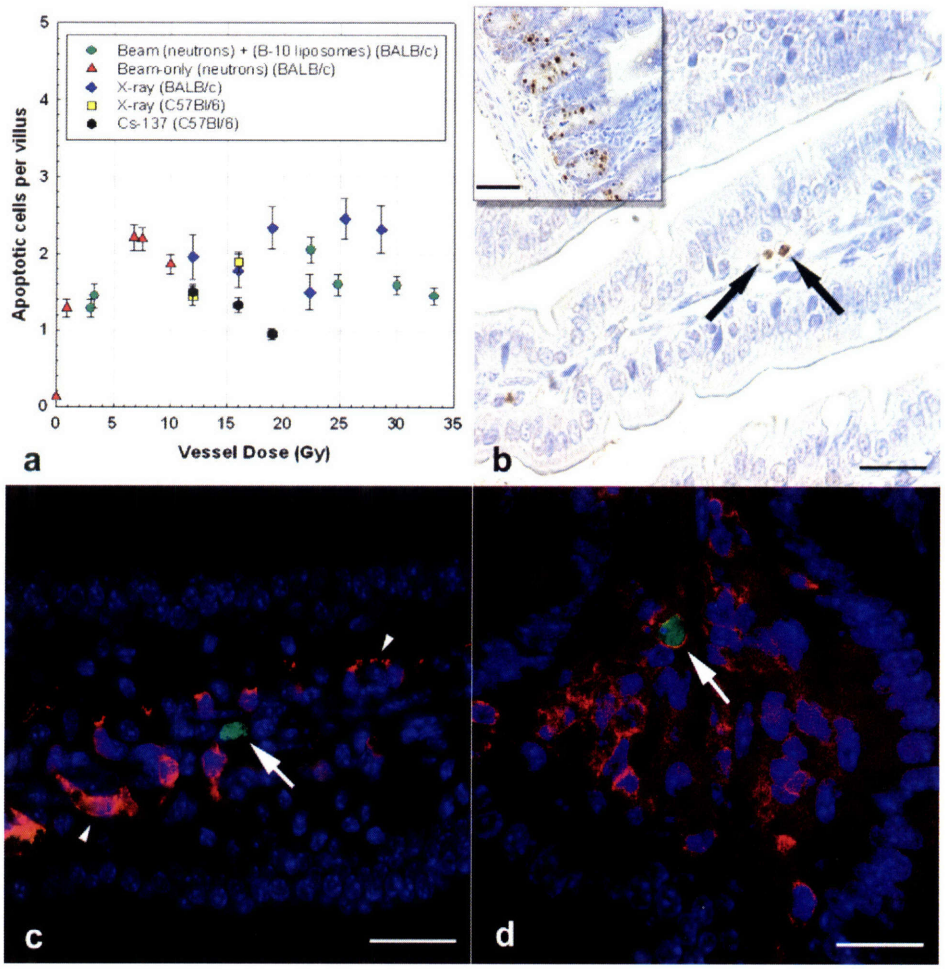

Figure 4-1. (a) TUNEL-positive nuclei in the lamina propria of mouse jejunal villi, at 4 h post-irradiation, as a function of blood vessel dose. Points represent the mean ± SEM, 50 villi per mouse, all scored by a single blinded observer. (b) TUNEL staining demonstrates few apoptotic cells in jejunal villi (arrows) when compared with intestinal crypt (inset); both at 4 h after 12 Gy 250 kVp x-rays. (c) Fluorescence imaging 4 h after 12 Gy of 250 kVp x-rays. The vascular endothelium (Meca-32, Cy3, red, arrowheads) and the apoptosis (caspase-3, fluorescine, green, arrow) labels do not co-localize. Nuclei were counter-stained blue with DAPI. (d) A lone caspase-3-positive cell (fluorescine, green, arrow) expresses on its surface the common leukocyte antigen CD45 (Cy3, red). Scale bars: (b) 50 µm; inset, 100 µm; (c) 50 µm; (d) 30 µm.

for 250 kVp x-rays; and 14-15 Gy for ^{137}Cs gamma rays. Scoring of TUNEL-positive cells per villus indicated 0.12 ± 0.04 apoptotic cells/villus for the unirradiated controls. When the data for all irradiation groups shown in Fig. 4-1a were combined (59 mice, 50 villi/mouse), the mean number of apoptotic cells scored per villus was 1.62 ± 0.03 (SEM) (range 0-12, median 1, mode 0). Apoptotic *epithelial* cells were, however, observed in intestinal crypts (Fig. 4-1b, inset) at all doses. These cells are radiation-sensitive and are known to exhibit an apoptotic dose-response that saturates at doses above ~ 1 Gy [7]. For the same irradiation groups shown in Fig. 4-1a, the number of apoptotic cells per crypt was 3.3 ± 0.1 (mean ± SEM, one mouse scored/point, 10 crypts/mouse). The number of apoptotic cells per crypt was significantly greater than the number per villus ($P<0.0001$). Scoring of TUNEL-positive cells per villus at 8 hrs post irradiation (12, 16 or 19 Gy, 250 kVp x-rays, C57Bl/6 mice, n=1/dose level) resulted in the same low level of apoptosis as shown in Fig. 4-1a for 4 hrs post irradiation. Representative thymus samples from all irradiated groups (250 kVp x-rays, ^{137}Cs gamma rays, neutrons alone, neutrons + liposomes) all showed extensive TUNEL staining at 4 hrs post-irradiation (data not shown).

The TUNEL method can be prone to false-positive labeling of cells in the intestinal villi related to tissue fixation or antigen retrieval procedures [15, 16]. To independently confirm and extend the TUNEL results, we used fluorescence immunohistochemistry for detection of activated caspase-3, which has been shown to correlate well with apoptosis identified using morphological criteria [16]. More cleaved caspase-3-positive cells were located in crypt epithelium than in

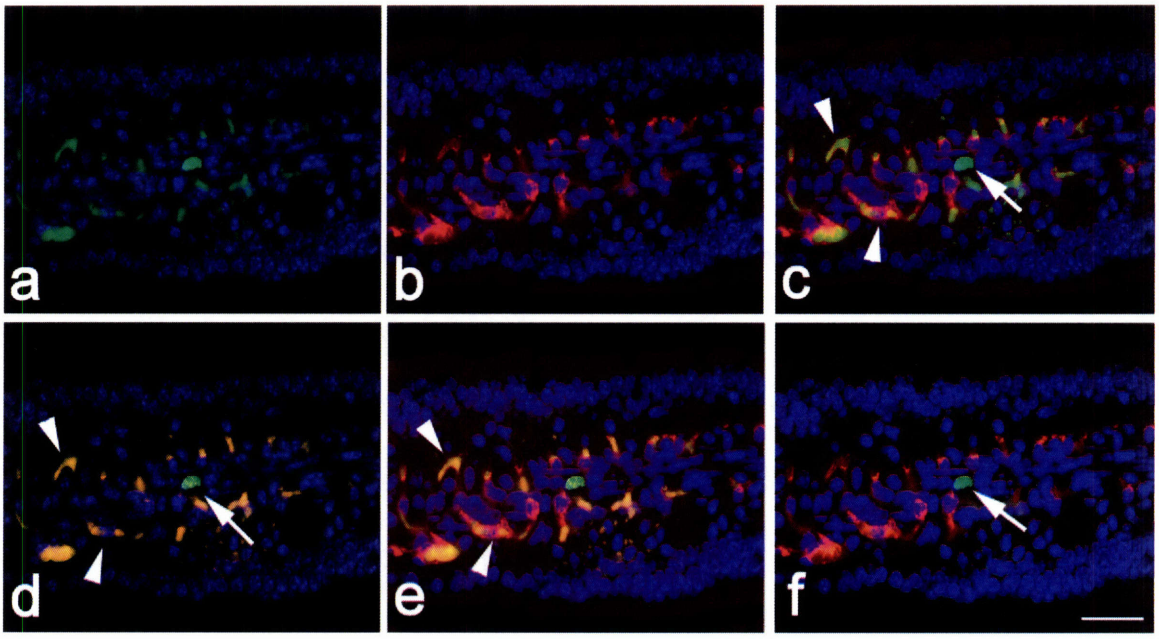

Figure 4-2. Double-label fluorescence immunohistochemistry in formalin-fixed, paraffin-embedded jejunum from a mouse irradiated with 12 Gy of 250 kVp x-rays, demonstrating elimination of confounding autofluorescence. (a) When excited at 450 - 490 Å and viewed through a narrow-pass emission filter (515-565 Å; green light only), there appear to be many cleaved-caspase 3-positive (fluorescein-labeled, green) cells in the villus. (b) Vascular endothelial cells are demonstrated by Meca-32 labeling (Cy3, red, excitation 546 Å, emission >590 Å). (c) Merged image appears to show both Meca-32-positive (arrowheads) and Meca-32-negative (arrow) cleaved caspase-3-positive cells. (d) When excited at 450 - 490 Å and viewed through a long-pass emission filter (allowing passage of all wavelengths > 515 Å) most fluorescent figures are shown to be the result of tissue autofluorescence (yellow, arrowheads) with only a single central figure retaining green fluorescent properties (arrow). (e) Meca-32 overlay demonstrates that endothelial cell-associated figures are autofluorescent erythrocytes. (f) Removing autofluorescence by color subtraction, only the central non-endothelial cell is confirmed to be a fluorescein-labeled cleaved caspase-3-positive cell (arrow). DAPI nuclear counterstain (blue) included in all panels (excitation 365 Å, emission >420 Å). Scale bar: 50 μm for all panels.

villi, in agreement with the TUNEL data shown in Fig. 4-1. We observed no co-localization of endothelial and apoptotic markers within intestinal villi (Fig. 4-1c). Most caspase-3-positive apoptotic cells within villi were localized to the central lamina propria, and not the subepithelial capillary bed, and were identified as CD45-positive leukocytes (Fig. 4-1d). Figure 4-2 illustrates the importance of background correction for tissue autofluorescence that we applied in this work. The multi-wavelength emission (yellow) of autofluorescent compounds, particularly in erythrocytes, is readily apparent when viewed through a long-pass filter (Fig. 4-2d), but produces false-positive labeling when viewed with a narrow-pass filter at the fluophore maximum emission (green) wavelength (Figs. 4-2a,c).

4.4 Discussion

Rapidly renewing normal tissues such as the bone marrow, the intestinal epithelium, and the oral mucosa are arranged into functional units that include a stem cell population and differentiated functional cells with a finite lifetime. The appearance of radiation-induced tissue damage is directly related to the cell turnover kinetics, and the finite lifetimes of the differentiated functional cells. Both the stem cells and the functional cells must be supplied by a network of blood vessels, also comprised of cells with a finite lifetime. Traditionally, it has been thought that acute effects result from the direct killing of the rapidly growing stem cell population and a loss of function because the differentiated functional cells are no longer being replaced. In the intestine, this assumption has been

supported by substantial experimental data showing a linear dose response relationship for crypt stem cell survival, (usually measured as regenerating crypts at 3-4 days post irradiation) [7, 17, 18].

Recent reports have suggested that early (4 hrs post-irradiation) endothelial cell apoptosis in the lamina propria is the primary lesion initiating the GI syndrome following whole-body photon irradiation [4, 19]. A massive increase in the extent of intestinal endothelial cell apoptosis was described when the radiation dose was increased above the threshold for death from the GI syndrome [4]. Deletion of acid sphingomyelinase changed the mode of death from the GI syndrome to the bone marrow syndrome; in effect, producing about 3 Gy of radioprotection [4]. The vascular endothelium in the acid sphingomyelinase-deficient mice exhibited a substantially reduced apoptotic response to radiation compared to wild-type mice [4]. Administration of basic fibroblast growth factor [4] or an angiopoietin analog [19] was shown to reduce the extent of apoptosis in intestinal endothelial cells and to provide some degree of radioprotection (increase in mean survival time). Apoptotic intestinal leukocytes, together with a subpopulation of apoptotic endothelial cells, have been described in irradiated mice with standard murine microflora [20]. Although the relative frequency of each population was not reported, the total number of apoptotic cells per villus was comparatively low in wild-type mice (approximately 3 per villus) after 16 Gy whole-body irradiation, which is consistent with the total number of apoptotic cells per villus that we report here (1.62 ± 0.03, Fig. 4-1a). Whereas it is possible that we overlooked a rare apoptotic endothelial cell, we

cannot envision a scenario by which such a small number could account for the massive tissue loss associated with the radiation-induced GI syndrome. Potten has also reported that although abundant apoptosis could be observed at early (4 hrs) and late (10 hrs) times in the crypt epithelial cells, little or no apoptosis was observed in the stroma or the endothelial cells [7].

Much of the disagreement over the sequence of events leading ultimately to the massive epithelial cell depletion that characterizes the GI syndrome, stems from the lack of experimental techniques to directly test hypotheses. We have developed a methodology that allows us to selectively increase the dose to vascular endothelial cells relative to the dose absorbed in the rest of the body by a factor of 3. This enables, for the first time, a direct investigation of the role of vascular damage in the response of normal tissues to irradiation. The selective vascular irradiation methodology depends on boron being present in the blood during the neutron irradiation and that it is retained within the lumen of the vessels. In our previous study of the mouse small intestine [10] we experimentally validated the method by performing biodistributions for boron in blood and other tissues at different time points following injection as well as quantifying the increased potency in crypt cell depletion with boron present outside the vessels during neutron irradiations. This was to simulate what might occur should boron leak from the vessel lumen when using the boronated liposomes. Briefly, a positive control group was included with 13 μg ^{10}B/g both in the blood and in the normal tissues, including the intestine. Neutron irradiation produced a significant shift in the crypt regeneration dose response curve which

indicates that the crypt regeneration assay is sensitive enough to allow us to discern the additional dose resulting from as little as 2 μg ^{10}B/g outside the vessels. In that study the crypt regeneration dose response data were the same for neutrons alone and neutrons in the presence of boronated liposomes (providing a concentration of 118 μg ^{10}B/g confined to the blood) from which it was concluded that there was no significant leakage of liposomal boron out of the blood vessels at the time of irradiation [10].

Data from the selective vascular irradiation experiments are inconsistent with the hypothesis that endothelial cell apoptosis is the cause of the GI syndrome. In our previous work, we examined the survival of crypt stem cells at 3.5 days post-irradiation and compared whole-body neutron irradiations with and without boronated liposomes to selectively increase the vessel dose. We showed that the greatly increased doses absorbed in the vasculature had no effect on crypt stem cell depletion at 3.5 days post-irradiation [10]. Here, we have examined the incidence of apoptosis in the mouse jejunum at 4 hours post-irradiation. For the same range of neutron doses and selective vascular irradiation conditions, we have demonstrated that the majority of apoptotic cells in irradiated mouse intestine are crypt epithelium, and that the few apoptotic cells present in villi are predominantly tissue-resident leukocytes. We have included whole-body photon irradiation groups in the present study. For both 250 kVp x-rays and ^{137}Cs gamma rays, the data are in agreement with our neutron ± liposome data: no dose response is evident in the number of apoptotic cells per villus for dose ranges that span the threshold for death from the GI syndrome.

Most significantly, we do not observe the high levels of apoptotic endothelial cells in the lamina propria of whole-body irradiated mice using the same experimental conditions reported by others [4, 19]. It was at 15 Gy (^{137}Cs) in C57Bl/6 mice that Paris *et al.* described a sharp increase in the number of apoptotic cells (~45% of crypt/villus units showing > 10, and ~25% showing > 20 apoptotic cells) which was attributed directly to apoptosis in vascular endothelial cells [4]. In summary, the selective vascular irradiation methodology we have described has provided an approach to directly address a long-standing and controversial issue in radiation biology. We conclude that early endothelial apoptosis is not the cause of the GI syndrome. The selective vascular irradiation methodology appears ideally suited for elucidating the role of vascular damage in the development of late effects in normal tissues or in the response of tumors to radiation. Such information could guide the development of protective or therapeutic strategies.

Acknowledgements

Supported by the Nuclear Engineering and Health Physics Fellowship Program (BWS), and the Innovations in Nuclear Infrastructure and Education Program (DE-FG07-02ID14420) of the U.S. Department of Energy, NIH Grant CA97342 (MFH), the Westaway Family Memorial Fund at MIT (JAC) and by the MIT Center for Environmental Health Sciences NIEHS P30 ES002109 (ABR, JAC).

References

1. Rubin, P., C.J. Johnston, J.P. Williams, S. McDonald, and J.N. Finkelstein, *A perpetual cascade of cytokines postirradiation leads to pulmonary fibrosis.* Int. J. Radiat. Oncol. Biol. Phys., 1995. **33**(1): p. 99-109.
2. Moulder, J.E., M.E. Robbins, E.P. Cohen, J.W. Hopewell, and W.F. Ward, *Pharmacologic modification of radiation-induced late normal tissue injury.* Cancer Treat Res, 1998. **93**: p. 129-51.
3. Barcellos-Hoff, M.H., *How tissues respond to damage at the cellular level: orchestration by transforming growth factor-{beta} (TGF-{beta}).* Brit.J. Radiol. Suppl., 2005. **27**: p. 123-7.
4. Paris, F., Z. Fuks, A. Kang, P. Capodieci, G. Juan, D. Ehleiter, A. Haimovitz-Friedman, C. Cordon-Cardo, and R. Kolesnick, *Endothelial apoptosis as the primary lesion initiating intestinal radiation damage in mice.* Science, 2001. **293**(5528): p. 293-297.
5. Suit, H.D. and H.R. Withers, *Endothelial cells and radiation gastrointestinal syndrome.* Science, 2001. **294**(5546): p. 1411.
6. Hendry, J.H., C. Booth, and C.S. Potten, *Endothelial cells and radiation gastrointestinal syndrome.* Science, 2001. **294**(5546): p. 1411.
7. Potten, C.S., *Radiation, the ideal cytotoxic agent for studying the cell biology of tissues such as the small intestine.* Radiat. Res., 2004. **161**(2): p. 123-136.
8. Coderre, J.A., Morris, G.M., Micca, P.L., Hopewell, J.W., Verhagen, I., Kleiboer, B.J., van der Kogel, A.J., *Late effects of radiation on the central nervous system: role of vascular endothelial damage vs glial stem cell survival.* Radiation Research, 2006. **166**: p. 495-503.
9. Otsuka, S., J.A. Coderre, P.L. Micca, G.M. Morris, J.W. Hopewell, R. Rola, and J.R. Fike, *Depletion of Neural Precursor Cells Following Local Brain Irradiation is due to Radiation Dose to the Parenchyma not the Vasculature.* Radiat. Res., 2006. **165**: p. 582-591.
10. Schuller, B.W., P.J. Binns, K.J. Riley, L. Ma, M.F. Hawthorne, and J.A. Coderre, *Selective irradiation of the vascular endothelium has no effect on the survival of murine intestinal crypt stem cells.* Proc Natl Acad Sci U S A, 2006. **103**(10): p. 3787-92.
11. Watson-Clark, R.A., M.L. Banquerigo, K. Shelly, M.F. Hawthorne, and E. Brahn, *Model studies directed toward the application of boron neutron capture therapy to rheumatoid arthritis: boron delivery by liposomes in rat collagen-induced arthritis.* Proc. Natl. Acad. Sci. USA, 1998. **95**(5): p. 2531-4.
12. Rydin, R.A., O.L. Deutsch, and B.W. Murray, *The effect of geometry on capillary wall dose for boron neutron capture therapy.* Phys. Med. Biol., 1976. **21**: p. 134 - 138.

13. Charlton, D.E. and B.J. Allen, *Monte Carlo calculations of ion passages through brain endothelial nuclei during boron neutron capture therapy.* Int. J. Radiat. Biol., 1993. **64**: p. 739 - 747.
14. Rogers, A.B., K.S. Cormier, and J.G. Fox, *Thiol-reactive compounds prevent nonspecific antibody binding in immunohistochemistry.* Lab Invest, 2006. **86**(5): p. 526-33.
15. Stahelin, B.J., U. Marti, M. Solioz, H. Zimmermann, and J. Reichen, *False positive staining in the TUNEL assay to detect apoptosis in liver and intestine is caused by endogenous nucleases and inhibited by diethyl pyrocarbonate.* Mol Pathol, 1998. **51**(4): p. 204-8.
16. Marshman, E., P.D. Ottewell, C.S. Potten, and A.J. Watson, *Caspase activation during spontaneous and radiation-induced apoptosis in the murine intestine.* J Pathol, 2001. **195**(3): p. 285-92.
17. Withers, H.R. and M.M. Elkind, *Microcolony survival assay for cells of mouse intestinal mucosa exposed to radiation.* Int. J. Radiat. Biol. Relat. Stud. Phys. Chem. Med., 1970. **17**(3): p. 261-7.
18. Hendry, J.H., C.S. Potten, and N.P. Roberts, *The gastrointestinal syndrome and mucosal clonogenic cells: relationships between target cell sensitivities, LD50 and cell survival, and their modification by antibiotics.* Radiat Res, 1983. **96**(1): p. 100-12.
19. Cho, C.H., R.A. Kammerer, H.J. Lee, K. Yasunaga, K.T. Kim, H.H. Choi, W. Kim, S.H. Kim, S.K. Park, G.M. Lee, and G.Y. Koh, *Designed angiopoietin-1 variant, COMP-Ang1, protects against radiation-induced endothelial cell apoptosis.* Proc Natl Acad Sci U S A, 2004. **101**(15): p. 5553-8.
20. Crawford, P.A. and J.I. Gordon, *Microbial regulation of intestinal radiosensitivity.* Proc Natl Acad Sci U S A, 2005. **102**(37): p. 13254-9.

Chapter 4 Appendix: Apoptosis in Cultured Human Microvascular Endothelial Cells (HMEC)

During the course of the apoptosis studies described in this chapter, the question arose asking whether endothelial cells exposed to high-LET radiation (the type used in the selective vascular irradiations) will actually undergo apoptosis or proceed down another pathway such as necrosis. To ascertain whether vascular endothelial cells will undergo apoptosis in response to high-LET radiation, human microvascular endothelial cells (HMEC) were irradiated *in vitro* using a custom apparatus designed in the Ph.D. thesis work of Rong Wang (Department of Nuclear Science and Engineering, 2005) [1]. This apparatus allows the direct irradiation of cultured cells with α-particles (high-LET) using ^{241}Am foils and subsequent *in situ* staining for DNA. Abundant apoptosis was found in cultured HMEC following either x-ray (low-LET) or α-particle irradiation (high-LET).

4A.1 Materials and Methods

To determine the response of microvascular endothelial cells to both high- and low-LET radiation, HMEC were cultured and exposed to either α-particles derived from an ^{241}Am source or 250 kVp x-rays. HMEC immortalized with SV40 were obtained from Dr. T. J. Lawley, Biologic Products Branch, Centers for

Disease Control, Atlanta, GA and grown as a monolayer on a 1.4 μm thick mylar membrane, which was part of a custom designed cell irradiation apparatus [1]. The monolayer was exposed to either α-particles (mean α-particle energy of 3.14 MeV, LET = 128 keV/μm) at a dose rate of 9.3 Gy min^{-1} or 250 kVp x-rays at a dose rate of 1.0 Gy min^{-1}. Absorbed doses of 1.0, 5.0 and 10.0 Gy were delivered. After irradiation, the HMEC were incubated at 37 °C for 4 hours, fixed to the mylar membrane with an ice-cold 3:1 methanol-to-acetic acid solution, and stained with 4,6,diamidino-2-phenylidole (DAPI) (10 μg ml^{-1}). The mylar membrane was then transferred to a glass slide (sandwiching the mylar membrane between a glass slide and cover-slip and cutting along the edge of the slide with a scalpel) for analysis by fluorescent microscopy. Apoptotic nuclei were scored based on the morphologic nuclear changes (condensed and fragmented), which are characteristic of apoptosis. All slides were scored by a single blinded observer.

4A.2 Results

The average percentage of apoptotic nuclei as a function of physical dose is shown in Figure 4A-1. The bars represent the mean of 3 different experiments (1000 total cells counted per experiment = 3000 total cells) ± 1 standard deviation. The incidence of apoptotic HMEC increases as a function of physical dose for both the low-LET x-rays and high-LET α-particles. Alpha-particles are more effective than x-rays at inducing apoptosis in that there is an apparent

relative biological effectiveness (RBE) of ~1.4.This experiment shows that high-LET radiation is able to induce an apoptotic response in microvascular endothelial cells. Furthermore, the incidence of apoptosis has been shown to occur after high-LET irradiation [2] and increase with increasing LET in Chinese hamster V79 cells [3]. Bovine derived microvascular endothelial cells have also been shown to undergo apoptosis *in vitro* using low-LET radiation [4]. Given that a mixture of both high- and low-LET radiation is delivered to the endothelial cells during our selective vascular irradiation technique (high vascular doses reaching ~27 Gy) [5], we were confident, at least from an *in vitro* perspective, that endothelial cells exposed to high-LET radiation would undergo apoptosis.

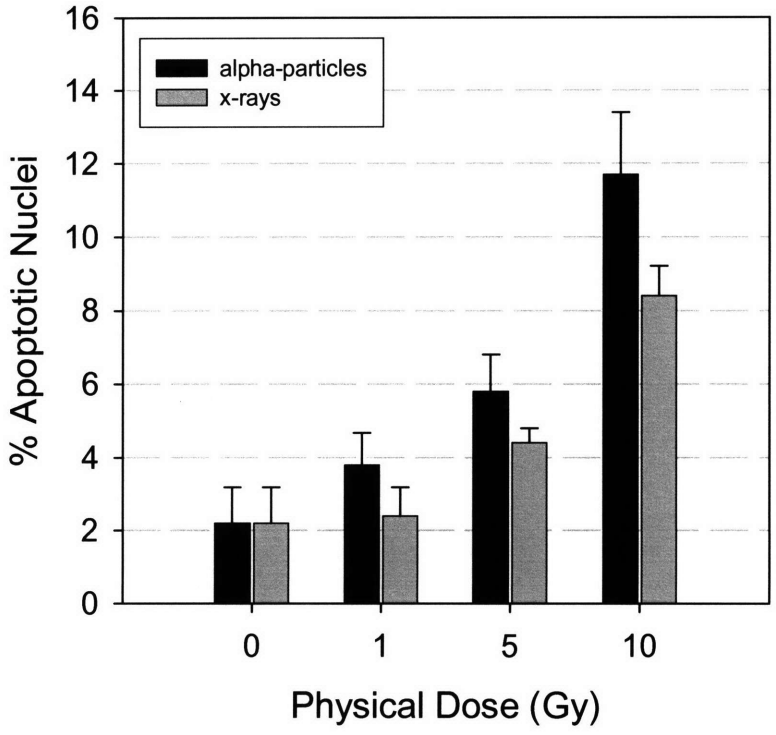

Figure 4A-3. Apoptotic HMEC nuclei (%) as a function of physical dose following α-particle or x-ray irradiation. Apoptosis in these cells increases as a function of dose for both α-particles (high-LET) and x-rays (low-LET).

However, despite the clear *in vitro* dose response for endothelial apoptosis presented here, we have shown that endothelial cells will not readily undergo radiation-induced apoptosis *in vivo*. This is because a situation is created *in vitro,* where cells are placed in an artificial context far removed from the tissue environment. In an *in vivo* environment, there must be many other cellular processes involved to prevent significant levels of endothelial apoptosis.

References

1. Wang, R. and J.A. Coderre, *A bystander effect in alpha-particle irradiations of human prostate tumor cells.* Radiat Res, 2005. **164**(6): p. 711-22.
2. Hendry, J.H., C.S. Potten, and A. Merritt, *Apoptosis induced by high- and low-LET radiations.* Radiat Environ Biophys, 1995. **34**(1): p. 59-62.
3. Aoki, M., Y. Furusawa, and T. Yamada, *LET dependency of heavy-ion induced apoptosis in V79 cells.* J Radiat Res (Tokyo), 2000. **41**(2): p. 163-75.
4. Langley, R.E., E.A. Bump, S.G. Quartuccio, D. Medeiros, and S.J. Braunhut, *Radiation-induced apoptosis in microvascular endothelial cells.* Br J Cancer, 1997. **75**(5): p. 666-72.
5. Schuller, B.W., P.J. Binns, K.J. Riley, L. Ma, M.F. Hawthorne, and J.A. Coderre, *Selective irradiation of the vascular endothelium has no effect on the survival of murine intestinal crypt stem cells.* Proc Natl Acad Sci U S A, 2006. **103**(10): p. 3787-92.

Chapter 5: Preliminary Study on Early Inflammatory Gene Expression Changes Following Selective Vascular Irradiation

5.1 Introduction

Nearly 50% of cancer patients receive some form of radiation therapy during the lifetime of their disease. Radiation therapy is an attractive option for patients and clinicians, because it is a non-invasive treatment modality that will preserve the tissue architecture while affording some curative or palliative effect, i.e. tumor shrinkage, pain relief, etc. [1]. However, radiation therapy does come with risk to the patient, as every cancer patient undergoing radiation therapy will experience some adverse side effects (early or late) from the treatment. The number of cancer survivors in the United States is increasing at a rapid rate. For example, the number of cancer survivors has more than tripled from 1971 to 2001, and this statistic has been met with an increasing concern about the quality of life for patients post-treatment [1]. Early and late radiation side-effects are the dose limiting factors during the course of radiation therapy treatment. The mechanisms underlying early radiation effects are relatively well understood in that they most often arise in stem-cell-based, rapidly renewing tissues, where radiation depletes the regenerative stem cell populations causing the ultimate

loss of tissue structure and function. In contrast, very little is known about the underlying mechanisms involved in the onset of late radiation effects.

The target-cell hypothesis for radiation damage in normal tissue was the established model to explain radiation damage for many years, and it more or less remains as the model used to explain early radiation effects today. However, recent investigations into the complex biochemical changes that take place in cells and tissues following irradiation suggest that late radiation effects are a result of the early activation of inflammatory cytokine cascades that ultimately lead to tissue changes months to even years after radiation exposure [1-10]. Inflammation is a normal component of wound healing where blood-lymphocytes and tissue resident macrophages are recruited to the site of injury through cytokine signaling to help ward off invading microbiota. Activated fibroblasts then deposit collagen to rebuild the tissue structure as angiogenesis takes place. Anti-fibrotic cytokines are then up-regulated to enlist the final tissue remodeling phase. In normal wound healing, activated fibroblasts disappear through active regulatory control and apoptosis, whereby the inflammation process eventually dissipates. In some cases a chronic inflammatory state is established where activated fibroblasts persist for long periods of time. This resembles a 'wound that does not heal' [11] but continues to release repair signals. The source of this chronic signaling cascade remains unknown.

The initial stages of radiation-induced fibrosis are indistinguishable from normal wound healing processes, where there is an almost immediate up-regulation of pro-inflammatory cytokines such as tumor necrosis factor-α (TNF-α)

[12] and interleukins 1 and 6 (IL1 and IL6). However, abnormal production of transforming growth factor-β (TGF-β), TNF-α and IL1 has been observed in irradiated tissues, including the small intestine [13], which may establish the active feedback loop necessary to establish a state of chronic inflammation. Recent evidence has suggested that direct damage to the vascular endothelium plays a critical role in the onset of this active feedback loop [14]. Studies have shown that radiation exposure in the small intestine will result in a decrease of microvascular thrombomodulin, which ultimately leads to inefficient reduction of thrombin, thereby disrupting the microvascular coagulation system [9, 15]. This excess thrombin has been shown to play a role in the activation of fibroblasts, thus perpetuating the inflammatory response leading to tissue fibrosis. Active feedback of TGF-β and TNF-α sustains the suppressed thrombomodulin levels, ultimately contributing to the chronic nature of the inflammation response.

Late radiation effects in the rat brain have been correlated to vascular radiation damage using a similar selective irradiation modality to what has been described in this thesis. Low molecular weight boron compounds (that do not cross the blood-brain barrier), coupled to thermal neutron irradiation, were used to selectively elevate the dose to the vascular endothelium in the rat brain. The main conclusions from these studies showed that vascular damage is the critical factor of the development of late white-matter necrosis [16], while neural progenitor cell loss in the subgranular zone (SGZ) is independent of vascular dose [17].

The selective vascular irradiation technique, which has been described in this thesis, is perfectly suited to elucidate the underlying mechanisms behind late radiation effects in normal tissues outside of the central nervous system. Various analytical techniques exist that allow for the direct measurement of inflammatory cytokine (e.g. - TNF-α, ICAM-1, IL-1b, IL-6 and TGF-β) levels in tissue following radiation exposure. Real-time polymerase chain reaction (PCR) and DNA microarray analyses were performed on tissue following uniform or selective vascular irradiation conditions. RNA extraction and real-time PCR protocols were established for mouse small intestine and brain. Independent real-time PCR measurements were performed on mouse tissue by the laboratory of M. Kerry O'Banion at the University of Rochester. DNA microarray analysis was performed on mouse tissue with the help of Rebecca Fry in the Center of Environmental Health Sciences (CEHS) at MIT. Inflammatory cytokines that were measured in more than one of the three different analysis techniques (real-time PCR at MIT, real-time PCR at University of Rochester, DNA microarray analysis MIT) were compared. The genome-wide data afforded by DNA microarray analysis allowed the construction of interactomes to reveal the signaling networks that were up-regulated due to radiation exposure in general and those networks that were uniquely up-regulated due to vascular damage. The pilot data obtained from these studies indicate that there may be a vascular component to the onset of late radiation effects in normal tissue. These results will serve as an interesting segue into another project exploring the specific role of vascular damage in the onset of late radiation effects. Details of the specific radiation damage

mechanisms could prove useful in the development of methods to treat or prevent radiation damage in normal tissues either during tumor therapy or after accidental or malevolent radiation exposures.

5.2 Materials and Methods

5.2.1 Mouse irradiations

Female C57Bl/6 mice (8-12 weeks old) were irradiated whole-body using ^{137}Cs gamma rays, epithermal neutrons, epithermal neutrons + boronated liposomes or epithermal neutrons + BPA. Gamma rays from a ^{137}Cs irradiator were delivered at a dose rate of 0.69 Gy min^{-1}, and epithermal neutrons from the MIT reactor were delivered at a dose rate of 0.57 Gy min^{-1}. The numbers of mice irradiated under each condition are summarized in Table 5-1 below:

Table 5-1: Mouse numbers and irradiation conditions

Irradiation Group	Number of Mice
Control	4
20 Gy gamma rays	4
11.9 Gy epithermal neutrons	4
3.8 Gy epithermal neutrons	4
3.8 Gy epithermal neutrons + boronated liposomes	4
3.8 Gy epithermal neutrons + BPA	3

^{10}B concentrations in blood at the time of neutron irradiation in mice that received boronated liposomes were 118±12 μg ^{10}B/g. ^{10}B concentrations in blood and tissue in mice that received BPA were ~13 μg ^{10}B/g. Mice were humanely killed 2 hrs after irradiation, and tissues were immediately processed for mRNA extraction.

5.2.2 RNA extraction and real-time PCR protocols for irradiated mouse tissue

mRNA was extracted from brain and small intestine (jejunum) using the RNeasy RNA extraction columns from Qiagen. Residual genomic DNA was removed by treatment with 1 unit DNAse I (Invitrogen) for 15 min at room temperature. The DNAse reactions were inactivated by addition of 1μL of 25mM EDTA and heating for 10 min at 65°C. Total RNA was quantified using standard spectrophotometric techniques. RNA (1 μg) was reverse transcribed using the Omniscript RT kit from Qiagen, and subsequent cDNA samples were stored at -80°C until further use. Real-time PCR was performed on the Applied Biosystems 7500 Fast Real-time PCR system while using SYBR Green PCR Master Mix (Applied Biosystems). Each reaction volume contained 25μL SYBR Green PCR Master Mix, 21μL RNAse-free water, 1.5μL forward primer (GAPDH, TNF-α or ICAM-1: final concentration 0.3 μM), 1.5μL reverse primer (GAPDH, TNF-α or ICAM-1 final concentration 0.3μM) and 1μL of cDNA for a total reaction volume of 50μL. The primers (Table 5-2) for GAPDH, TNF-α and ICAM-1 were designed using the Primer3 software package (MIT).

Table 5-2: PCR primer design

Gene	Primer Sequence	Accession Number for Gene Sequence
GAPDH	f- 5'-aacctgccaagtatgatgac r- 5'-gtccagggtttcttactcct	BC096440
ICAM-1	f- 5'-atgtttataaccgccagaga r- 5'-tcacacgtgttcacagtctt	NM_010493
TNF-α	f- 5'-gccgatttgctatctcatac r- 5'-tgggtagagaatggatgaac	NM_013693

GAPDH, which was assumed to be present in constant amounts through all experiments, was used as the 'housekeeping' gene in this study. The log of the fluorescence signal (log R_n) was plotted versus cycle number, and an arbitrary line was drawn through the linear portion of the amplification curves. The value, C_t, was defined as the cycle number where the amplification curve crossed this threshold. The fold-change in the target genes relative to GAPDH values was calculated using:

$$\text{Fold Change} = 2^{-\Delta\Delta Ct},$$

where $\Delta\Delta C_t = (C_{t\,\text{Target}} - C_{t\,\text{GAPDH}})_{\text{Dose x}} - (C_{t\,\text{Target}} - C_{t\,\text{GAPDH}})_{\text{Dose 0.}}$

Real-time PCR data was obtained by M. Kerry O'Banion (University of Rochester) using the same RNA samples that were obtained in the previously described RNA extraction protocol. Instead of using the SYBR Green PCR

reaction protocol, TaqMan® probes were used to measure the mRNA levels in the mouse tissue.

5.2.3 DNA microarray experiments

mRNA samples used for the previously described real-time PCR experiments were used in DNA microarray experiments performed by Lisa Smeester (CEHS) and Rebecca Fry (CEHS). mRNA samples from control mice, mice irradiated with 3.8 Gy of epithermal neutrons and mice irradiated with 3.8 Gy of epithermal neutrons plus boronated liposomes in the blood were used for the microarray experiments. The data were processed by Rebecca Fry (CEHS), and a genome-wide analysis was performed to determine the genes that were up- and down-regulated in response to uniform and selective vascular irradiation conditions. An interactome, based on this information, was then constructed, which highlighted the signaling networks that were activated within the tissue following radiation exposure. For clarity, the genes that were uniquely up-regulated due to vascular damage were individually labeled in red.

5.3 Results

5.3.1 Real-time PCR results (MIT and University of Rochester)

Figure 5-1 is a plot of the real-time PCR data (MIT) from mouse small intestine exposed to both uniform and selective vascular irradiation conditions. There is strong up-regulation of ICAM-1 in mice irradiated with epithermal neutrons with corresponding weaker up-regulation of TNF-α in the same animals. Interestingly, there is little up-regulation of both ICAM-1 and TNF-α in the animals exposed to gamma rays. Even though ICAM-1 and TNF-α are up-regulated in all groups exposed to epithermal neutrons, there is no evidence from this study that vascular damage plays a role in the expression of these two inflammatory cytokines in the mouse small intestine, as there are no differences between mice that received a low dose of neutrons and those that received the same neutron dose with extra dose selectively delivered to the vasculature.

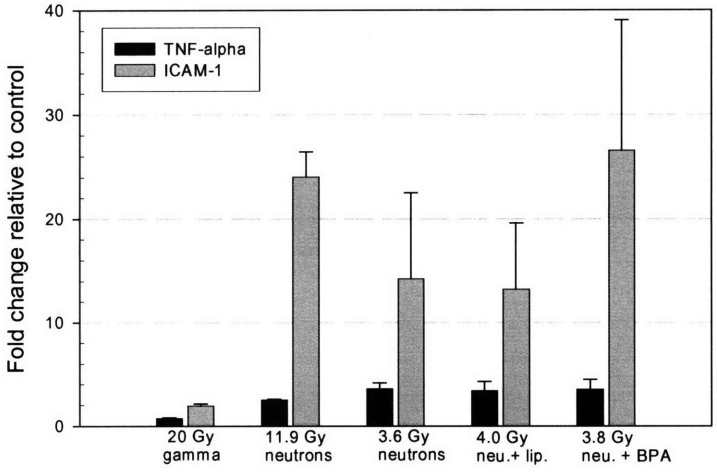

Figure 5-1. TNF-α and ICAM-1 mRNA levels in mouse small intestine following irradiation with ^{137}Cs gamma rays (gamma), epithermal neutrons (neutrons), epithermal neutrons + BPA (neu.+BPA) or epithermal neutrons + boronated liposomes in the blood (neu.+lip., selective vascular irradiation).

Figure 5-2 is a plot of the real-time PCR data (MIT) from mouse brain exposed to both uniform and selective vascular irradiation conditions. Compared to the mouse small intestine data, there is weaker up-regulation of ICAM-1 in mice irradiated with epithermal neutrons with corresponding weak up-regulation of TNF-α in the same animals. Even though ICAM-1 and TNF-α are up-regulated in all groups exposed to epithermal neutrons, there is no evidence from this study that vascular damage plays a role in the expression of these two inflammatory cytokines in the mouse brain.

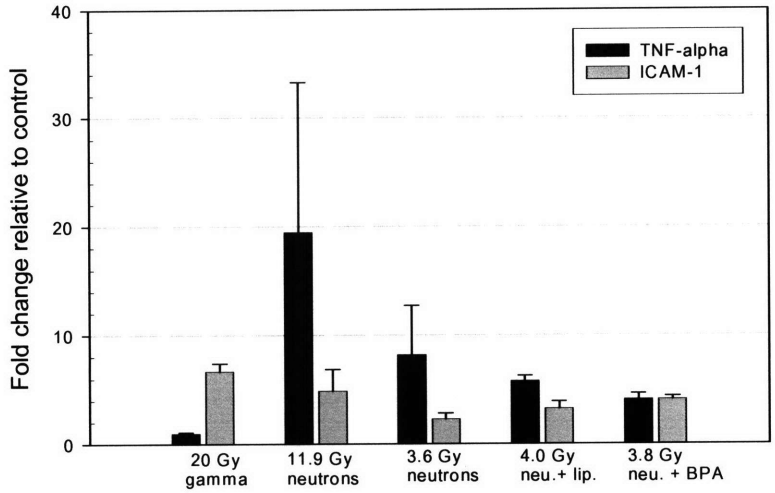

Figure 5-2. TNF-α and ICAM-1 mRNA levels in mouse brain following irradiation with ^{137}Cs gamma rays (gamma), epithermal neutrons (neutrons), epithermal neutrons + BPA (neu.+BPA) or epithermal neutrons + boronated liposomes in the blood (neu.+lip., selective vascular irradiation).

Figure 5-3 is a plot of the real-time PCR data (mouse small intestine) obtained by M. Kerry O'Banion at the University of Rochester on the same RNA samples used in the MIT real-time PCR studies. 11.9 Gy of neutrons caused a higher up-regulation in TNF-α, IL-6 and ICAM-1 than 20 Gy of gamma rays. Figure 5-3 (A) represents inflammatory cytokine expression after a low dose of epithermal neutrons. In Figure 5-3 (B), extra dose was selectively delivered to the vasculature to result in a vascular dose of ~ 12 Gy. One can see from this study that the added dose selectively delivered to the vasculature may have caused an increase in inflammatory cytokine levels compared to Figure 5-3 (A) ($p<0.001$ for IL-6. The difference between A and B is not statistically significant for TNF-α and ICAM-1).

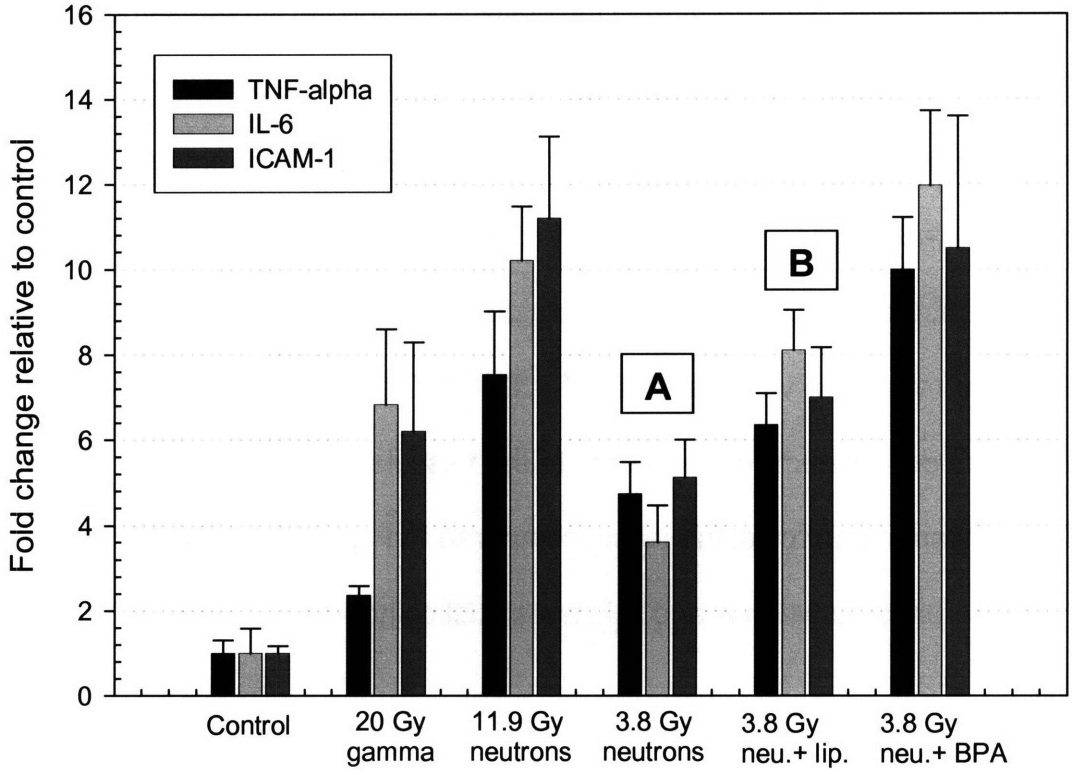

Figure 5-3. Expression of TNF-α, IL-6 and ICAM-1 in mouse small intestine following uniform whole-body and selective vascular irradiation conditions; measured using real-time PCR. A) Inflammatory cytokine levels following uniform neutron irradiation. B) Inflammatory cytokine levels following selective vascular irradiation conditions.

Figure 5-4 is a plot of the real-time PCR data (mouse brain) obtained by M. Kerry O'Banion at the University of Rochester on the same RNA samples used in the MIT real-time PCR studies. IL-6 expression was suppressed in the mouse brain, while TNF-α and ICAM-1 were up-regulated (but to a lesser extent than in the small intestine). Unlike the response in the small intestine, 20 Gy of gamma

rays elicited the largest response in terms of TNF-α and ICAM-1 expression. Figure 5-4 (A) represents inflammatory cytokine expression after a low dose of epithermal neutrons. In Figure 5-4 (B), extra dose was selectively delivered to the vasculature to result in a vascular dose of ~ 12 Gy. One can see from this study that the added dose selectively delivered to the vasculature may have caused an increase in inflammatory cytokine levels compared to Figure 5-4 (A) ($p<0.04$ for ICAM-1. The difference between A and B is not statistically significant for TNF-α and IL-6.).

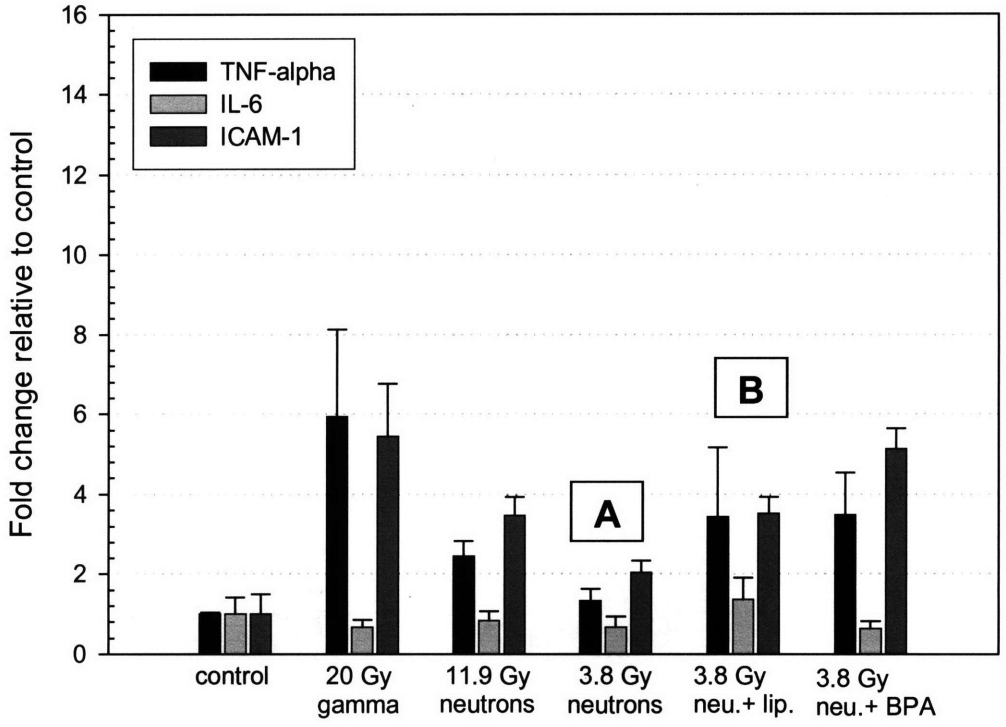

Figure 5-4. Expression of TNF-α, IL-6 and ICAM-1 in mouse brain following uniform whole-body and selective vascular irradiation conditions; measured using real-time PCR. A) Inflammatory cytokine levels following uniform neutron irradiation. B) Inflammatory cytokine levels following selective vascular irradiation conditions.

5.3.2 DNA microarray results (MIT CEHS)

DNA microarray analysis was performed on RNA samples (brain and small intestine) taken from control mice and mice irradiated with neutrons alone or neutrons plus boronated liposomes in the blood. The relative genome-wide changes caused by irradiation with neutrons alone or neutrons plus boronated liposomes were examined in these experiments. The total number of genes screened in the microarray experiments was 28,295. Of these, 679 were modulated by treatment with neutrons alone (where modulation is defined as a 1.5-fold change relative to controls at $p<0.05$), whereas treatment with neutrons

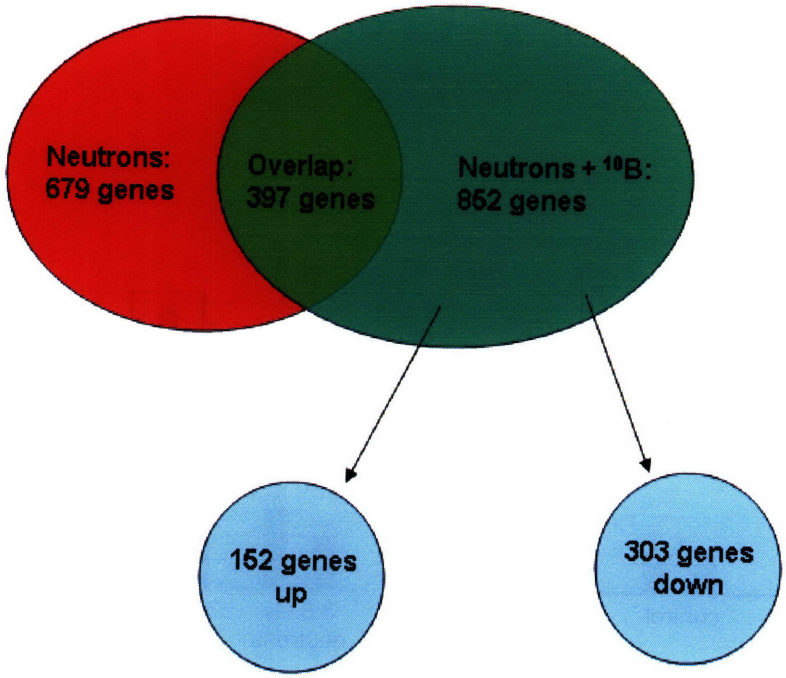

Figure 5-5. Venn diagram showing the numbers of modulated genes measured in the DNA microarray experiments (mouse small intestine).

plus liposomes resulted in modulation of 852 genes, relative to control mice. Many of these genes (397) were shared by the two conditions (neutrons alone or neutrons plus boronated liposomes). Of particular interest to us is the subset of 455 modulated genes that were uniquely modulated due to selective vascular irradiation. Specifically, 152 genes were uniquely up-regulated and 303 genes were down-regulated in response to selective vascular irradiation (Figure 5-5).

We analyzed the interactions and molecular pathways of the gene products and transcripts that were uniquely up-regulated due to selective vascular irradiation. We identified a highly significant ($p<10^{-18}$) large interactome that connects the up-regulated genes unique to the selective vascular irradiation groups. Figure 5-6 shows part of the genome-wide interactome that was created from the microarray data. It shows that the NF-κB sub-network was activated due to radiation exposure, and the genes that were uniquely up-regulated due to vascular damage are indicated in red. It turns out that NF-κB was up-regulated due to vascular damage and is connected to the TNF-α signaling cascade. The fact that TNF-α is not highlighted in red does not mean that it was not up-regulated in the neutrons plus boronated liposomes group. It happened to be up-reguated in both the neutrons only and selective vascular irradiation groups (see Figure 5-3).

Key players in the inflammation response and cellular function are embedded within the large interactome. The signaling networks that were most strongly expressed in the neutrons only (Figure 5-5; 679 genes) and overlap groups (Figure 5-5; 397 genes) are involved in the cell cycle, cell death, cancer,

DNA repair and the immune response. Those networks up-regulated in the neutrons plus boronated liposomes group (Figure 5-5; 852 genes) are also involved in the cell cycle, DNA repair and cell death, but when the overlap genes are subtracted from the neutrons plus ^{10}B group, the network most strongly up-regulated in the remaining group (Figure 5-5, 152 genes) is intimately involved in cell death, hematological system development, inflammatory disease and the immune response. These results support our hypothesis that vascular damage may be involved in the inflammation response following radiation exposure.

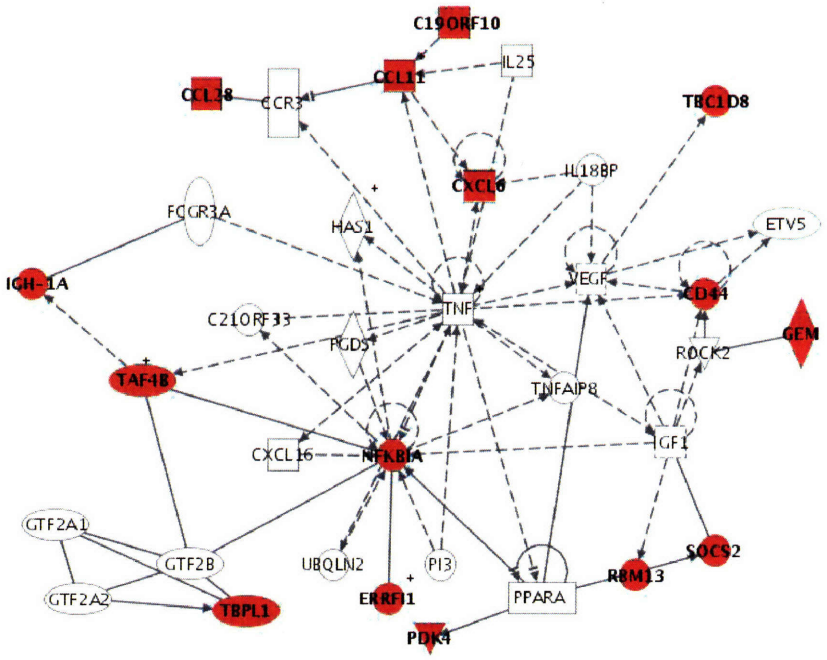

Figure 5-6. Interactome indicating the specific up-regulation of the NF-κB sub-network. The red-highlighted genes represent those uniquely up-regulated due to vascular damage.

5.3.3 Trend comparison between genes that were measured in more than one of the analysis techniques described above

Table 5-3 lists the fold-change values for the genes that were measured in more than one of the three analysis techniques (real-time PCR (Schuller), real-time PCR (O'Banion), DNA microarray analysis (Fry)). Most of the genes show a similar trend when compared across the three analysis techniques. The exceptions (Table 5-3, yellow highlighted) are: TNF-α (20 Gy gamma-rays) measured by Schuller (down-regulation) and O'Banion (up-regulation); IL-6 (3.8 Gy N and 3.8 Gy N+L) measured by O'Banion (up-regulation) and Fry (no change). In all cases, the magnitudes of gene expression measured in each analysis technique were different. The differences in overall magnitude of gene expression between the three analysis techniques can be attributed to differences in primer design (and type) and laboratory technique for real-time PCR, or, in the case of the DNA microarray results, a different analysis technique altogether. Therefore, the overall trend of gene expression is a better metric to use when comparing the gene expression levels. The threshold for change (either up- or down-regulation) was a 1.5-fold change from control values. A student's t-test was applied to each comparison to determine if values were significantly different from control values when the decision of up-regulation, down-regulation or 'no change' was made ($p<0.05$ was considered significant for these comparisons).

Table 5-3: Values for gene expression from Schuller, O'Banion and Fry.

Gene	20 Gy γ			11.9 Gy N			3.8 Gy N			3.8 Gy N+L			3.8 Gy N+BPA		
	S[1]	O[2]	F[3]	S	O	F	S	O	F	S	O	F	S	O	F
TNF-α	0.7	2.4		2.5	7.5		3.6	4.7	1.7	3.4	6.4	1.6	3.5	9.9	
ICAM-1	1.9	6.2		24.1	11.2		14.2	5.1	3.4	13.2	7.0	3.7	26.5	10.5	
IL-1b								1.6*	-1.1		1.1	-1.1			
IL-6								3.1	1.1		8.1	1.1			
TGF-β								1.3	1.2		1.2	1.3			

[1] Real-time PCR performed by Schuller at MIT.
[2] Real-time PCR performed by O'Banion at University of Rochester.
[3] DNA microarray analysis performed by Fry at MIT.
* Not statistically different from control.
n.b. – A blank cell indicates that the gene was not measured using that particular technique.

5.4 Discussion

The technique for selective irradiation of the vascular endothelium, as described in this thesis, allows for the study of the role vascular radiation damage in the normal tissue radiation response, both early and late. The technique is ideally suited for mechanistic studies involving vascular damage in tissue outside of the central nervous system (CNS), where the blood-brain barrier can be used to selectively manipulate the microvasculature. Coderre *et al.* have previously employed a similar methodology in the rat CNS where the blood-brain barrier was used to restrict the widely used BNCT compound, BSH, to the blood. Subsequent irradiation with thermal neutrons selectively elevated the dose delivered to the CNS microvasculature. They were able to show that vascular

damage was responsible for the onset of late (7 months) necrosis in the rat spinal cord [16, 18-21]. In these studies, O-2A glial progenitor cells survived selective vascular irradiation conditions, which indicated that vascular radiation damage played a critical role in the onset of late radiation effects but had no effect on the early radiation response in that system. Similar studies were carried out in the rat brain where the loss of neural precursor cells was correlated with stem cell dose and not the added dose selectively delivered to the vasculature [17]. A similar, biphasic trend has emerged from the mouse small intestine studies conducted in this thesis; that early radiation effects (intestinal crypt stem cell loss and the gastrointestinal syndrome) are due to direct radiation damage to the proliferative stem cell populations regenerating the tissue, while late effects (chronic inflammation and fibrosis) may be due to damage to the vasculature.

Inflammation is a normal response to tissue injury that starts with the activation of vascular endothelial cells by pro-inflammatory cytokines (such as IL-1, IL-6 and TNF-α) and the recruitment of neutrophils to the site of injury. Circulating neutrophils attach to the activated vascular endothelium through receptor-ligand interactions between integrins and selectins that are expressed on both neutrophils and activated vascular endothelial cells. Upon attachment, endothelial cells allow for the extravasation of neutrophils from the blood stream to the site of injury, where chemotactic molecules are released that serve to recruit other players in the inflammation response such as macrophages and mast cells. In normal wound healing, the production of pro-inflammatory

cytokines is closely followed by the release of anti-inflammatory cytokines to ultimately lead to full tissue recovery [17].

Chronic inflammation is a process where either the initiating damage stimulus remains present at the site of tissue injury or the active mechanism for suppressing pro-inflammatory signaling has been distrupted. Chronic inflammation is also involved with neoplastic progression [22, 23]. Radiation has been shown to initiate the inflammation response in normal tissues [24], and it has been shown to initiate the activation of inflammatory cytokines ultimately leading to fibrosis [25]. Late radiation effects exhibit many of the same characteristics present in chronic inflammation, such as a continuous cytokine signaling cascade and neoplastic progression. This radiation-induced cytokine cascade establishes a state of chronic inflammation, which ultimately leads to permanent tissue changes such as fibrosis [10].

In normal wound healing, fibrosis promoting proteins such as transforming growth factor-β (TGF-β) and connective tissue growth factor (CTGF) are in a delicate balance with fibrosis inhibiting proteins such as TNF-α among others [1, 8, 26-28]. However, in the late fibrogenic response to radiation, this balance between fibrosis promoters and inhibitors is disrupted, and the wound healing process is perpetuated over long periods of time [1]. This type of radiation response has been likened to a 'wound that does not heal' [11, 15, 29].

TGF-β is a strong profibrotic molecule that is intimately tied to cellular differentialtion and proliferation. As such, it has been classified as both a cytokine and growth factor (as its name suggests). It is involved with embryonic

development, cell-cycle control and wound healing, and its dysfunction has been linked to cancer and fibrotic diseases such as arteriosclerosis, rheumatoid arthritis and scleroderma [1]. TGF- β accumulates in the extra-cellular matrix in an inactive form, and must be activated by dissociation from its associated latency associated peptide (LAP) [1, 30]. Thus, an abundant supply of inactive TGF- β is present in tissue that can be rapidly activated in response to a damage event. It is known that ionizing radiation can activate TGF- β, and activation occurs rapidly (~1h post-irradiation) starting with doses as low as 0.1 Gy [1, 31-33].

The TGF- β signaling pathway is known in great detail, but the reason for the persistent cytokine signaling cascades in chronic inflammation is still unknown. Some evidence suggests that damage to the microvasculature and subsequent tissue hypoxia could motivate fibrogenesis in tissues following radiation exposure [34, 35]. Radiation damage has been described as a complex wound caused by vascular damage and subsequent dysregulation of the coagulation system leading to chronic inflammation and fibrosis [15, 36]. The radioprotector, amifostine, which does not cross the blood-brain barrier, has been used to selectively protect the vasculature of the rat brain. These studies have shown that selective protection of the vascular endothelium in the CNS can save the CNS from late radiation effects [37-40]. Clearly, vascular damage plays an integral role in the onset of late radiation effects in the CNS, and the results from the preliminary studies presented in this chapter may indicate that vascular

damage may play a similar role in the onset of late effects (fibrosis) outside of the CNS; in this case, the mouse small intestine.

The process of fibrogenesis in normal tissues following radiation exposure is a complex interplay between multiple cell types and signaling pathways. Our selective vascular irradiation technique allows us to irradiate one target cell population (vascular endothelium) while keeping all others relatively unscathed (3x less dose). We have used various molecular biology techniques (real-time PCR and DNA microarray analysis) to measure inflammatory cytokine (mRNA) levels in tissue following uniform and selective vascular irradiation conditions. Although it is impossible, at this time, to make absolute conclusions about specific radiation damage mechanisms involved with the radiation-induced inflammation response from the data presented in this chapter, it is possible to define overall trends in inflammatory cytokine expression that will hopefully lead to further studies in the future.

We set out to concentrate on some of the primary molecules involved with the inflammation response. We chose to concentrate on TNF-α, ICAM-1 (intercellular adhesion molecule-1), IL-6, IL-1b and TGF-β in these pilot studies. TNF-α and ICAM-1 levels were measured using the three available analysis techniques described earlier (real-time PCR at MIT and University of Rochester; DNA microarray analysis at MIT), while the rest of the cytokines were measured using two of the available three techniques (real-time PCR at MIT and University of Rochester; real-time PCR at University of Rochester and DNA microarray analysis at MIT). TNF-α and ICAM-1 were up-regulated in all three of the analysis

techniques (Table 5-3) and for each of the irradiation conditions outlined above (except Schuller 20 Gy gamma rays). IL-6, IL-1b and TGF-β levels were measured by O'Banion and Fry (Table 5-3). IL-6 was up-regulated in the O'Banion real-time PCR measurements but did not change in the Fry DNA microarray measurements (for 3.8 Gy N and 3.8 Gy N+L). IL-1b levels did not change relative to control levels in both the O'Banion and Fry measurements (for 3.8 Gy N and 3.8 Gy N+L). TGF-β levels did not change relative to control levels for both O'Banion and Fry (3.8 Gy N and 3.8 Gy N+L). The trends that arose from the comparison between O'Banion and Fry for IL-6, IL-1b and TGF-β may have resulted from fundamental differences between real-time PCR and DNA microarray analysis. Also, each gene might follow a different time-course in terms of up- or down-regulation following radiation exposure. Given that these studies were conducted at one fixed time point (2 hrs post-irradiation), further time-course studies might reveal interesting kinetics for these three genes. We would expect to see persistent up-regulation of inflammatory signaling molecules weeks to months after radiation exposure, specifically in the selective vascular irradiation groups.

While the real-time PCR measurements performed by Schuller at MIT do not show evidence that vascular radiation damage plays a role in the early release of inflammatory cytokines, TNF-α and ICAM-1, in the mouse small intestine and brain (Figures 5-1 & 5-2), the O'Banion real-time PCR and Fry DNA microarray analysis techniques do show evidence that vascular damage may be involved in the inflammation response (Figures 5-3, 5-4 & 5-6). Figure 5-3 shows

the results from the O'Banion measurements in the small intestine under uniform and selective vascular irradiation conditions. Figure 5-3 (A) shows the results for TNF-α, IL-6 and ICAM-1 after a uniform neutron beam dose of 3.8 Gy. Figure 5-3 (B) shows the results for the same three genes and neutron dose but with a higher dose selectively delivered to the vasculature (~12 Gy). Although there seems to be an indication that the added dose selectively delivered to the vasculature caused the increase in levels seen in Figure 5-3 (B), IL-6 is the only gene in Figure 5-3 (B) that is significantly greater than (A). Figure 5-4 shows the results from the O'Banion measurements in the mouse brain under uniform and selective vascular irradiation conditions. Figure 5-4 (A & B) are the results of same irradiation conditions as Figure 5-3 (A & B). Again, there seems to be an indication that the added dose selectively delivered to the vasculature caused the increase in levels seen in Figure 5-4 (A). ICAM-1 is the only gene in Figure 5-4 (B) that is significantly greater than (A). Figure 5-6 is an interactome (created by Rebecca Fry from the group of genes up-regulated due to vascular damage (Figure 5-5; 152 genes)) that shows the up-regulation of the NF-κB sub-network. The genes highlighted in red are those uniquely up-regulated due to vascular damage. Other networks upregulated from that same group are involved in cell death, the cell cycle, inflammatory disease and the immune response.

These preliminary data merely hint at the role of vascular damage in the onset of late radiation effects in normal tissues. The selective vascular irradiation technique that has been developed in this thesis is ideally suited to elucidate the subtle role of vascular damage in the complex process of chronic inflammation

and fibrogenesis. The beauty of this technique is that it can be applied to any tissue where vascular damage may play an important role in the radiation response. This is also true for tumors where there has been intense research into the role of tumor vasculature in tumor growth and development, which has led to anti-angiogenic therapies. Radiation endotheliology is a fruitful and interesting field that will have far reaching impact in radiation oncology and nuclear medicine.

References

1. Bentzen, S.M., *Preventing or reducing late side effects of radiation therapy: radiobiology meets molecular pathology.* Nat Rev Cancer, 2006. **6**(9): p. 702-13.
2. Boerma, M., C.I. Schutte-Bart, L.E. Wedekind, H. Beekhuizen, and J. Wondergem, *Effects of multiple doses of ionizing radiation on cytokine expression in rat and human cells.* Int J Radiat Biol, 2003. **79**(11): p. 889-96.
3. Calveley, V.L., M.A. Khan, I.W. Yeung, J. Vandyk, and R.P. Hill, *Partial volume rat lung irradiation: temporal fluctuations of in-field and out-of-field DNA damage and inflammatory cytokines following irradiation.* Int J Radiat Biol, 2005. **81**(12): p. 887-99.
4. Handschel, J., C. Sunderkotter, B. Kruse-Losler, F.J. Prott, U. Meyer, J. Piffko, and U. Joos, *Late effects of radiotherapy on oral mucosa in humans.* Eur J Oral Sci, 2001. **109**(2): p. 95-102.
5. Rube, C.E., D. Uthe, K.W. Schmid, K.D. Richter, J. Wessel, A. Schuck, N. Willich, and C. Rube, *Dose-dependent induction of transforming growth factor beta (TGF-beta) in the lung tissue of fibrosis-prone mice after thoracic irradiation.* Int J Radiat Oncol Biol Phys, 2000. **47**(4): p. 1033-42.
6. Rube, C.E., F. Wilfert, D. Uthe, K.W. Schmid, R. Knoop, N. Willich, A. Schuck, and C. Rube, *Modulation of radiation-induced tumour necrosis factor alpha (TNF-alpha) expression in the lung tissue by pentoxifylline.* Radiother Oncol, 2002. **64**(2): p. 177-87.
7. Rube, C.E., F. Wilfert, D. Uthe, J. Konig, L. Liu, A. Schuck, N. Willich, K. Remberger, and C. Rube, *Increased expression of pro-inflammatory cytokines as a cause of lung toxicity after combined treatment with gemcitabine and thoracic irradiation.* Radiother Oncol, 2004. **72**(2): p. 231-41.
8. Barcellos-Hoff, M.H., *How tissues respond to damage at the cellular level: orchestration by transforming growth factor-{beta} (TGF-{beta}).* BJR Suppl, 2005. **27**: p. 123-7.
9. Hauer-Jensen, M., L.M. Fink, and J. Wang, *Radiation injury and the protein C pathway.* Crit Care Med, 2004. **32**(5 Suppl): p. S325-30.
10. Okunieff, P., T. Cornelison, M. Mester, W. Liu, I. Ding, Y. Chen, H. Zhang, J.P. Williams, and J. Finkelstein, *Mechanism and modification of gastrointestinal soft tissue response to radiation: role of growth factors.* Int J Radiat Oncol Biol Phys, 2005. **62**(1): p. 273-8.
11. Eckes, B., P. Zigrino, D. Kessler, O. Holtkotter, P. Shephard, C. Mauch, and T. Krieg, *Fibroblast-matrix interactions in wound healing and fibrosis.* Matrix Biol, 2000. **19**(4): p. 325-32.
12. Gaber, M.W., O.M. Sabek, K. Fukatsu, H.G. Wilcox, M.F. Kiani, and T.E. Merchant, *Differences in ICAM-1 and TNF-alpha expression between*

large single fraction and fractionated irradiation in mouse brain. Int J Radiat Biol, 2003. **79**(5): p. 359-66.
13. McBride, W.H., C.S. Chiang, J.L. Olson, C.C. Wang, J.H. Hong, F. Pajonk, G.J. Dougherty, K.S. Iwamoto, M. Pervan, and Y.P. Liao, *A sense of danger from radiation.* Radiat Res, 2004. **162**(1): p. 1-19.
14. Hopewell, J. and H.R. Withers, *Proposition: long-term changes in irradiated tissues are due principally to vascular damage in the tissues.* Med Phys, 1998. **25**(12): p. 2265-8.
15. Denham, J.W. and M. Hauer-Jensen, *The radiotherapeutic injury--a complex 'wound'.* Radiother Oncol, 2002. **63**(2): p. 129-45.
16. Coderre, J.A., G.M. Morris, P.L. Micca, J.W. Hopewell, I. Verhagen, B.J. Kleiboer, and A.J. van der Kogel, *Late effects of radiation on the central nervous system: role of vascular endothelial damage and glial stem cell survival.* Radiat Res, 2006. **166**(3): p. 495-503.
17. Otsuka, S., J.A. Coderre, P.L. Micca, G.M. Morris, J.W. Hopewell, R. Rola, and J.R. Fike, *Depletion of neural precursor cells after local brain irradiation is due to radiation dose to the parenchyma, not the vasculature.* Radiat Res, 2006. **165**(5): p. 582-91.
18. Morris, G.M., J.A. Coderre, A. Bywaters, E. Whitehouse, and J.W. Hopewell, *Boron neutron capture irradiation of the rat spinal cord: histopathological evidence of a vascular-mediated pathogenesis.* Radiat Res, 1996. **146**(3): p. 313-20.
19. Morris, G.M., J.A. Coderre, J.W. Hopewell, P.L. Micca, and C. Fisher, *Boron neutron capture irradiation of the rat spinal cord: effects of variable doses of borocaptate sodium.* Radiother Oncol, 1996. **39**(3): p. 253-9.
20. Morris, G.M., J.A. Coderre, J.W. Hopewell, P.L. Micca, M.M. Nawrocky, H.B. Liu, and A. Bywaters, *Response of the central nervous system to boron neutron capture irradiation: evaluation using rat spinal cord model.* Radiother Oncol, 1994. **32**(3): p. 249-55.
21. Morris, G.M., J.A. Coderre, E.M. Whitehouse, P. Micca, and J.W. Hopewell, *Boron neutron capture therapy: a guide to the understanding of the pathogenesis of late radiation damage to the rat spinal cord.* Int J Radiat Oncol Biol Phys, 1994. **28**(5): p. 1107-12.
22. Rao, V.P., T. Poutahidis, Z. Ge, P.R. Nambiar, B.H. Horwitz, J.G. Fox, and S.E. Erdman, *Proinflammatory CD4+ CD45RB(hi) lymphocytes promote mammary and intestinal carcinogenesis in Apc(Min/+) mice.* Cancer Res, 2006. **66**(1): p. 57-61.
23. Coussens, L.M. and Z. Werb, *Inflammation and cancer.* Nature, 2002. **420**(6917): p. 860-7.
24. Quarmby, S., P. Kumar, and S. Kumar, *Radiation-induced normal tissue injury: role of adhesion molecules in leukocyte-endothelial cell interactions.* Int J Cancer, 1999. **82**(3): p. 385-95.
25. Rubin, P., C.J. Johnston, J.P. Williams, S. McDonald, and J.N. Finkelstein, *A perpetual cascade of cytokines postirradiation leads to pulmonary fibrosis.* Int J Radiat Oncol Biol Phys, 1995. **33**(1): p. 99-109.

26. Leask, A. and D.J. Abraham, *TGF-beta signaling and the fibrotic response.* Faseb J, 2004. **18**(7): p. 816-27.
27. Moussad, E.E. and D.R. Brigstock, *Connective tissue growth factor: what's in a name?* Mol Genet Metab, 2000. **71**(1-2): p. 276-92.
28. Border, W.A. and N.A. Noble, *Transforming growth factor beta in tissue fibrosis.* N Engl J Med, 1994. **331**(19): p. 1286-92.
29. Martin, M., J. Lefaix, and S. Delanian, *TGF-beta1 and radiation fibrosis: a master switch and a specific therapeutic target?* Int J Radiat Oncol Biol Phys, 2000. **47**(2): p. 277-90.
30. Lawrence, D.A., *Latent-TGF-beta: an overview.* Mol Cell Biochem, 2001. **219**(1-2): p. 163-70.
31. Ehrhart, E.J., P. Segarini, M.L. Tsang, A.G. Carroll, and M.H. Barcellos-Hoff, *Latent transforming growth factor beta1 activation in situ: quantitative and functional evidence after low-dose gamma-irradiation.* Faseb J, 1997. **11**(12): p. 991-1002.
32. Ewan, K.B., R.L. Henshall-Powell, S.A. Ravani, M.J. Pajares, C. Arteaga, R. Warters, R.J. Akhurst, and M.H. Barcellos-Hoff, *Transforming growth factor-beta1 mediates cellular response to DNA damage in situ.* Cancer Res, 2002. **62**(20): p. 5627-31.
33. Ewan, K.B., G. Shyamala, S.A. Ravani, Y. Tang, R. Akhurst, L. Wakefield, and M.H. Barcellos-Hoff, *Latent transforming growth factor-beta activation in mammary gland: regulation by ovarian hormones affects ductal and alveolar proliferation.* Am J Pathol, 2002. **160**(6): p. 2081-93.
34. Delanian, S. and J.L. Lefaix, *The radiation-induced fibroatrophic process: therapeutic perspective via the antioxidant pathway.* Radiother Oncol, 2004. **73**(2): p. 119-31.
35. Vujaskovic, Z., M.S. Anscher, Q.F. Feng, Z.N. Rabbani, K. Amin, T.S. Samulski, M.W. Dewhirst, and Z.A. Haroon, *Radiation-induced hypoxia may perpetuate late normal tissue injury.* Int J Radiat Oncol Biol Phys, 2001. **50**(4): p. 851-5.
36. Wang, J., H. Zheng, X. Ou, L.M. Fink, and M. Hauer-Jensen, *Deficiency of microvascular thrombomodulin and up-regulation of protease-activated receptor-1 in irradiated rat intestine: possible link between endothelial dysfunction and chronic radiation fibrosis.* Am J Pathol, 2002. **160**(6): p. 2063-72.
37. Plotnikova, E.D., M.K. Levitman, V.V. Shaposhnikova, J.V. Koshevoj, and L.K. Eidus, *Protection of microvasculature in rat brain against late radiation injury by gammaphos.* Int J Radiat Oncol Biol Phys, 1988. **15**(5): p. 1197-201.
38. Plotnikova, E.D., M.K. Levitman, V.V. Shaposhnikova, V. Koshevoy Ju, and L.K. Eidus, *Protection of microcirculation in rat brain against late radiation injury by gammaphos.* Int J Radiat Oncol Biol Phys, 1984. **10**(3): p. 365-8.
39. Nieder, C., N.H. Andratschke, N. Wiedenmann, and M. Molls, *Prevention of radiation-induced central nervous system toxicity: a role for amifostine?* Anticancer Res, 2004. **24**(6): p. 3803-9.

40. Lyubimova, N. and J.W. Hopewell, *Experimental evidence to support the hypothesis that damage to vascular endothelium plays the primary role in the development of late radiation-induced CNS injury.* Br J Radiol, 2004. **77**(918): p. 488-92.

Chapter 6: Future Work

This thesis describes a generalized methodology to selectively irradiate the vascular endothelium. Careful dosimetric considerations were made for both the uniform neutron beam dose and the added dose selectively delivered to the vascular endothelium from the boron neutron capture reactions restricted to the blood. Even though the thermal neutron flux and blood-boron concentrations are known at the time of irradiation, the final dose to the vascular wall is a calculation that includes not only those measured parameters but also terms that are based in modeling and simulation. Therefore, the dose to the vascular endothelium is not a measured value but, rather, a calculation that is based in real measurement. Current radiation dosimetry techniques do not allow for intravascular (*in vivo*) measurements to determine the dose delivered to the vascular wall. Therefore, it is necessary to conduct studies to directly measure the damage to the vascular endothelium in a biological system, where the physiological response to selective vascular irradiation can be used to determine the extent of vascular damage.

Blood-brain barrier dispruption following selective vascular irradiation is one such physiological response that may directly reveal the extent of vascular damage in that system [1, 2]. One potential experiment could involve subjecting the CNS to selective vascular irradiation conditions, waiting an appropriate period of time to allow blood-brain barrier disruption to occur, introducing a dye that will pass through the blood-brain barrier following disruption and measuring the amount of dye leakage into the CNS tissue using spectrophotometric techniques (to measure dye concentration). The amount of dye leakage could then be

correlated to vascular dose and serve as a measure of vascular damage following selective vascular irradiation conditions*.

Another physiological response that could be useful in determining the extent of vascular damage due to selective vascular irradiation, and one that has been studied in great detail, is brain capillary drop-out following radiation exposure. Lyubimova and Hopewell used the radio-protector, Gammaphos, to selectively protect the brain endothelium from a dose sufficient to cause late radiation necrosis in the rat CNS. They scored the number of surviving endothelial cells at various times post-irradiation (up to 65 weeks), and were able to correlate endothelial cell loss with the onset of necrosis and vascular abnormalities. Gammaphos selectively protected the brain endothelium, which resulted in reduced radiation-induced necrosis [3]. Similar histological techniques can be used to measure capillary drop-out and necrosis following selective vascular irradiation conditions, and these can be used to determine the extent vascular damage.

The gene expression studies conducted in Chapter 5 indicate that there are inflammatory changes in the small intestine following selective vascular irradiation, and that there may be a vascular component to these changes. In those studies mice were subjected to a variety of irradiation conditions, but gene expression was only measured at one time point (2 hrs post-irradiation). A complete time course (2 hrs to months post-irradiation) and dose response for inflammatory cytokine expression using DNA microarray and real-time PCR

* Rebecca L. Raabe is currently performing these studies for her master's thesis (Department of Nuclear Science and Engineering, MIT, expected August, 2007).

analysis may reveal the specific role of vascular damage in the onset of chronic, radiation-induced inflammatory signaling leading to fibrosis in the small intestine. It might also be pertinent to conduct low dose experiments to establish dose thresholds for inflammatory cytokine expression. Increasing the blood-boron concentration as high as possible (using new ^{10}B compounds) will allow one to use lower neutron beam doses to achieve similarly high vascular doses to the ones used in Chapter 5. Reducing the tissue damage due to the neutron beam dose will allow one to observe cytokine expression due to vascular damage alone.

The goal of this thesis was to develop a generalized methodology to selectively irradiate the vascular endothelium that can be applied to any tissue or tumor. The small intestine was chosen for proof-of-principle studies, because it has interesting radiation pathology, both early and late. This same methodology can also be applied to other tissues where the role of vascular damage in the onset of early and late effects is still a question. There have been extensive studies in the CNS (described earlier) using similar vascular irradiation techniques. The technique described in this thesis can be applied to the lung and tumor where there are, as yet, unresolved controversies (described earlier) regarding the role of vascular damage in these tissues.

The results from these proposed studies will lend remarkable insight into the role of vascular damage in normal tissue radiation pathology. These insights will probably contain information on specific damage mechanisms involved in early and late radiation effects. Based on this information, interventional drugs

can be developed that can be used to protect tissues from debilitating radiation effects. This will prove invaluable to clinicians and first responders as they try to subvert normal tissue radiation damage following radiation therapy or potential nuclear accidents.

References

1. Li, Y.Q., P. Chen, A. Haimovitz-Friedman, R.M. Reilly, and C.S. Wong, *Endothelial apoptosis initiates acute blood-brain barrier disruption after ionizing radiation.* Cancer Res, 2003. **63**(18): p. 5950-6.
2. Yuan, H., M.W. Gaber, K. Boyd, C.M. Wilson, M.F. Kiani, and T.E. Merchant, *Effects of fractionated radiation on the brain vasculature in a murine model: blood-brain barrier permeability, astrocyte proliferation, and ultrastructural changes.* Int J Radiat Oncol Biol Phys, 2006. **66**(3): p. 860-6.
3. Lyubimova, N. and J.W. Hopewell, *Experimental evidence to support the hypothesis that damage to vascular endothelium plays the primary role in the development of late radiation-induced CNS injury.* Br J Radiol, 2004. **77**(918): p. 488-92.